Doctorate Dissertation (Censored)

博士論文（要約）

# Function and formation of neuronal circuits that regulate divergent action selection

# （多様な行動選択を制御する神経回路の機能と形成）

A Dissertation Submitted for Degree of Doctor of Philosophy

December 2018

博士（理学）申請

平成 30 年 12 月

Department of Physics, Graduate School of Science,

The University of Tokyo

東京大学大学院理学系研究科物理学専攻

Suguru Takagi

髙木　優

# Abstract

Animals process sensory inputs from the environment to produce adaptive motor outputs. Importantly, due to the size and nature of animal bodies, animals must discriminate the geometric position of the sensory input on the body. The mechanism of neuronal circuits that realizes such somatotopically-organized action selection has largely remained elusive.

In the current dissertation, I studied the function and formation of tactile-induced action selection circuitry using *Drosophila melanogaster* larvae, which escape by backward locomotion when touched on the head, while they crawl forward when touched on the tail.

First, I identify a class of segmentally repeated second-order somatosensory interneurons, that I named Wave, whose activation in anterior and posterior segments elicits backward and forward locomotion, respectively. Anterior and posterior Wave neurons extend their dendrites in opposite directions to receive somatosensory inputs from the head and tail, respectively. Downstream of the anterior Wave neurons, I identify premotor circuits, which together with Wave, are necessary for the backward locomotion touch response.

Next, I show the developmental process of the formation of Wave neuron morphology. Stage-by-stage observation suggested that Wave neurons are identical to a class of known pioneer neurons. I show the recruitment of Wnt/Fz signaling in guiding axons of posterior Wave neurons onto more posterior neuromeres. Furthermore, cell-specific knock-down of DFz4 partially inhibited the commandability of fictive forward locomotion but not of backward locomotion.

Taking these together, I propose that segment-specific neurite extension of Wave neurons mediates divergent action selection. As these neurons are likely to be conserved across species, the present study may serve as a model to study the general principle of action selection circuits.

# List of Abbreviations

| Abbreviation | Meaning |
|---|---|
| A | Anterior |
| ABD | Abdomen |
| AC | Anterior commissure |
| aCC | Anterior corner cell |
| AD | Activation domain |
| ALM | Anterior lateral microtubule cell |
| AVA | (not available; defined in White et al., 1986) |
| AVB | (not available; defined in White et al., 1986) |
| A-P | Anterior-posterior |
| BL | Brain Lobe |
| CNS | Central nervous system |
| CPG | Central pattern generator |
| D | Dorsal |
| DBD | DNA binding domain |
| EM | Electron microscopy |
| Fas2 | Fasciclin 2 |
| FLP | Flippase |
| FRT | Flippase recognition site |
| Fz | Frizzled |
| GF | Giant fiber |
| GFP | Green fluorescent protein |
| hAEL | hours after egg laying |
| HRP | Horseradish peroxidase |
| L | Lateral |

| | |
|---|---|
| LG | Lateral giant axon |
| M | Medial |
| MCFO | MultiColor FlpOut |
| MD | Multidendritic |
| MG | Medial giant axon |
| MN | Motor neuron |
| MoG | Giant motoneurons |
| P | Posterior |
| PBS | Phosphate-buffered saline |
| PC | Posterior commissure |
| PLM | Posterior lateral microtubule cell |
| ROI | Region of interest |
| SN | Sensory neuron |
| TeTxLC | Tetanus toxin light chain |
| TX | Thorax |
| UAS | Upstream activating sequence |
| V | Ventral |
| VNC | Ventral nerve cord |

# List of Figures and Tables

Figure 1.1 Somatotopic action selection across phyla. ..... 14

Figure 1.2 Segmental divergence of homologous neurons underpins somatotopic tactile responses in the *Drosophila melanogaster* larva. ..... 23

Figure 1.3 Atlas of Wave neurons. ..... 24

Figure 2.1 Genetic neuronal targeting. ..... 28

Figure 2.2 Schematic function of GCaMP as a neuronal activity visualizer. ..... 31

Figure 2.3 Schematic function of ChR2 and CsChrimson as a neuronal excitators. ..... 32

Figure 2.4 Scheme of FlpOut-based mosaic analyses ..... 35

Figure 3.1 Characterization of body location-dependent somatosensory touch responses (see also Figure 3.2). ..... 57

Figure 3.2, related to Figure 3.1 ..... 59

Figure 3.3 Identification and characterization of Wave neurons, candidate command neurons for backward locomotion (see also Figure 3.4). ..... 63

Figure 3.4, related to Figure 3.3 ..... 65

Figure 3.5 Confined optogenetic activation of Wave neurons elicits fictive backward locomotion (see also Figures 3.6 and 3.7). ..... 68

Figure 3.6, related to Figure 3.5 ..... 70

Figure 3.7, related to Figure 3.5 ..... 72

Figure 3.8 Segmental difference in the function and morphology of Wave neurons (see also Figure 3.9). ..... 76

Figure 3.9, related to Figure 3.8 ..... 78

Figure 3.10 Single-cell activation of Wave neurons *in vivo*. ..... 80

Figure 3.11 Nociceptive sensory neurons activate Wave neurons in a segment-specific manner. ..... 83

Figure 3.12 Neuronal circuitry involving Wave neurons. ..... 86

Figure 3.13, related to Figure 3.12 ..... 88

Figure 3.14, related to Figure 3.12 ..... 90

Figure 3.15 Sensorimotor pathways recruited in anterior touch-triggered backward response. . 93

Figure 3.16, related to Figure 3.15 ..... 95

Figure 3.17, Overall summary of the sensorimotor pathway that realizes backward motor outputs in response to head touch perception ..... 97

# Table of Contents

*Abstract* 3

*List of Abbreviations* 5

*List of Figures and Tables* 7

*Chapter 1. General introduction* 12

**Background** 12

**Somatotopic tactile response: simple reflex** 16

**Somatotopic tactile response: rhythmic motor activity** 17

**Development of adaptive wiring** 19

**Research questions and outlines of the present dissertation** 20

*Chapter 2. General methodology* 26

**Genetic neuronal targeting** 26

**Analyses of neural circuits** 29

**Loss-of-function genetic screen: RNAi** 33

**Mosaic analyses** 33

*Chapter 3. Divergent connectivity of homologous command-like neurons mediates segment-specific touch responses in Drosophila* *36*

**Introduction** **36**

**Materials and Methods** **40**

Experimental Model and Subject Details 40

Method details 42

**Results** **55**

Different Larval Responses are Induced by Noxious Touch Depending on the Body Location of the Stimulation 55

Identification of Wave as a Candidate Command Neuron for Backward Locomotion 61

Confined Optogenetic Activation of a Single Wave Neuron Elicits Fictive Backward Locomotion 66

Wave Neurons are Activated by Nociceptive Sensory Stimuli on the Head 81

Circuit Mapping Showed that Wave Neurons Relay Nociceptive Sensation to Motor Outputs 84

Wave and its Downstream Motor Circuits are Required for the Execution of Touch-Triggered Backward Response 91

**Discussion** **96**

Command-like Neurons Elicit Larval Escape Behaviorss 97

Lateral Interaction between Distinct Command Systems 99

Segmental Interneurons are Diverged to Drive Adaptive Behaviors 100

*Chapter 4. Formation of neuronal connectivity that regulates divergent action selection 104*

*Chapter 5. Conclusions* _____ *105*

**Action selection circuitry** _____ **105**

**Diversification of homologous ganglia** _____ **107**

*Notes on the dissertation* _____ *108*

*Acknowledgements* _____ *110*

*References* _____ *112*

# Chapter 1. General introduction

This chapter is modified and reproduced from the following publication:

Takagi, S. & Nose, A. (2018) Circuit architecture for somatotopic action selection in invertebrates. *Neurosci. Res.*, 10.1016/j.neures.2018.08.008

**Background**

Animals have prospered through their ability to process ever-changing sensory inputs from the environment and to dynamically produce adaptive motor outputs. As Nikolaas Tinbergen proposed in the 1950s, the causal structure underlying animal behaviors can be described as a function of the nervous system, in concert with the sensory organs and muscles (Tinbergen, 1951). Although the internal structure of the nervous system was largely a "black box" at that time, the field of ethology has progressed dramatically since then, in harmony with neuroscience, to describe the mechanistic aspects of behavior as a response to external stimuli. For instance, animals can discriminate sensory inputs of different modalities (such as light, heat, and mechanical inputs) by perceiving them at the dedicated sensory neurons, which in turn activate a specific downstream central circuitry to interpret the valence of the input, and subsequently select an appropriate motor program to adaptively respond to the input. However, due to the size and nature of animal bodies, animals must discriminate not only the modality of the sensory inputs but also the geometric position of the sensory input on the body. Wilder Penfield introduced the concept of "somatotopy," which refers to the presence of one-to-one

correspondence between the sensory receptive field on the body and the brain region (Penfield and Boldery, 1937). This correspondence is known as the cortical homunculus. The presence of somatotopic processing is not limited to the mammalian cortex though, but is also seen across a broad range of phyla, such as Annelida, Nematoda, and Arthropoda (Figure 1.1A; Bezares-Calderón et al., 2018; Chalfie et al., 1985; Edwards et al., 1999; Islam and Zelenin, 2008; Kristan, 1982). Invertebrate species have served as excellent models for studying the brain function because of the reliable accessibility to individual neurons using physiological and/or genetic toolkits. This feature enables the pursuit of understanding of the brain function across multiple levels of analyses, such as computational, representational, and implementational levels, which David Marr proposed as the key requirements when trying to understand the information processing mechanism (Marr, 2010). In this chapter, I would first like to introduce the neuronal wiring schemes that enable somatotopic action selection, and the general relationship between neuronal morphology, circuit structure, and animal behavior. I then pose the questions that will be addressed in the present dissertation.

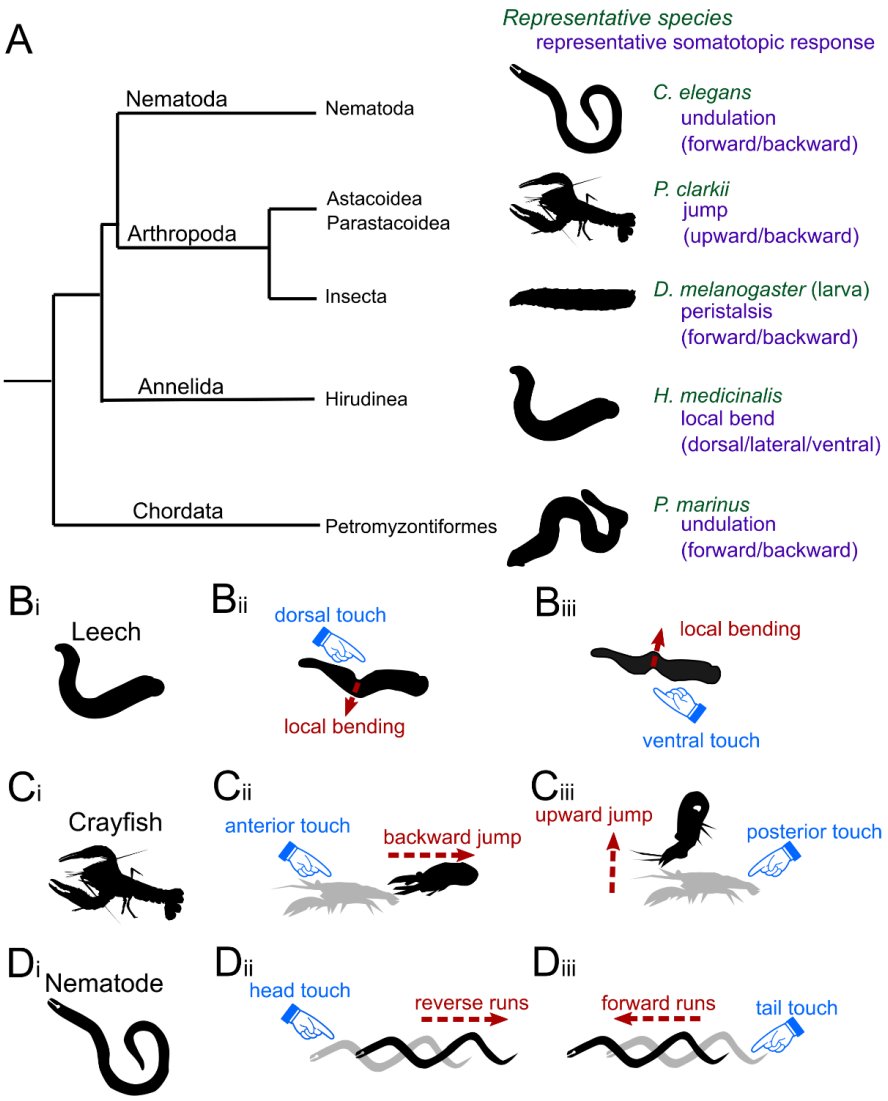


**Figure 1.1 Somatotopic action selection across phyla.**

**(A)** Example animal species and their somatotopic tactile responses. **($B_{i-iii}$)** Somatotopic tactile responses in the leech *H. medicinalis* **($B_i$)**. A touch on a certain angular location on the body induces local bending in the stimulated direction **($B_{ii}$, $B_{iii}$)**. **($C_{i-iii}$)** Somatotopic tactile responses in crayfish *P. clarkii* **($C_i$)**. A touch on the head induces a backward jump **($C_{ii}$)**, whereas a touch on the tail induces an upward jump **($C_{iii}$)**. **($D_{i-iii}$)** Somatotopic tactile responses in the nematode *C. elegans* **($D_i$)**. A gentle touch on the head induces

reverse runs **($D_{ii}$)**, whereas a touch on the tail induces forward runs **($D_{iii}$)**. Figures reproduced from Figure 1 in Takagi and Nose, 2018.

**Somatotopic tactile response: simple reflex**

Simple reflex, which consists of transient contraction of a subset of skeletal muscles, often suffices to allow the animal to evade a tactile stimulus, which leads to the question: what is the circuit architecture that links localized tactile inputs to transient muscle contraction?

In the medicinal leech (*Hirudo medicinalis*), which comprises a tubular body, evasion from a tactile input from a certain angle is achieved by a local bending of the body wall at the same angle and simultaneous extension of that at the opposite angle (Figure 1.1$B_{i\text{-}iii}$). Among the two mechanosensory neurons (T and P cells, respectively) in the leech body, the P cells play more prominent roles in producing local bending (Kristan, 1982). The four P cells are distributed in an angularly even manner, and activation of each leads to a unique motor pattern contributing to local bending (Lockery and Kristan, 1990a). The local bending is accomplished by unique activity patterns of four classes of motoneurons (DE, DI, VE, and VI) that innervate the longitudinal muscles. Therefore, the network wiring pattern from the mechanosensory P cells to each type of motoneuron is crucial for computing the bending angle of the leech body. Such sensorimotor pathways are regulated by several classes of interneurons, each of which induces unique motoneuron activity patterns contributing to local bending (Lockery and Kristan, 1990b). Each interneuron receives similar, but not identical, weights of synaptic inputs from the P cells (Lockery and Kristan, 1990b), and the interneuron function is distributed rather than dedicated to bending reflexes of different angles (Lockery and Sejnowski, 1992). Such redundancy in part enables the computation of the bending angle as a population vector of the P cell activity pattern (Lewis and Kristan, 1998). Thus, precise connectivity and synaptic weighting, which is likely to be underpinned by the unique morphology of each of the classes of

local bending interneurons (Lockery and Kristan, 1990b), is critically important for the local bending network.

Another famous example of touch reflex is the jumping behavior of crayfish. Crayfish jump upward in response to tail touch, whereas they jump backward in response to head touch (Figure 1.1$C_{i\text{-}iii}$; Edwards et al., 1999). Studies on the jumping reflex have established the "command neuron concept," which is the notion that a dedicated class of interneurons, whose activation is necessary and sufficient to induce a specific behavior and is simultaneous to the behavioral epochs, regulates each patterned motor output (Kupfermann and Weiss, 1978; Wiersma and Ikeda, 1964). The first command neurons identified include two classes of giant fibers (GFs): the medial giant axons (MGs) and the lateral giant axons (LGs). Although both MGs and LGs provide excitatory inputs onto segmental motoneruons (the giant motoneruons, or MoGs), activation of these GFs produces distinct motor outputs. Namely, MGs induce a backward jump and LGs induce an upward jump. These divergent motor outputs are underpinned by segment-specific wiring patterns. MGs provide synaptic inputs onto MoGs in all abdominal segments, thereby inducing transient muscle contraction of all body segments, which yields a backward jump. LGs, on the other hand, provide synaptic inputs onto MoGs only in anterior abdominal segments, thereby inducing a local bend in the anterior abdominal segments that curves the middle of the body, which results in an upward jump (Mittenthal and Wine, 1973).

**Somatotopic tactile response: rhythmic motor activity**

I have up to now discussed the input location-specific reflexes and their circuit architectures. Many animal species, however, developed a more complex form of motor outputs that requires

the coordination of muscles across the whole body, which is denoted the patterned motor outputs. Patterned motor outputs are thought to be regulated by a rhythm generating circuit in the central nervous system (CNS), which is called the central pattern generator (CPG). The concept of a CPG emerged from an experiment showing that the isolated nerve cord of the grasshopper can produce patterned motor activity reflecting flight behavior (Wilson, 1961), and it is now appreciated as a common mechanism across the animal kingdom (Marder and Bucher, 2001). Thus, if a complex motor output is to be commanded, such a decision should be made by an action selection circuitry, which resides upstream of the dedicated CPG for the behavior. In the case of somatotopic responses, the action selection circuitry would include divergent neural pathways that connect sensory inputs at distinct locations to respective CPGs.

One of the best-studied examples of such a location-specific wiring scheme is the touch response in the *C. elegans* nematode. *C. elegans* performs forward and reverse runs, which are performed by dedicated populations of segmental motoneurons (B- and A-type motoneurons, respectively (Chalfie et al., 1985)). A light touch on the head of *C. elegans* induces reverse runs, whereas a touch on the tail induces forward runs (Figure 1D$_{i\text{-}iii}$; Chalfie et al., 1985). A light touch is primarily sensed by ALM and PLM sensory neurons, which sense touch in the head and the tail, respectively. ALM in turn activates AVA, a command neuron for reverse runs, whereas PLM is thought to activate AVB, a command neuron for forward runs (Pirri et al., 2009). Both AVB and AVA are directly upstream of dedicated motoneurons (the B- and A-type motoneurons, respectively). The runs (whether in forward or reverse direction) are accomplished by rhythmic and sequential activity of motoneurons that propagates along the body axis, implying the existence of CPGs. Where does the CPG circuitry for locomotion reside in the *C. elegans* nervous system? Interestingly, a recent study has shown that the CPGs for

reverse runs are the dedicated motoneurons themselves; the A-type motoneurons exhibit intrinsic and oscillatory activity so that they can generate rhythmic reverse runs even in the absence of premotor neurons such as AVA (Gao et al., 2018). Hence, activation of motoneurons is sufficient to trigger runs with the direction matched to the location of the touch on the body.

How is the somatotopic tactile response regulated in animals with segmented central nervous systems, such as insects and vertebrates? The spinal cord in vertebrates and the nerve cord in insects both have segmentally repeated units of somatosensation and motor regulation. Each segment of the nerve cord (neuromere) receives somatosensory inputs from, and regulates, muscle contraction of the corresponding body segment. Each neuromere is highly homologous to the others in terms of the composite primary afferents, local and projection interneurons, and motor efferents. Hence, in order to realize segment-specific tactile responses, each of the homologous neuromeres must possess unique neural architectures that match its receptive field to distinct motor programs, which implicates the presence of divergent wiring of the same class of neurons across segments. Such architecture and its function, though, remains elusive.

**Development of adaptive wiring**

As reviewed so far, adaptive wiring of neuronal elements (somatotopically organized sensorimotor connectivity) underlies the somatotopic action selection. The question of how this wiring emerges is another topic that needs to be discussed. The development of neuronal connectivity has been a central question in neuroscience, from axon guidance to target selection. Up to now, various families of proteins have been attributed to axon guidance in many animal species. Recent studies also begin to reveal how neuronal wiring mediated by axon guidance molecules shapes adaptive animal behaviors. For instance, a study in the nematode *C. elegans*

showed that Wnt-mediated neuronal wiring realizes somatotopic action selection. The ALM neuron resides in the middle of the antero-posterior axis and extends its neurite towards the anterior end of the body. Since ALM is known to be critical for sensing gentle touch (Pirri et al., 2009), the anterior projection of the ALM is thought to be crucial for the mechanosensation on the head. Mutations in Wnt family orthologues, *cwn-1* and *egl-20*, cause defects in the anterior projection of the ALM neurite, implying that Wnt signaling regulates the maturation of the neurite polarity (Hilliard and Bargmann, 2006). Notably, the mutations not only cause neurite polarity defects in ALM but also behavioral defects in the anterior touch response (Hilliard and Bargmann, 2006). Thus, Wnt likely realizes adaptive somatotopic action selection by regulating neurite polarity crucial for the behavior.

However, such gene knock-out strategies not only affect the neuron of interest but also all the other cells that normally express the gene, thus failing to show the causal link between gene function, neuronal circuits, and behaviors. Due to the technical limitations in gene disruption, whether a perturbation of neurite guidance in a specific neuron of interest alters the function of the neuronal circuits or not has been difficult to prove. Hence, how a somatototpic action selection circuitry is formed still remains an open question.

**Research questions and outlines of the present dissertation**

The questions asked in the present dissertation are as follows:

(1) What is the neuronal circuit structure/function that processes location-specific sensory inputs and subsequently triggers the appropriate sequence of motor outputs? (Chapter 3)

(2) What is the developmental mechanism that forms the location-specific sensorimotor circuitry? (Chapter 4)

To address these questions, I studied the function and formation of tactile-induced action selection circuitry using *Drosophila melanogaster* larvae (Figure 1.2A$_i$). Similarly to *C. elegans*, *D. melanogaster* larvae perform a backward crawl in response to head touch and forward crawl in response to tail touch (Figure 1.2B; Kernan et al., 1994; Robertson et al., 2013; Titlow et al., 2014). *D. melanogaster* has enriched genetic tools to drive gene expression in cells in spatiotemporally targeted manners, thus allowing investigation of the function of each neuron in behavior and development.

The *Drosophila* larva is a segmented animal with its body largely divided into thorax, abdomen, and a specialized structure in the anterior and posterior end (Figure 1.2A$_i$). The thorax consists of three segments (T1, T2, T3), and the abdomen seven segments (A1, A2, ... A7). The *Drosophila* nervous system can be divided into the central (CNS) and the peripheral (PNS) nervous systems. The CNS in *Drosophila* can further be subdivided into the brain and ventral nerve cord (VNC), a chain of ganglia homologous to the spinal cord in mammals (Figure 1.2A$_i$). Each body segment is connected to the correspondent segmentation of the VNC, known as the neuropile.

Tactile inputs are first detected by the somatosensory neurons in the PNS, which transmit signals into the correspondent neuromere in the VNC. The sensory input is processed by the interneuronal circuit in the CNS, and ultimately produces coordinated motor activities. Larval crawling, or peristalsis, is accomplished by the sequential activity of the MNs in each neuromere (Figure 1.2A$_{ii}$). Here, forward crawling is accomplished by motor recruitment from posterior-to-anterior neuromeres, whereas backward crawling is accomplished by the direction the other way around (Figure 1.2B).

In Chapter 3, I identify a segment-specific wiring scheme present in the larvae of the fruit fly *D. melanogaster*. Key players of the wiring scheme are the segmentally repeated interneurons, which I named Wave neurons, present in the abdominal neuromeres of the VNC. Wave neurons mediate the location-specific touch response by acting as command-like neurons: activation of Wave neurons in anterior segments elicits the backward crawl, whereas activation in posterior segments elicits the forward crawl. Wave neurons in different neuromeres not only elicit distinct behaviors but also exhibit distinct axonal and dendritic morphology. Namely, anterior Wave neurons project their axon and dendrite anteriorly, whereas the posterior Wave neurons project their axon and dendrite primarily towards the posterior. The diverged connectivity suggests the presence of segment-specific axon/dendrite guidance mechanisms. Electron microscopy (EM)-based mapping of the circuits around anterior Wave neurons showed that Wave neurons are direct synaptic targets of the touch receptor afferents (MD III/IV). Importantly, since anterior Wave neurons extend dendrites anteriorly, they receive synaptic inputs from the touch receptors in the head. EM-based mapping also identified, in the downstream circuitry of an anterior Wave neuron, a class of premotor neurons named A03a5, whose activity, together with Wave, is necessary for the larvae to perform a backward crawl in response to head touch. Thus, Wave neurons match their tactile receptive fields with appropriate motor programs by diverging their axon/dendrite extension patterns. Such segment-specific wiring architecture could be a general strategy for somatotopic responses across animal species with segmented central nervous systems.

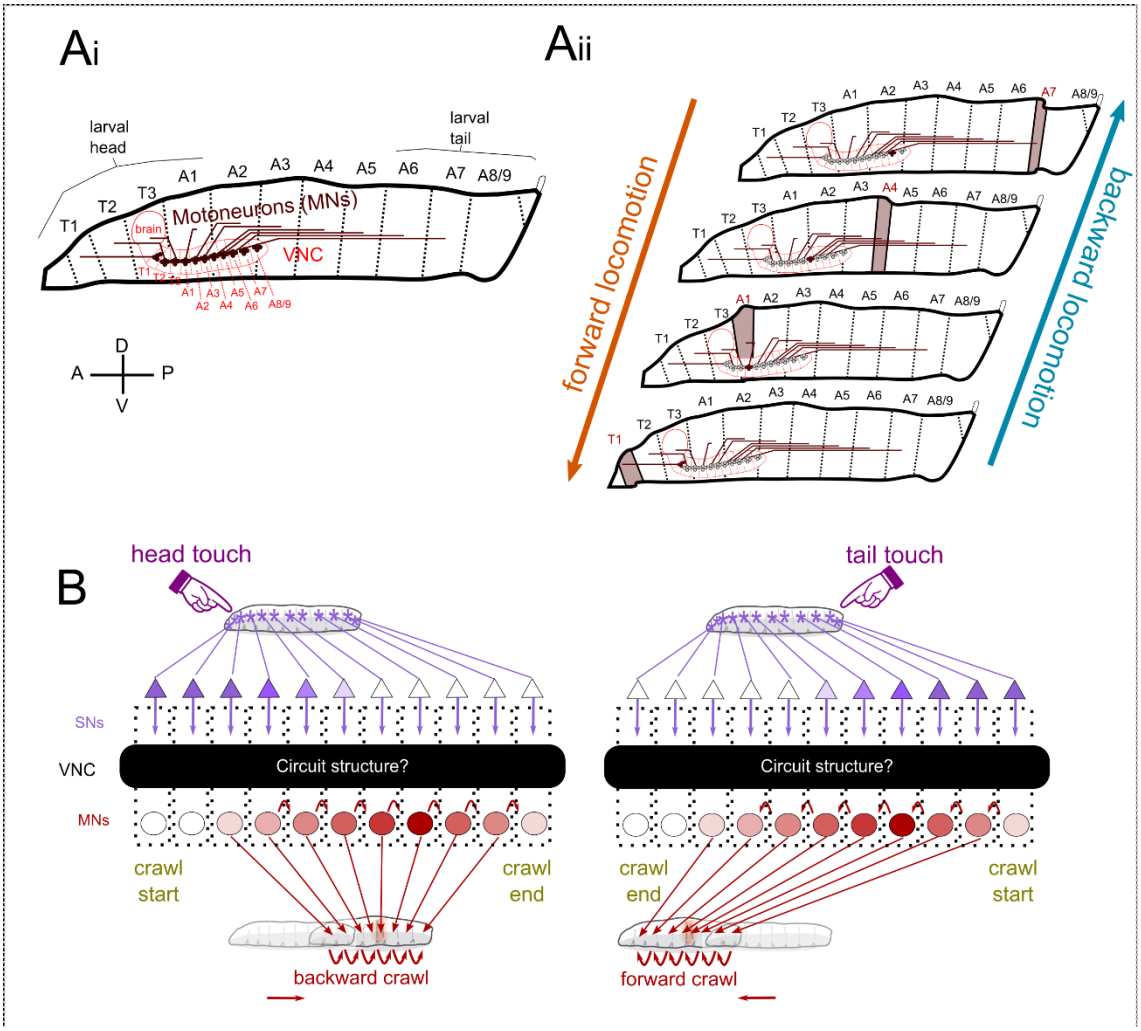


**Figure 1.2 Segmental divergence of homologous neurons underpins somatotopic tactile responses in the *Drosophila melanogaster* larva.**

**($A_i$)** Schematic lateral view of the *D. melanogaster* larval body, with the atlas of the central nervous system (the brain and the ventral nerve cord (VNC)) and the body wall. Both the body wall and the VNC are segmented (boundaries shown as dotted lines) and are connected to each other via nerve roots. **($A_{ii}$)** Scheme of forward and backward locomotion. Forward locomotion is accomplished by sequential contraction of segmental muscles (shown as light brown) from posterior to anterior segments, which is regulated

by sequential activity of motoneurons (MNs) in the VNC (shown as dark brown). Backward locomotion is largely a time reversal of the forward locomotion. **(B)** Schematic diagram of sensorimotor pathways that mediate segment-specific tactile responses to head and tail touch**.** The internal structure in the VNC has remained elusive. SNs: sensory neurons, MNs: motor neurons. Figure (**B**) modified and reproduced from Figure 2 in Takagi and Nose, 2018.

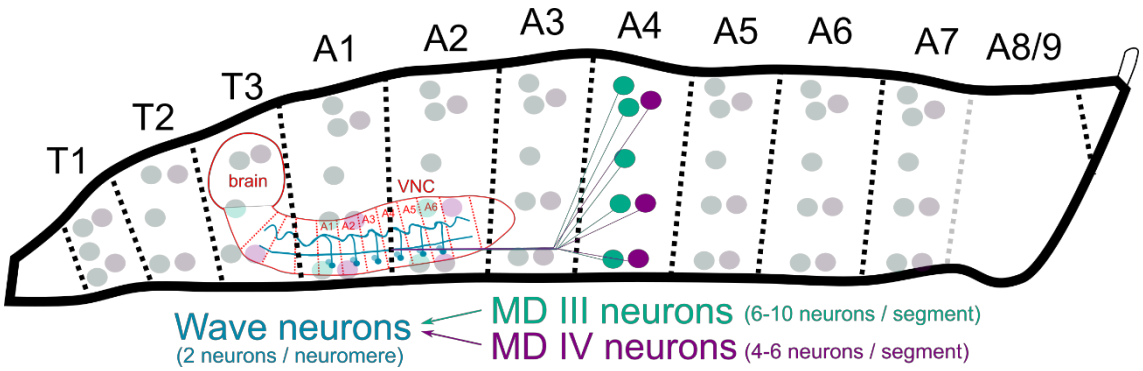


**Figure 1.3 Atlas of Wave neurons.**

Schematic lateral view of the *D. melanogaster* larval body, with the atlas of Wave neurons and their upstream sensory neurons (MD III/IV).

In Chapter 4, I examine the developmental mechanisms of the Wave neurite formation. I first identify a GAL4 driver line that targets Wave neurons throughout embryonic to larval stages. Stage-by-stage observation using the identified driver suggests that Wave neurons correspond to embryonic vMP2 neurons, which were known to pioneer the longitudinal connectives in the VNC at an early embryonic stage. RNAi-based knock-down of candidate neurite guidance

receptors using the identified driver reveals an essential role of DFz4, a member of the Frizzled protein family that function as Wnt receptors, in guiding the posterior axon of Wave neurons specifically in a posterior neuromere. I also show the requirement of DWnt4, a ligand for DFz4, as a potential extrinsic guidance cue for the posterior Wave neurons. Knock-down of DFz4 specifically in Wave neurons decreased the ability of Wave neurons to induce fictive forward, but not backward, locomotion. Thus, a segment-specific neurite guidance mechanism plays an essential role in gaining motor commandability, presumably through local neuronal circuit formation.

Taken together, the present study shows that a class of segmentally-repeated neurons diverge their neurite extension pattern to form a functional circuitry that triggers distinct behaviors in response to sensory inputs on different body-locations. As these neurons and the molecular mechanisms are likely to be conserved across species, the present study may pave a way towards understanding the general principle of somatotopic action selection.

# Chapter 2. General methodology

Here, I introduce the genetic targeting methods and neural-circuit analyses that are used in the current dissertation.

**Genetic neuronal targeting**

Although all cells are implemented with a full set of genomes, not all the genes are expressed in a single cell. The expression pattern of a specific gene in a specific cell is regulated by specific sequences in the genome called enhancers. Hence, genetic manipulation of a specific gene (*gene A*) under regulation of the enhancer of another gene (*gene B*) enables one to drive expression of the *gene A* in *gene B*-expressing cells. This is called the ectopic expression. The targeted gene expression has become even more sophisticated since the invention of the GAL4/UAS system (Brand and Perrimon, 1993) in *Drosophila*. In this method, the GAL4 gene is expressed under regulation of endogenous enhancers, resulting in GAL4 protein expression in specific cells. The GAL4 protein is a class of transcription factor that drives expression of the target gene under regulation of the upstream activating sequence (UAS). By generating transgenic GAL4 lines with various enhancers, and UAS lines with various genes of interest, one can test their multiple combinations only by crossing the GAL4 lines and the UAS lines (Figure 2.1A, B). Thousands of GAL4 lines are now available in stock centers, making large-scale screens in genetics and cell biology possible. Using the GAL4/UAS system, one can test the function of neurons using

artificially engineered molecular tools enabling calcium imaging, optogenetics and thermogenetics (as will be described).

A similar system to the GAL4/UAS system, called the lexA binary system was recently invented (Lai and Lee, 2006). In this system, the DNA binding domain (DBD) of lexA was fused with the activation domain (AD) derived from other transcription factors (such as GAL4). The lexA binds with the lexA operator (lexAop) sequence, thus driving gene expression downstream of lexAop. This lexA binary system can function independently of the GAL4/UAS system, and thus can be applied in the same animal (Figure 2.1C).

Repressing GAL4 activity in specific cells can sometimes be helpful to confine ectopic gene expression in a smaller subset of cells. The GAL80 protein is used for such analyses (called the two-hybrid system), and several GAL80 transgenic lines are available for this purpose (Figure 2.1D).

Intersection between two independent enhancers allows confined gene expression. The split-GAL4 system realizes such approach by independently expressing the AD and DBD of the GAL4 protein (Figure 2.1E, Luan et al., 2006).

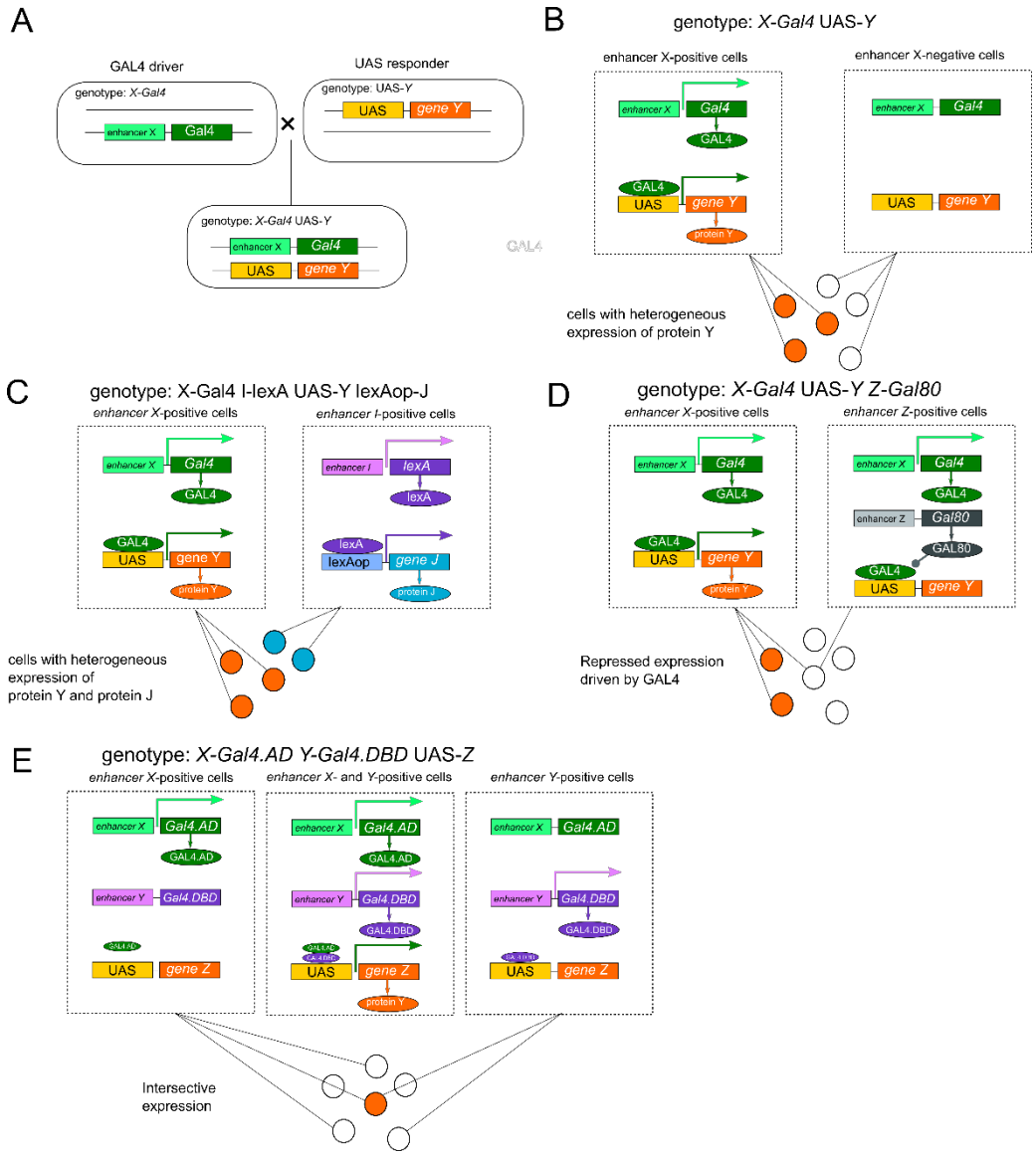


**Figure 2.1 Genetic neuronal targeting.**

**(A)** Genetic cross in GAL4/UAS system. **(B)** GAL4 drives expression of reporter gene downstream the UAS. **(C)** lexA binary system can be used independently of the GAL4/UAS system. **(D)** GAL80 two-hybrid system can be used to confine the gene expression driven by GAL4/UAS system. **(E)** Split-GAL4 system enables intersective expression of reporter gene downstream the UAS.

## Analyses of neural circuits

Studying neural circuits focuses on the connectivity of each neuron, and aims to understand the flow and calculation of information. Here, methods used in this study for dissecting these distinct contexts of neural connectivity are described.

### *Connectomics*

Structural connectivity among neurons refers to information on how neurons are synaptically coupled to each other. The whole set of information of this structural connectivity in the nervous system is called the connectome, and the research area of building a connectome is called connectomics. The structure of a synapse is on approximately the $10^{-8}$ meter scale, which can only be imaged using electron microscopy. The connectome in nematodes met completion using the electron microscopy, where all 302 neurons are identified as well as their synaptic connectivity (White et al., 1986).

Until recently, knowing the connectivity of central neurons in *Drosophila* has not been easy. One of the techniques to visualize synaptic coupling among neurons is the GFP Reconstitution Across Synaptic Partners (GRASP) (Feinberg et al., 2008), which was originally developed in *C. elegans*. In *Drosophila*, this method takes advantage of the GAL4/UAS system and the lexA binary system as follows. A fragment of GFP, which itself is not fluorescent, is expressed in one of the putative synaptic partner neurons using the GAL4/UAS system. A complementary fragment of GFP, which also is non-fluorescent, is expressed in the other putative synaptic partner neuron by using the lexA binary system. When these two cells locate close enough to make synaptic contacts, the fragments of GFP reconstitutes, and fluorescence

reemerges. Thus, one can estimate the possibility that the candidate synaptic partners in fact connect to each other. However, to apply this method, one must have candidates for the synaptic partners in the beginning, which is not always the case. Also, the GRASP signal does not assure that there actually is a synapse, since cell-cell contacts outside the synapse could generate the signal.

Another approach in knowing the connectivity of neurons in *Drosophila* is reconstructing neurons from 3D images of serial electron microscopy. Unlike nematodes, the *Drosophila* larval CNS consists of too many neurons, thus it is almost impossible for a single researcher to reconstruct all the synapses. This problem is now being overcome by a new method named Collaborative Annotation Toolkit for Massive Amounts of Image Data (CATMAID) (Saalfeld et al., 2009). This method enables researchers to do such reconstruction of neurons and annotation of synapse in a world-wide, collaborative manner and reveal the whole connectivity of the neuron of interest to other neurons (Schneider-Mizell et al., 2016)

.

*Calcium imaging*

Recording the activity of neurons has classically been accomplished by electrophysiological methods. However, applying such methods to multiple neurons is difficult, particularly as the number of neurons increases. Optical imaging of the neuronal activities has recently been developed, and has become popular since the invention of GCaMP (Nakai et al., 2001). GCaMP is engineered as intervening CaM and M13 to circularly-permutated GFP (cpGFP; non-fluorescent), and shows $Ca^{2+}$ dependent fluorescence due to the structural changes in CaM

and M13 (Figure 2.2). Since GCaMP can be genetically encoded, it can be expressed in neurons of interest using the GAL4/UAS system mentioned.

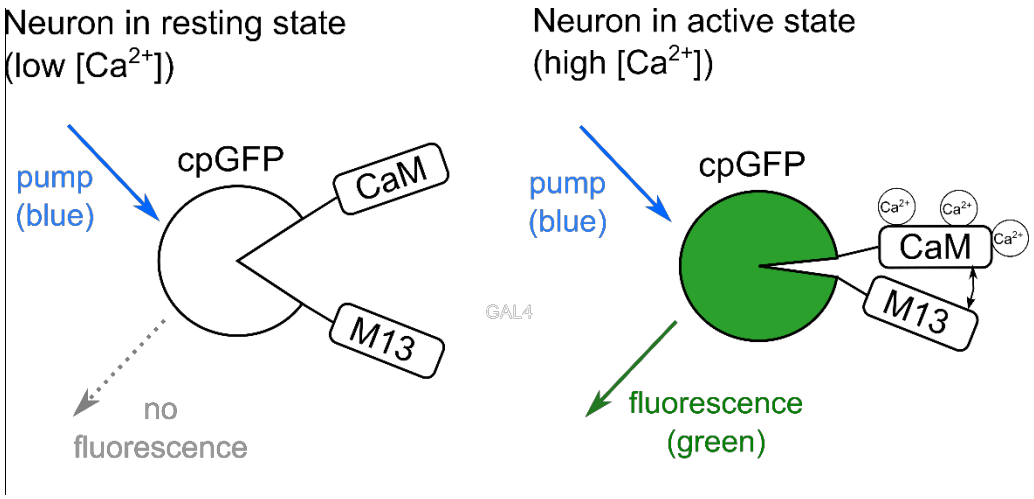


**Figure 2.2 Schematic function of GCaMP as a neuronal activity visualizer.**

cpGFP: circularly permuted GFP, CaM: Calmodulin, M13: a CaM-binding peptide

*Optogenetics and thermogenetics*

Although neuronal recording raises the possibility of neurons' direct connection, it is still unclear whether there is causal relationship between them. This causal relationship can be only tested by manipulation of neuronal activities.

Recently, methods for optical activation of neurons have been developed (Lima and Miesenböck, 2005; Zemelman et al., 2002). Chanelrhodopsin-2 (ChR2) is a class of light-gated cation channel, and can be expressed in the membrane of neurons, depolarizing the neurons when activated by blue light (Nagel et al., 2003). Thus, driving the expression of ChR2 to specific cells enables one to control the timing of neuronal activation using light. A red-shifted variant of ChR2 was also invented recently (Figure 2.3).

An alternative method for manipulating the activity of neurons, applicable to poikilotherm, uses temperature shift. Shibire is a class of dynamin that is required in endocytosis of neurotransmitters. Thermosensitive mutants of Shibire (Shibire$^{ts}$) dysfunctions in restrictive temperature, above 29 degrees Celsius. The dysfunction of Shibire is known to impair the whole endocytosis of the expressing neurons, probably because dynamins functions as a multimer. Thus, ectopic expression of Shibire$^{ts}$ impairs the neuron with neurotransmitter recycling, and blocks synaptic transmission (Kitamoto, 2001, 2002).

Similarly, but without temperature shifts, targeted expression of tetanus toxin light chain (TeTxLC) impairs exocytosis and therefore results in blockage of synaptic transmission (Sweeney et al., 1995).

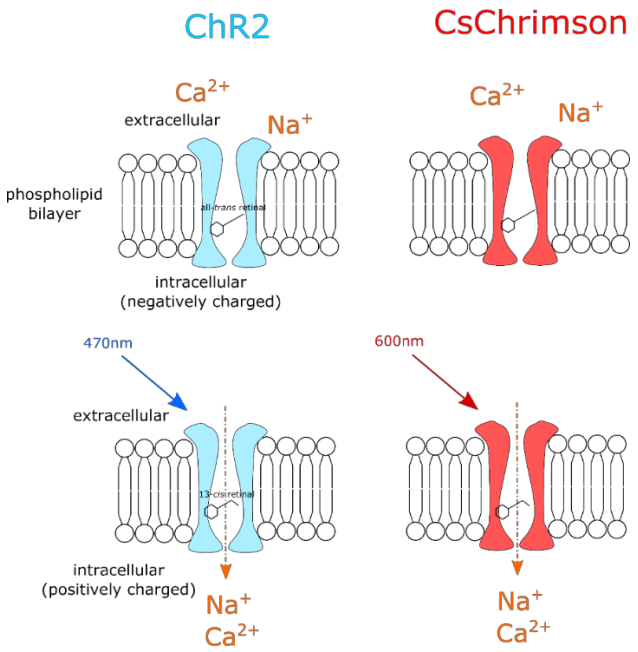


**Figure 2.3 Schematic function of ChR2 and CsChrimson as a neuronal excitators.**
Light illumination triggers *trans*- to *cis*- conversion of retinal, followed by conformational change of ChR2. As ChR2 is a non-selective cation channel, opening of the channel pore results in net inward current.

**Loss-of-function genetic screen: RNAi**

A gene is a sequence of DNA that codes a specific protein. Gene expression refers to a process in which a gene is first transcribed into an mRNA and then translated into a protein. Loss-of-function studies provide an insight on the necessity of a gene of interest and can be accomplished by disrupting either the DNA sequence (knock-out) or the transcribed mRNA (knock-down). In this study, I used the RNA interference (RNAi) method to perform knock-down experiments. RNAi is a phenomenon in which an mRNA with a specific sequence is degraded by a double-stranded RNA (dsRNA) with the complementary sequence (Fire et al., 1998). By encoding dsRNA for each gene sequence under the control of UAS, one can knock-down a specific gene in a GAL4-dependent manner. In this study, comprehensive UAS-RNAi resources generated by the *Drosophila* Transgenic RNAi Project (TRiP) at Harvard Medical School were used (Perkins et al., 2015).

**Mosaic analyses**

Restricting gene expression/disruption in a single-cell resolution is essential to probe the function of a specific cell of interest. For this purpose, generating an individual animal composed of cells with heterogeneous genotype is a powerful approach. Such approach is known as the mosaic analysis (Hotta and Benzer, 1970, 1972).

In this study, I took advantage of site-directed DNA recombination to generate mosaic animals. Recombination is accomplished by Flippase (FLP), which recognizes a specific DNA sequence (FRT). It is known that a DNA sequence sandwiched by FRT sites will be excised from the genome when the FLP is present (Golic and Lindquist, 1989), which is referred to as

FlpOut. Hence, a FlpOut-oriented reporter line for *gene A* (UAS-FRT-STOP-FRT-*A*) allows generation of genetic mosaics for protein A expression. The following two reporters were used in the current study.

*MultiColor FlpOut (MCFO)*

MultiColor FlpOut (MCFO) is a FlpOut-oriented reporter line for multiple epitope tags (such as V5, HA, and FLAG), which are inserted into a backbone of membrane-bound nonfluorescent superfolder GFP (Figure 2.4A; (Nern et al., 2015)). Among several variants of MCFO, MCFO-4 and -6 take advantage of FLP introduced by a neuronal Synaptobrevin (nSyb) promoter, which results in stochastic FlpOut only in neurons. As a whole, MCFO allows labeling of GAL4-targeted neurons in a single-cell resolution.

*FlpOut optogenetics*

A FlpOut-oriented reporter line for CsChrimson is used to understand the function of a neuron in a single-cell resolution (Figure 2.4B). The FLP is induced under the regulation of a heat shock promoter. Thus, heat shock (above 37 degrees Celsius) would induce FlpOut in a stochastic manner, resulting in sparse expression of CsChrimson.

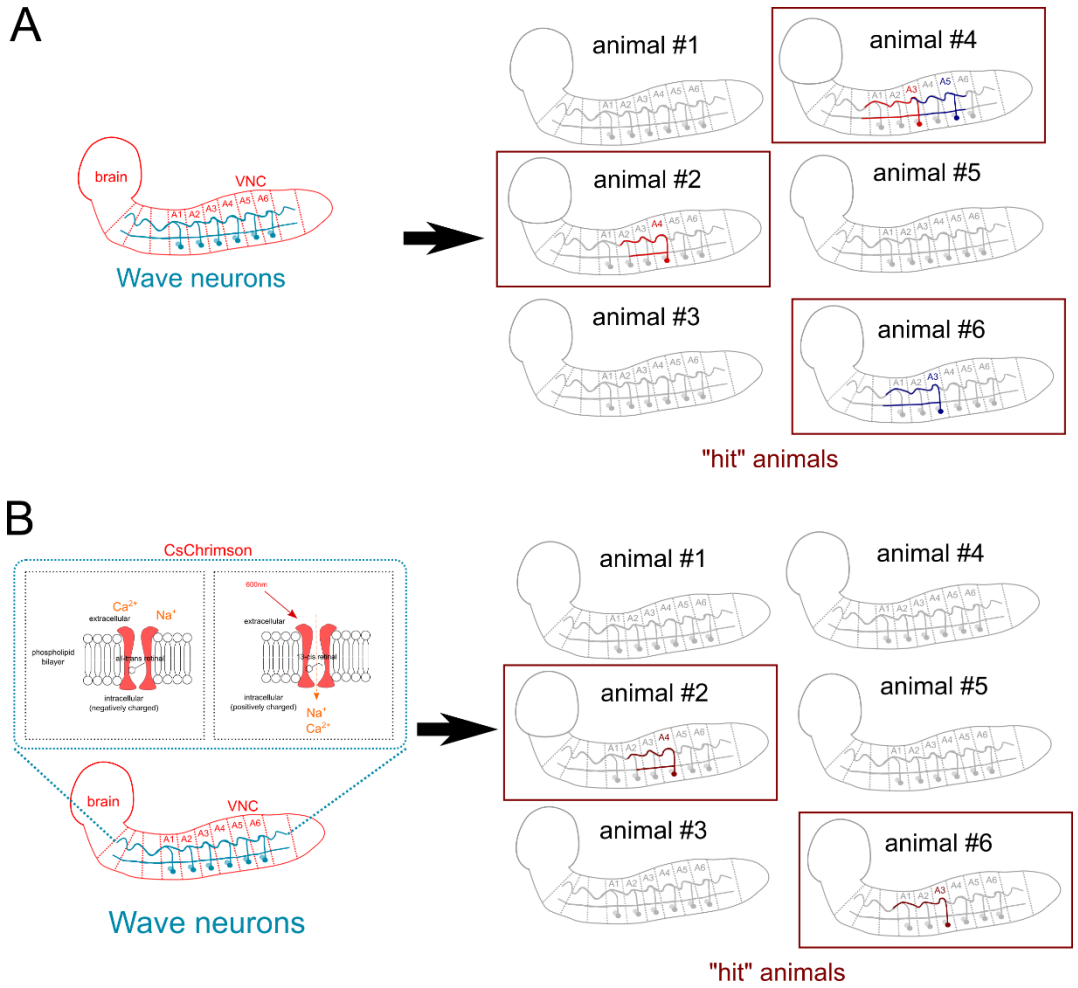


**Figure 2.4 Scheme of FlpOut-based mosaic analyses**

(**A**) Outline of MCFO. Epitope tags (such as V5 and HA) are stochastically expressed under GAL4 regulation. By avoiding neurite overlaps, MCFO allows to analyze the morphology of individual neurons (such as Wave neurons in each neuromere). (**B**) Outline of FlpOut optogenetics. CsChrimson is stochastically expressed under GAL4 regulation, allowing the functional characterization of individual neurons (such as Wave neurons in each neuromere).

# Chapter 3. Divergent connectivity of homologous command-like neurons mediates segment-specific touch responses in *Drosophila*

This chapter is modified and reproduced from the following publication:

Takagi, S., Cocanougher, B.T., Niki, S., Miyamoto, D., Kohsaka, H., Kazama, H., Fetter, R.D., Truman, J.W., Zlatic, M., Cardona, A., & Nose, A (2017). Divergent Connectivity of Homologous Command-like Neurons Mediates Segment-Specific Touch Responses in *Drosophila*. *Neuron* 96, 1373–1387.e6

## Introduction

Appropriate response to tactile sensory stimuli is crucial for animal survival. Upon sensing a tactile stimulus, animals respond by choosing the most ethologically adequate behavior depending on the body location of the stimulus (Di Giminiani et al., 2013; Kristan et al., 2005). For instance, crayfish perform upward jumps in response to a posterior touch and backward jumps in response to an anterior touch (Edwards et al., 1999). Similarly, leeches shorten in response to an anterior touch, bend to a midbody touch, and crawl/swim to a posterior touch (Kristan et al., 2005; Palmer et al., 2014). Somatosensory inputs, such as mechanical and/or noxious cues, are sensed by receptors in the periphery and the information is passed along to the

CNS. The spinal cord in vertebrates and nerve cord in invertebrates consist of homologous repeating units, neuromeres, each of which communicates with a corresponding skin area via the peripheral nerves. A somatosensory input from a specific location in the periphery is transmitted to the correspondent neuromere and the information is then processed to generate motor programs appropriate for the origin of the stimulus (Abraira and Ginty, 2013; Duan et al., 2014; Hwang et al., 2007; Ohyama et al., 2013, 2015; Tsubouchi et al., 2012; Yan et al., 2013; Zhang et al., 2013). Hence, each of the homologous neuromeres must possess unique neural architectures that match its receptive field (the segmental origin of the stimulus) to distinct motor programs.

A common form of location-dependent behavioral responses is seen when an animal chooses the direction of movement upon encountering somatosensory stimuli. In many animal species, including nematodes (Chalfie et al., 1985), insects (Green et al., 1983; Orlovsky et al., 1999), and lampreys (Islam and Zelenin, 2008; McClellan, 1989), a stimulus in the head induces backward escape responses, whereas that in the tail induces forward movements. For instance, in *C. elegans* command interneuron AVA or AVB induces backward or forward locomotion, respectively, in response to localized touch stimuli in the tail or head (Piggott et al., 2011; Pirri et al., 2009). In adult *Drosophila*, a descending command-like neuron triggers backward walking, a behavior induced when the flies encounter impassable barriers or looming visual stimuli (Bidaye et al., 2014; Sen et al., 2017). However, network mechanisms that process location-specific sensory inputs and subsequently trigger the appropriate sequence of motor outputs remain largely unknown.

Here, I combined electron microscopy (EM) circuit mapping, opto- and electrophysiology, and behavioral analysis, to identify the circuitry basis for differential

responses to body touch in *Drosophila* larvae. On soft substrates, the wandering larvae mainly perform forward locomotion (Berni et al., 2012), whereas backward locomotion is infrequent except when encountering noxious and/or mechanical stimuli (Green et al., 1983; Kernan et al., 1994; Ma et al., 2016). A noxious touch (such as a pinprick) or a gentle touch to a freely behaving larva yields distinct responses depending on the location of the stimulation on the body (Titlow et al., 2014). The larvae transiently perform backward locomotion in response to touch on the larval head (which is defined here as the anterior end of the larva), whereas they escape by forward locomotion if touched on the tail (Figure 3.1A). Execution of forward/backward locomotion requires sequential activation of motoneurons (Fushiki et al., 2016; Hasegawa et al., 2016; Itakura et al., 2015; Kohsaka et al., 2014; Zwart et al., 2016), whereas the identity of its actuator circuitry remains largely elusive.

I first tried to identify the sensory neurons that mediate the body-location-dependent touch responses to a pinprick. Previous studies have shown that a class of multidendritic sensory neurons, MD class IV (multidendritic [MD] IV), are responsible for mechanical (Hwang et al., 2007; Kim et al., 2012; Tracey et al., 2003), thermal (Ohyama et al., 2013; Tracey et al., 2003), and light (Xiang et al., 2010) nociception, suggesting that MD IV neurons function as a polymodal nociceptor (Terada et al., 2016; Zhong et al., 2010). Also, MD III neurons are known to mediate gentle-touch responses including backward locomotion (Kernan et al., 1994; Tsubouchi et al., 2012; Yan et al., 2013). I tested the requirement of these neurons in intact animal as well as in *ex vivo* CNSs, in which the segmental motoneurons are sequentially activated(Pulver et al., 2015)

I found a segmentally repeated neuron, which I named Wave, whose activation in anterior segments sufficed to elicit backward locomotion, and in posterior segments sufficed to

elicit forward locomotion. The unique morphological characteristics of the neurons, including the bifurcated, ipsi-lateral, and anteriorly projecting neurite projection, enabled me to identify the cells as the A02o neuron, annotated by EM reconstruction as a postsynaptic target of MD IV (Ohyama et al., 2015). Although all Wave neurons are postsynaptic to both nociceptive (MD IV) and mechanoreceptive (MD III) somatosensory neurons (as was previously shown by the reconstruction in two independent EM volumes (Ohyama et al., 2015; Schneider-Mizell et al., 2016)), anterior and posterior Wave neurons differed in their receptive fields, both behaviorally and in the spatial extent of their dendritic arbors. By using CATMAID software (Saalfeld et al., 2009; Schneider-Mizell et al., 2016), I also identified circuits downstream of Wave both driving motoneurons and laterally interacting with circuits for other escape responses such as rolling (Ohyama et al., 2015). My findings indicate that homologous command-like interneurons can induce distinct escape behaviors by selectively integrating spatially localized stimuli and targeting distinct downstream circuits mediating different motor programs, thereby implementing location-dependent sensorimotor responses.

## Materials and Methods

### Experimental Model and Subject Details

*Drosophila melanogaster* strains

The following fly strains were used in this study. Both male and female wandering 3rd-instar larvae were used for all functional and histological experiments. No randomization or blinding was performed throughout.

•*yw* (Bloomington *Drosophila* Stock Center, #6598)

•*VT25803-GAL4* (VDRC Stock Center, VT ID: 202269, RRID: FlyBase FBst0485707)

•*eve[RRa-F]-GAL4* (Specifically targets aCC motoneurons (Fujioka et al., 2003), gift from Dr. Miki Fujioka)

•*ppk-GAL4* (Specifically targets MD IV (Grueber et al., 2007), gift from Dr. Yuh Nung Jan)

•*19-12-GAL4* (Specifically targets MD III when combined with *repo-GAL80* (Yan et al., 2013), gift from Dr. Yuh Nung Jan)

•*repo-GAL80* (Suppress GAL4 activity in glial cells, gift from Dr. Yuh Nung Jan)

•*clh24-GAL4* (Targets MD IV (Hughes and Thomas, 2007), gift from Dr. Cynthia L. Hughes)

•*UAS-CD4::GCaMP6f* (A membrane-fused GCaMP, H.K. and A.N., unpublished)

•*UAS-DenMark, UAS-syt::GFP/CyO* (UAS-TLNs-21; Markers for pre- and post-synaptic sites (Nicolaï et al., 2010), gift from Dr. Bassem A. Hassan)

•*UAS-shibire$^{ts}$;;UAS-shibire$^{ts}$* (A synaptic transmission blocker; Aso et al., 2010)

•*UAS-CsChrimson::mVenus* (A red-shifted Channelrhodopsin variant (Klapoetke et al., 2014), Bloomington *Drosophila* Stock Center, #55136, RRID: BDSC 55136)

•*UAS-ChR2[T159C]* (A Channelrhodopsin variant (Berndt et al., 2011), transgenic flies generated as described in (Fushiki et al., 2016)

•*UAS-TeTxLC-H* (A synaptic transmission blocker (Sweeney et al., 1995), gift from Dr. Hideyuki Okano)

•*UAS-Kir3.1::GFP* (A rectifying potassium channel used to hyperpolarize neurons (Baines et al., 2001), gift from Dr. Richard A Banes)

•*UAS-ChAT-RNAi* (An RNAi construct used to knock down ChAT. Generated by the Transgenic RNAi Project (TRiP), Bloomington *Drosophila* Stock Center, #60028)

•*UAS-VGlut-RNAi* (An RNAi construct used to knock down vGluT. Generated by the Transgenic RNAi Project (TRiP), Bloomington *Drosophila* Stock Center, #40845)

•*20XUAS > dsFRT > -CsChrimson::mVenus (attP18), pBPhsFlp2::Pest (attP3)*; Express CsChrimson under GAL4 control when the STOP cassette is removed by hsFlp2, a heat-shock-dependent recombinase that targets FRT, Drs. Stefan Pulver, Karen Hibbard, and the Rubin lab members, personal communication)

•*tsh-GAL80* (Suppress GAL4 activity in thoracic and abdominal neuromeres (Clyne and Miesenböck, 2008), gift from Dr. Julie Simpson)

•*Cha3.3kbp-GAL80* (Suppress GAL4 activity in a subset of cholinergic neurons, (Kitamoto, 2002), gift from Dr. Toshihiro Kitamoto)

•*tub-LexA* (Targets all cells, (Lai and Lee, 2006), gift from Dr. Tzumin Lee)

•*VGlut-LexA* (Targets glutamatergic neurons including motoneurons, Bloomington *Drosophila* Stock Center, #60314)

•*LexAop-R-GECO-1* (A red-shifted genetically encoded calcium indicator (GECI), (Kohsaka et al., 2014; Zhao et al., 2011))

•*LexAop-RCaMP2* (A red-shifted calcium indicator (Inoue et al., 2015), generated by S.T., E. Hasegawa, and H.K., unpublished)

•*R57C10-FlpL;;pJFRC201-10XUAS-FRT > STOP > FRT-myr::smGFP-HA, pJFRC240-10XUASFRT > STOP > FRT- myr::smGFP-V5-THS-10XUAS-FRT > STOP > FRT-myr::smGFP-FLAG, pJFRC210-10XUAS-FRT > STOP > FRT-myr::smGFP-OLLAS* (Named shortly as MCFO-6 in (Nern et al., 2015). Bloomington *Drosophila* Stock Center (#64090), RRID: BDSC 64090)

•*R57C10-Flp2;;pJFRC201-10XUAS-FRT > STOP > FRT-myr::smGFP-HA, pJFRC240-10XUASFRT > STOP > FRT- myr::smGFP-V5-THS-10XUAS-FRT > STOP > FRT-myr::smGFP-FLAG* (Named shortly as MCFO-4 in (Nern et al., 2015). Bloomington *Drosophila* Stock Center (#64087), RRID: BDSC 64087)

•*MB120B-spGAL4* (A combination of GAL4.AD and GAL4.DBD that specifically targets Wave neurons, Generated by J.W.T. and M.Z.)

•*SS02064-spGAL4* (A combination of GAL4.AD and GAL4.DBD that specifically targets A03a5 neurons Generated by J.W.T.)

Method details

Immunohistochemistry

The larvae were pinned down on a sylgard-coated dish, and dissected in calcium free HEPES buffered saline (HEPES 5 mM, NaCl 140 mM, KCl 2 mM, MgCl2 6 mM, sucrose 36 mM, pH = 7.1), washed with phosphate buffered saline (PBS), and were fixed in 4% paraformaldehyde in PBS for 30 min at room temperature. After two 15 min washes with 0.2% Triton X-100 in PBS

(PBT), the larvae were incubated with 5% normal goat serum (NGS) in PBT for 30 min. The larvae were then incubated over one night or two at 4°C with the primary antibodies. After two 15 min washes, the larvae were incubated overnight at 4°C with the secondary antibodies. Fluorescent images were acquired using a confocal microscope (FV1000, Olympus).

The list of the antibodies used and the dilution is as follows:

•rabbit anti-GFP (Af2020, Frontier Institute; 1:1000; RRID: AB 10615238)

•mouse anti-Fas2 (1D4, Hybridoma Bank (University of Iowa); 1:10; RRID: AB 528235)

•guinea pig anti-GFP (Af1180, Frontier Institute; 1:1000; RRID: AB 2571575)

•rabbit anti-HA (C29F4, Cell Signaling Technology; 1:1000; RRID: AB 1549585)

•mouse anti-V5 (R960-25, Invitrogen; 1:500; RRID: AB 2556564)

•mouse anti-ChAT (4B1, Hybridoma Bank (University of Iowa); 1:50; RRID: AB 528122)

•mouse anti-GABA (A2052, Sigma; 1:100; RRID: AB 477652)

•mouse anti-vGluT (Gift from Dr. Hermann Aberle; 1:1000; RRID: AB 2315544)

•goat Alexa Fluor 488 or Cy3-conjugated anti-rabbit IgG (A-11034 or A-10520, Invitrogen Molecular Probes; 1:300; RRID: AB 2576217 or AB 10563288)

•goat Alexa Fluor 555 or Cy5-conjugated anti-mouse IgG (A-21424 or A-10524, Invitrogen Molecular Probes; 1:300; RRID: AB 141780 or AB 2534033)

•goat Alexa Fluor 488-conjugated anti-guinea pig IgG (A-11073, Invitrogen Molecular Probes; 1:300; RRID: AB 142018)

Optogenetics (with CsChrimson) in free-moving larvae

The larvae were grown at 25°C. Second or third instar larvae were picked, gently washed, and transferred onto an apple-juice agar plate coated with yeast paste, either containing 1mM of

all-trans retinal (ATR) or none (ATR concentration was calculated based on the volume of the dry yeast. Note that the same amount of distilled water was added to make yeast paste). The plate was covered with the plastic cover and aluminum foil, and placed at 25°C for one night. The behavioral experiment was conducted on an apple juice agar plate, which was placed on a heating plate to set the surface temperature of the agar within 25°C ± 1°C. The larvae were placed on the fresh apple-plate for over 5 min before the behavioral assays. 660 nm LED light at the density of 20~25 $\mu W/mm^2$ (THORLABS) was used for the stimulation of CsChrimson. The stimulation trials were delivered three times for each animal, with a duration of 10-15 s for each trial, and >15 s intervals between each trial. Video recording was conducted under a stereo-microscope (SZX16, Olympus), while the background illumination was minimized so as not to activate CsChrimson.

Local-area optogenetics using one-photon excitation (ChR2[T159C])

The larvae were grown at 25°C. First or second instar larvae were picked, gently washed, and transferred onto an apple-juice agar plate coated with yeast paste containing 10 mM ATR. The plate was covered with the plastic cover and aluminum foil, placed in 25°Celcius for two nights. The larvae were dissected on a sylgard-coated dish in TES buffered solution (TES 5 mM, NaCl 135 mM, KCl 5 mM, $MgCl_2$ 4 mM, $CaCl_2$ 2 mM, sucrose 36 mM, pH = 7.15). The CNSs of the larvae were isolated from the body wall, and the buffered solution was refreshed before the sample was set under the stereo-microscope (FV1000, Olympus). For the brain ablation experiments, the VNC was set on a MAS-coated slide glass (S9215, Matsunami Glass Ind.).

The microscope was fitted with two optical paths: one is for area-confined stimulation and the other for calcium imaging. The two paths were isolated by using a dichroic mirror

(ADM 405/488, Olympus). The isolated CNS was placed under a water immersion lens (20x, XLUMPLFLN, NA1.0, WD 2 mm, Olympus). Fluorescence derived from the YFP tagged to the ChR2[T159C] protein was scanned using the 515 nm Ar laser, to confirm the expression of ChR2.T159 in the GAL4-expressing cells. For image acquisition, attached software (Olympus FLUOVIEW Ver.4.2) was used.

The stimulation was achieved using the 488 nm Ar laser, which can be confined to 10 μm in diameter. The spot of stimulation was selected based on the image obtained with scanned YFP. The intensity of stimulation was set to 8.3 μW. Concurrently with the stimulation, calcium imaging was done by expressing RGECO (Zhao et al., 2011), a class of red-shifted GECI, under the regulation of tub-LexA to enable panneuronal imaging. The imaging was achieved by recording the fluorescence with an EMCCD camera (iXon3, ANDOR TECHNOLOGY). The pump light for imaging was derived from Xe lamp (X-Cite, Excelitas Technologies). Positions of the cell bodies were confirmed by scanning YFP tagged to the ChR2[T159C] protein. Animals that failed to show the expression in Wave neurons were excluded from the experiment. Trains of 5 s light were applied with intervals of more than 10 s.

The motor outputs were monitored by imaging the RGECO fluorescence, in the region of dorsal neuropile where the motoneurons dendrites are concentrated (Figure 3.5B). The motoneurons dendrites are clustered in each neuromere, thus it is possible to distinguish the activity of the motoneurons from one neuromere to another.

Local-area optogenetics using two-photon excitation (CsChrimson)

The preparation of the larvae was the same as in the one-photon excitation experiment, except that they were fed with yeast paste containing ATR for only one night.

The stimulation was achieved using a femtosecond laser (Chameleon Vision II, Coherent). The wavelength was mode-locked to 930 nm. The isolated CNS was placed under a water immersion lens (Objective W Plan- Apochromat 20x/1.0 DIC D = 0.17 M27 75mm, Carl Zeiss Microscopy), and imaged with an upright microscope (LSM 710 NLO, Carl Zeiss Microscopy). In this experiment, GAL4-targeted cells expressed both CsChrimson and CD4::GCaMP6f. Both optogenetics (CsChrimson) and imaging (CD4::GCaMP6f) was achieved by two-photon excitation. Each trial consisted of an imaging period and a stimulation period. During the imaging period, low intensity light (~10 mW at the back aperture of the objective lens) was focused to the motor pattern indicator neurons for monitoring fictive waves. During the stimulation period, higher intensity light (~30 mW at the back aperture) was focused on the cell body of the target neuron.

The frame size was fixed to 70.30 × 70.30 μm, and the image was taken at the resolution of 128 × 128 pixels. Dwell time in a single pixel was set to 3.15 μs.

For the quantification of fictive backward waves, the occurrence of sequential recruitment of the motor pattern indicator neurons from A1 to A3 within 3 s after the stimulation cessation was the criteria for positive events.

Electrophysiological nerve stimulation

Electrophysiological nerve stimulation was achieved by suction glass electrode with the inner diameter of 5-8 μm. Electrical pulses (Square pulses, interval: 10 ms, duration: 5 ms) were generated by an electronic stimulator (SEN-3301, Nihon Kohden), passed through an isolator (SS-302J, Nihon Kohden) for modulating stimulus intensity (max amplitude: 27.5 V), and applied to platinum electrode fiber inserted in the glass pipette filled with TES buffered saline.

The imaging was achieved by recording the fluorescence with an EMCCD camera (iXon3, ANDOR TECHNOLOGY) mounted on an upright confocal microscope (spindisc, CSU21, Yokogawa; microscope, upright microscope Axioskop2 FS (Zeiss, Germany) equipped with EMCCD camera iXon, Andor). The larvae were dissected on a sylgard-coated dish in TES buffered solution. The CNSs of the larvae were isolated from the body wall, and fixed on a MAS-coated slide glass (S9215, Matsunami Glass Ind.) in the puddle of TES buffer.
For experiments in Figure 3.1, either OK6-GAL4 (which targets all motoneurons) or VGluT-LexA (which specifically targets glutamatergic neurons including motoneurons) was used to monitor fictive locomotion by using the 10X objective lens (Zeiss Achroplan 10x / 0.30 Infinity/0 W Ph1 Water Immersion Microscope Objective). 10 s of stimulation was repeated four to seven times per each animal, and the number of wave-like activities during stimulation was averaged within each animal.

For experiments in Figure 3.11, the activity in the neurites of Wave neurons residing between A1 and T3 neuromeres (extended by Wave neurons in anterior neuromeres) were imaged by using the 20X objective lens (Olympus LUMPlanFl 20x /0.50 W Infinity/0 Water Immersion Microscope Objective) and quantified using ImageJ. Jump rate was calculated as the average of the value described below for first and second stimulation events:

$$J_t = \frac{F_t + F_{t+1}}{F_{t-2} + F_{t-1}}$$

Here, *F* denotes the fluorescence, and t stands for the frame when the electrophysiological stimulation initiated.

Statistical significance was calculated for the jump rate after logarithmic transformation.

Thermogenetic inhibition (Shibire$^{ts}$)

Female UAS-shibire$^{ts}$ flies were crossed with GAL4 males. The larvae were grown at 25°C. Third instar larvae were picked, gently washed, and transferred onto an apple-juice agar plate to habituate the larvae. Another apple-plate was heated to 31 ± 1 for behavioral experiments (25 ± 1 for one of the control groups in Figure 8A as indicated in the panel), and the larvae were transferred onto the heated plate for over 3 min, in order to inactivate neurons. Video recording was conducted under a stereo microscope (SZX16, Olympus).

Touch assay

As a noxious touch, a pinprick was delivered by hand with insect pins held by forceps. To minimize the variance of the stimulation intensity, the pinprick was applied so that the body wall of the targeted site (dorsal side of T3 ± 1 segment) was clearly dented upon the prick, but not penetrated. Trials with penetration or those without an obvious dent were excluded from the analyses. Three trials or more were performed for each animal.

For gentle touch, von Frey filament (Touch Test Sensory Evaluator (0.07 g), North Coast; #NC12775-04) was used. Gentle touch was applied to the target site in the same manner as for the noxious touch, and was applied until the larva showed a behavioral response (forward locomotion, head sweep, or backward locomotion). Five trials were performed for each animal.

Sparse activation of Wave neurons in vivo using FLP-out technique

Female 20XUAS > dsFRT > -CsChrimson::mVenus (attP18), pBPhsFlp2::Pest (attP3) flies were crossed with *MB120B- spGAL4* males. Eggs were collected for 24 hr on an apple-juice agar plate with a moderate amount of yeast paste.

The eggs were raised in the plate at 25°C for 24 hr. Then, heat shock was induced by placing the plate into an incubator set to 37°C for 1 hr. The plate was put back to 25°C and two days later, the larvae were transferred to and raised in another plate that contained 1mM ATR-containing yeast paste for approximately 24 hr. The larvae were tested in the behavioral assay as described above, except that the light stimulations were delivered only twice for each animal. 54 animals were tested, and the expression of CsChrimson::mVenus was confirmed as described above. The segment identities of Wave neurons were determined by observing the entry point of the neurite from the soma, based on Fas2 tracts (TPs 1, 4, and 5).

Dual-color calcium imaging

I used an emission splitting system (DV2 Multichannel Imaging System, Photometrics) to perform dual-color imaging of GCaMP6m and R-GECO-1.

EM reconstruction using CATMAID

EM reconstruction was performed as described previously (Fushiki et al., 2016; Ohyama et al., 2015) using a modified version of CATMAID (Schneider-Mizell et al., 2016), which includes application based on a Django web framework (https://www.djangoproject.com) and a database PostgreSQL (http://www.postgresql.org). The reconstruction was based on a manually-sectioned serial-section EM volume of a 1$^{st}$ instar larval CNS (Generated by Dr. Richard Fetter;

Schneider-Mizell et al., 2016). Each neuron is reconstructed as a skeleton, which consists of one or more nodes in each cross-section of the neuron being present. Synapses are annotated as a directed connection from a node of one neuron (i.e. pre) to that of another neuron(s) (i.e. post). Synapses must match the following four criteria that are evident from the EM images: active zone, vesicles, and presynaptic T-bar, and postsynaptic densities (PSDs) (Ohyama et al., 2015). Based on such manually-annotated synapses, synapse flow centrality (SFC; see Schneider-Mizell, 2016) was calculated to cluster each neuronal arbor as a dendrite or an axon (this calculation is implemented in the CATMAID software).

I manually traced the axonal and dendritic processes of Wave (A02o) neurons and identified the location of the pre- and post-synapses. I then reconstructed the presynaptic and postsynaptic neurons from the synaptic sites. I mapped the circuit by the iterative method as described (Schneider-Mizell et al., 2016), in which iterative reviews on the traced neurons and comparison of the mapped circuits on the left and right halves of each segment were performed to identify further issues to resolve.

Finding identified neurons in the EM volume

Finding neurons in the EM volume identical to those in light microscopy (visualized using GAL4 drivers) was performed as described previously (Fushiki et al., 2016), as follows. Each lineage in the *Drosophila* larval nerve cord holds 10-15 neurons, which are separable from each other by their distal arbors. In the EM dataset, I located the entry point from the cortex into the neuropile of the lineage bundle of interest, and then reconstructed the low-order branches. Matching these partially reconstructed neurons to light microscopy images allowed me to uniquely identify the neuron of interest in the EM volume.

Representations of sample sizes

The representations of sample sizes ("*n*") are indicated within the respective figure panels, except for the following for which the representations are indicated in the corresponding figure legends: Figures 3.8B, 3.8C, and 3.7A–3.7C'.

Quantification of larval behaviors

Larval behaviors were manually quantified for the data presented in Figures 3.1, 3.3, 3.10, 3.15, and 3.16. Larval locomotion was counted when a sequence of muscle contraction across segments was observed, with the direction from anterior to posterior being backward locomotion and the other way around being forward locomotion (Berni et al., 2012). For the data presented in Figures 3.10D and 3.10D', wiggle/bend was defined as one or more bout(s) of transient, left-right asymmetric muscle contraction across multiple abdominal segments.

In quantification of larval behaviors upon optogenetic stimulation, the first 10 s after stimulation onset in each trial was used for quantification (to avoid the effect of desensitization). For data in Figure 3.3A, the average of three trials in each animal tested was used for quantification. For data in Figure 3.10, the sum of two trials (10 s + 10 s) was used for quantification.

In quantification of behaviors upon mechanical or aversive stimulation, either the probability or the number of the backward locomotion that larvae performed was used for quantification. In quantification of the probability (as in Figures 3.1B' and 3.16D), the probability was calculated by dividing the number of positive trials by that of total trials. A trial was marked as positive when a larva showed one or more backward response(s) to the stimulus

between stimulus onset and forward resumption. In quantification of the number (as in Figures 3.15A, 3.15G, and 3.16B), the number was calculated as the average of backward responses in each trial between stimulus onset and forward resumption.

Direction of fictive locomotion

In order to detect fictive locomotion in calcium imaging, I set the imaging ROIs in each of the neuromeres A1 to A7 to include dendrites of motoneurons in each neuromere, which are spatially segregated from each other. Since wave-like activity is most salient in neuromeres A1 to A7, I defined a fictive forward wave as a bilateral and sequential motor activity propagating from A7 to A1, and a fictive backward wave as that in the opposite direction. In some cases when the magnification is too high to image the entire abdominal neuromeres, sequential recruitment of motor activity in three neuromeres or more was used to identify fictive waves. In quantification of the fictive locomotion upon stimulus onset (nerve root stimulation and area-confined optogenetics), the waves that emerged before the stimulus onset were not taken into account.

In quantification of the coincidence of fictive waves in two neuronal populations (as in Figures 3.6C and 3.7C''), the waves were separately counted in each of the calcium traces and then the coincidence was examined.

Quantification of calcium transients

The quantification of signals of calcium probes was first performed by Fiji (Fiji is just ImageJ). The ROIs were set to the neurites of interest, and the mean signal within each ROI was used as the representative signal intensity in each frame. Letting $n$ be the ROI identity and $t$ be the frame

number, I obtained the raw signal intensity $F_{ROI[n]}(t)$. The signals were normalized by calculating the baseline $F_{ROI[n]}$, which was calculated as the average of the bottom 30 values of $F_{ROI[n]}(t)$ (from this point, the calculation was performed by Microsoft Excel). Thus, I calculated the normalized calcium transient in each ROI as:

$$\frac{\Delta F}{F} = \frac{F_{ROI[n]}(t) - F_{ROI[n]}}{F_{ROI[n]}}$$

Quantification of a phase lag during fictive locomotion

In order to quantify the peak shift of the wave-like activity along neuromeres, I calculated the phase as follows. I first extracted time bins corresponding to the entire forward or backward wave. Next, I calculated the cross-correlation function (CCF) of the activity traces in two neuromeres of interest, and the lag that maximizes the CCF was defined as the time lag of the peak. The time lag was normalized by the time bins and indicated as the phase $\theta$, where $-180^\circ < \theta < 180^\circ$.

Quantification of immunoreactivities

In order to identify neurotransmitter phenotypes (as in Figures 3.4C, 3.4D', 3.16E, and 3.16E'), I performed immunohistochemistry by using anti-GFP and anti-ChAT/vGluT primary antibodies, which were subsequently tagged by Alexa 488- and Cy3-conjucated secondary antibodies respectively. The laser intensities for the scanning of each channel (Alexa 488 and Cy3) were fixed throughout. After image acquisition, I used Fiji (Fiji is just ImageJ) to quantify the immunoreactivity of the neurotransmitter marker antibodies. The ROIs were manually set as ovals that surround each cell of interest (by observing the Alexa 488 channel), and the

fluorescence were calculated for both the Alexa 488 and Cy3 channels. In order to normalize the immunoreactivity between each cell, the quantification was performed by dividing the fluorescence of anti-ChAT/vGluT by that of anti-GFP.

Statistical analyses

All statistical tests were performed using R-project (http://www.r-project.org) or Microsoft Excel. I performed non-parametric tests throughout to determine statistical significance (with the pooled data being represented as boxplots), except for the data presented in Figures 3.5D', 3.8B, 3.8C, 3.11E, 3.2, 3.7B, and 3.9A–3.9C'. No methods were used to determine whether the data met assumptions of the statistical approach taken. The error bars (in Figures 3.8B, 3.8C, 3.11E, and 3.9A–3.9C') represents standard errors of the mean (SEM).

## Results

### Different Larval Responses are Induced by Noxious Touch Depending on the Body Location of the Stimulation

I first tested whether the activity of MD IV is necessary for the larval response to localized mechanical nociception. I found that the probability of performing backward locomotion in response to head prick was significantly reduced upon inhibition of synaptic transmission from MD IV neurons (Figures 3.1B and 3.1B'), indicating that these neurons are partly required for the touch response. I also tested the requirement of another class of multidendritic sensory neurons, MD class III (MD III), and found that inhibition of MD III also resulted in significant reduction in the induction of backward locomotion upon a pinprick (Figure 3.1B'). These results suggest that both MD IV and MD III are involved in the touch response.

I further studied the roles of the sensory neurons in an isolated CNS. I electrically stimulated the nerve root, which contains axons of all somatosensory neurons in a specific body wall hemisegment (to mimic head or tail touch), while performing calcium imaging of the motoneurons (to detect fictive locomotion, Figure 3.1C). I found that electrical stimulation of the nerve root in an anterior segment (A1) induced fictive backward locomotion (Figure 3.2). In contrast, electrical stimulation of the nerve root in a posterior segment (A7) induced fictive forward locomotion (Figure 3.2), indicating that location-dependent somatosensory responses are preserved in this physiological assay. The occurrence of the backward motor pattern was greatly reduced when synaptic transmission from MD IV or MD III was inhibited (Figure

3.1C'). Thus, MD IV and MD III neurons are partly required for backward response to localized sensory inputs both *in vivo* and *ex vivo*.

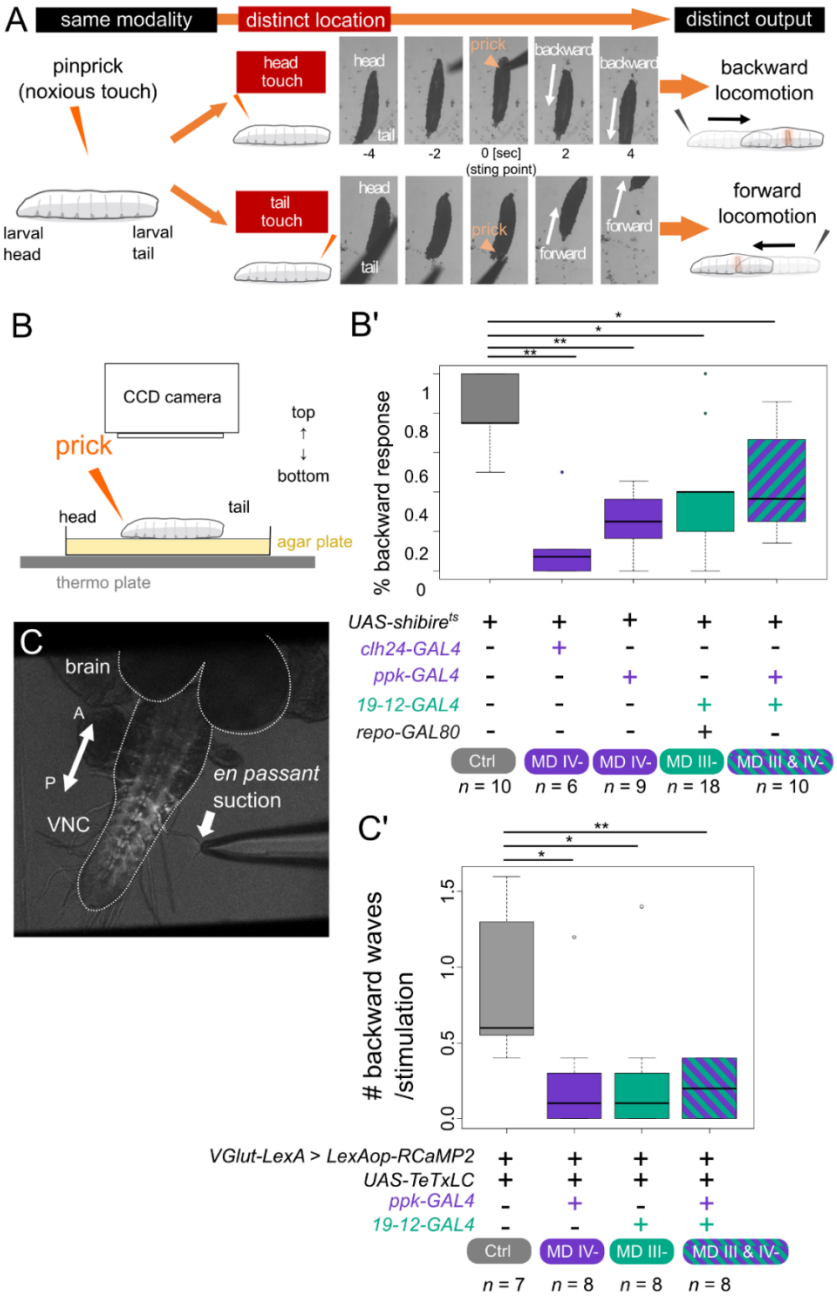


**Figure 3.1 Characterization of body location-dependent somatosensory touch responses (see also Figure 3.2).**

(**A**) Body location-dependent touch responses to pinpricks. Stimulus on the head induces backward locomotion whereas stimulus on the tail induces forward locomotion. (**B, B'**) Inhibition of nociceptive/mechanosensory neurons reduces backward response to a

pinprick. (**B**) The behavior of the larvae was observed on an apple juice agar plate. (**B'**) Quantification of the probability of backward responses to a head touch. Inhibiting the transmission of MD IV (purple), MD III (green), or both (purple/green stripes) significantly reduces the probability. *: $p < 0.05$, **: $p < 0.01$, no indications: $p > 0.05$, Kruskal-Wallis test followed by Steel-Dwass post-hoc analysis. The + labels in the horizontal axis denote the transgenes used for the experiments (listed on the left). (**C**) Experimental setup of electrically stimulating A1 (anterior) nerve root. The activity of motoneurons was monitored by calcium imaging, while the nerve root was electrically stimulated by a glass electrode. (**C'**) Quantification of the occurrence of fictive backward locomotion. Blocking the transmission of MD IV (purple), MD III (green), or both (purple/green stripes) significantly reduces the occurrence of backward locomotion to A1 nerve root stimulation. **: $p < 0.01$, *: $p < 0.05$, no indications: $p > 0.9$, Kruskal-Wallis test followed by Steel-Dwass post-hoc analysis. Figures reproduced from Figure 1 in Takagi et al., 2017.

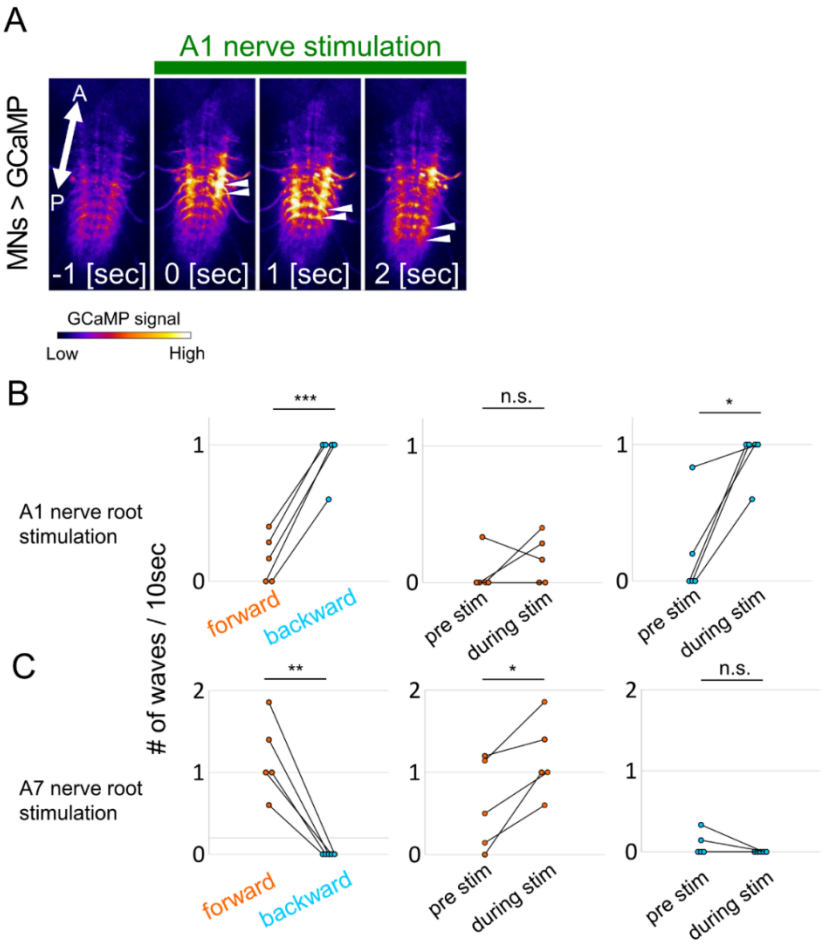


**Figure 3.2, related to Figure 3.1**

**(A)** Example image of fictive backward locomotion in an isolated CNS upon stimulation of the A1 nerve root. The double arrowheads show the progression of the wave front. A: anterior, P: posterior. (**B, C**) Quantification of fictive locomotion induced by the nerve root stimulation in an anterior (**B**) and posterior (**C**) neuromere. The number of forward versus backward waves during stimulation (left), number of forward waves before versus during stimulation (middle), and number of backward waves before versus during stimulation (right) are compared. Electrical stimulation to an anterior nerve root (A1, **B**) elicits backward motor waves, whereas stimulation to a posterior nerve root (A7, **C**)

elicits forward motor waves. *: $p < 0.05$, **: $p < 0.01$, ***: $p < 0.001$, paired *t*-test.

Figures reproduced from Figure S1 in Takagi et al., 2017.

Identification of Wave as a Candidate Command Neuron for Backward Locomotion

I searched for neurons whose activation induces backward locomotion in the larvae, by expressing the red-shifted channelrhodopsin CsChrimson in different subsets of GAL4-targeted cells, and identified *VT25803-GAL4*-targeted cells (hereafter called VT25803 cells) as a candidate (Figures 3.3A and 3.4A). Interestingly, in four of the nine cases examined, where photostimulation was applied during forward locomotion, backward locomotion was immediately induced before the completion of the forward peristalsis, and initiated in a middle segment near the segment contracted at the time of photostimulation (Figure 3.3A'). Such reversal in the middle of peristalsis is rarely seen in normal larvae; backward locomotion normally starts in the anterior-most segment and only after completion of the preceding forward peristalsis. *VT25803-GAL4* drove expression in small subsets of cells in the brain and the ventral nerve cord (VNC) (Figure 3.3B). I used the GAL80-mediated intersectional method (Lue et al., 1987) to narrow down the candidate neuron(s) eliciting the backward locomotion among GAL4-targeted cells. I found both *tsh-GAL80*, which represses GAL4-mediated expression in the VNC (Figure 3.4A), and *Cha3.3kbp-GAL80*, which represses GAL4 activity in subsets of cholinergic neurons (Figure 3.4B), significantly reduced the frequency of backward locomotion triggered by the optogenetic activation (Figure 3.3A). This led me to identify a single class of segmentally repeated pairs of abdominal neurons as the candidate, since they were the only cells that were Cha3.3kbp positive and present in the VNC.

Morphology of the candidate neurons was studied in single-cell images generated by the MultiColor FLP-Out (MCFO) method (Figure 3.3C). I named the neuron as Wave for its characteristic wavy axon. Wave neurons extend their dendrites to the ventro-medial neuropile.

Wave neurons extend their axons to the dorsal neuropile where motoneuronal dendrites are present. The axons of Wave neurons in each neuromere are bundled to form a unique dorso-ventrally winding fascicle that extends the entire anteroposterior axis in the VNC, which is the origin of the name of the neurons. These characteristics suggest that Wave neurons receive synaptic inputs from sensory neurons including MD IV and MD III, and send information to the motor circuits. Immunostaining for neurotransmitter markers showed that Wave neurons were immunoreactive both to anti-choline acetyltransferase (ChAT) and anti-vGluT (Figures 3.4C–3.4D') but not to anti-GABA (Figure 3.4E), suggesting that the neurons are cholinergic and glutamatergic.

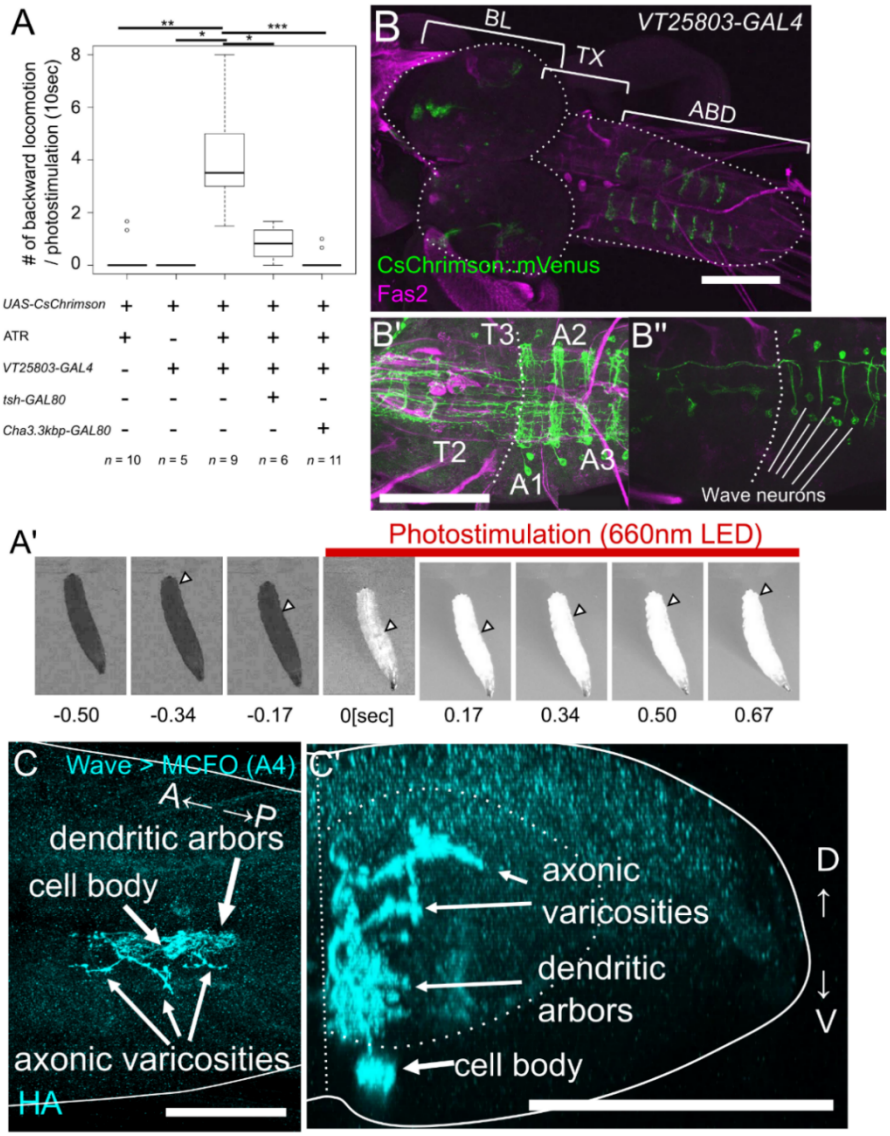


**Figure 3.3 Identification and characterization of Wave neurons, candidate command neurons for backward locomotion (see also Figure 3.4).**

(**A, A'**) Optogenetic activation of *VT25803* cells elicits backward locomotion in free-moving larvae. (**A**) Quantification of the induced backward locomotion upon LED onset. *: $p < 0.05$, **: $p < 0.01$, ***: $p < 0.001$, no indications: $p > 0.05$, Kruskal-Wallis test followed by Steel-Dwass post-hoc analysis. (**A'**) An example image of the induced backward locomotion. The propagation of muscle contraction reversed upon

photostimulation halfway through the peristalsis. The arrows indicate the position of muscle contraction at each time frame. (**B, B', B"**) Expression driven by *VT25803-GAL4* assessed by using CsChrimson::mVenus as a reporter. (**B**) A stack image in a low magnification view of the entire CNS. BL= brain lobe, TX = thorax, ABD = abdomen. (**B'**) A full stack image across the VNC. (**B"**) A stack image of the ventral-half of the VNC showing expression in Wave neurons. Scale bar = 100 $\mu$m. (**C, C'**) Morphology of Wave in A4 neuromere in dorsal view (**C**) and anterior view (**C'**), captured in an MCFO image (Nern et al., 2015) using *VT25803-GAL4*. Scale bar = 50 $\mu$m. Figures reproduced from Figure 2 in Takagi et al., 2017.

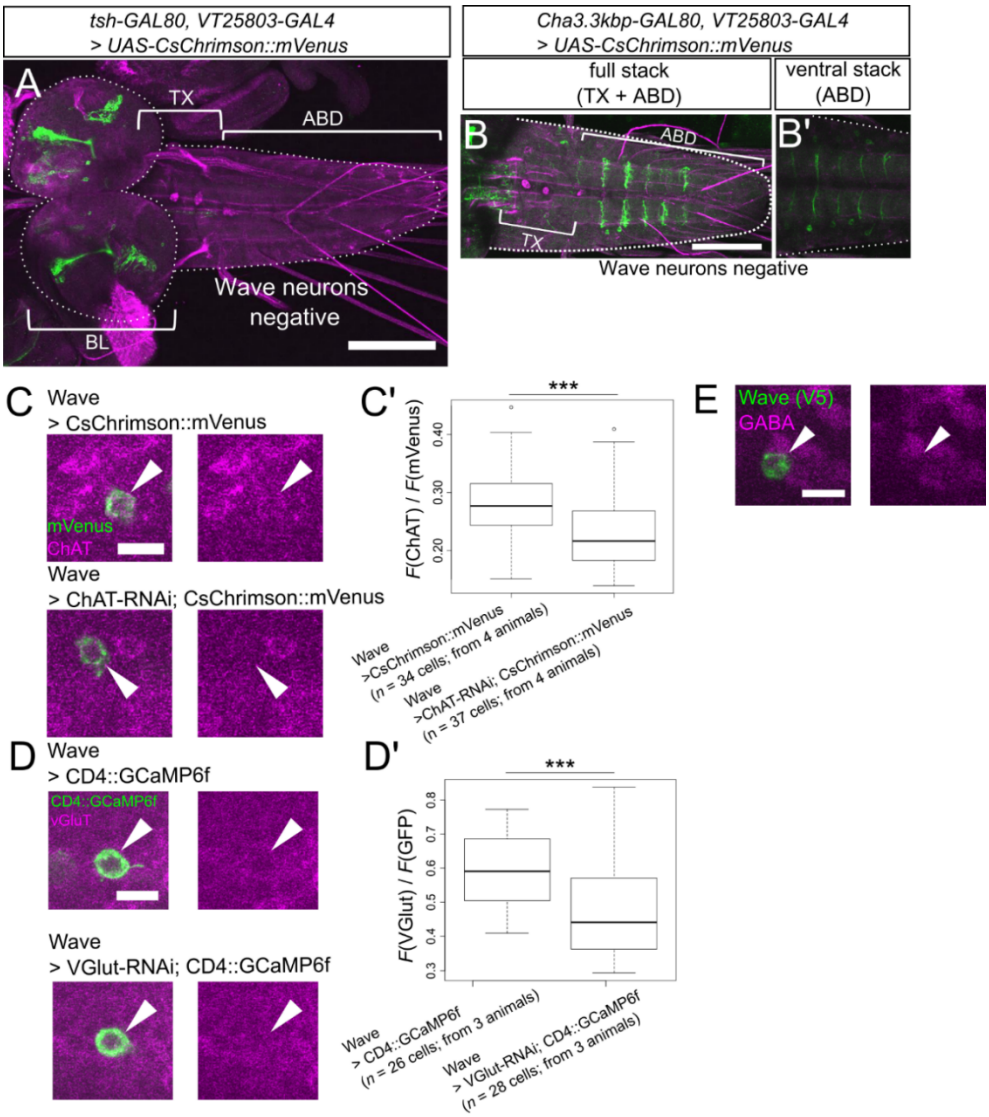


**Figure 3.4, related to Figure 3.3**

**(A, B)** The GAL80-mediated intersectional method identified Wave neurons as candidate backward-inducing neurons. (**A**) Expression driven by *VT25803-GAL4, tsh-GAL80*. Scale bar = 100 $\mu$m. (**B, B'**) Expression driven by *VT25803-GAL4, Cha3.3kbp-GAL80*. (**B**) A stack image of the whole VNC. (**B'**) A stack image of the ventral VNC. Note that expression in Wave neurons is absent. Scale bar = 50 $\mu$m. (**C-E**) Wave neurotransmitter phenotype. (**C, D**) Wave neurons are immunoreactive both to ChAT (**C**) and VGlut (**D**)

antibodies, which is diminished by ChAT-RNAi (**C**) and VGlut-RNAi (**D**) induction, respectively. Scale bar = 10 $\mu$m. (**C', D'**) Quantification of immunoreactivity to ChAT (**C'**) and VGlut antibodies (**D'**), respectively. ***: $p < 0.001$, Mann-Whitney's $U$ -test. (**E**) Wave soma is GABA negative. Scale bar = 10 $\mu$m. Figures modified and reproduced from Figure S2 in Takagi et al., 2017.

Confined Optogenetic Activation of a Single Wave Neuron Elicits Fictive Backward Locomotion

To further confirm that Wave neurons elicit backward locomotion and also to study the effect of locally activating a subset of Wave neurons, I conducted the following two lines of experiments to specifically manipulate the activity of Wave neurons.

First, by using a split GAL4 line (*MB120B-spGAL4*) that drives expression only in Wave neurons (generated by Drs. James W. Truman and Marta Zlatic, Figure S2F in Takagi et al., 2017), I performed an area-confined optogenetics assay. In this assay, I applied light in an area-confined manner (~10 μm in diameter) to activate a subset of GAL4-targeted neurons (by using ChR2[T159C]) in one or a few segments, while monitoring motor activity by calcium imaging (by expressing R-GECO, a red fluorescent genetically encoded $Ca^{2+}$ indicator (Zhao et al., 2011), under the regulation of *tub-LexA*) in an isolated CNS (Figures 3.5A, 3.6A, and 3.6B; see also Method Details). While *tub-LexA* drives expression of R-GECO pan-neuronally, directional activity propagation recorded in the dorsal neuropile perfectly coincided with fictive forward or backward locomotion detected in motoneurons (Figures 3.6B–3.6E). Focal

stimulation spotted within A1–A3 neuromeres induced consecutive backward waves, indicating that activation of Wave neurons in these neuromeres is sufficient to induce backward locomotion (Figures 3.5C, 3.5D, and 3.5D'). The induced backward waves initiated in the abdominal segment A1, unlike the spontaneously occurring backward waves, which initiate in the first thoracic neuromere (T1; Berni, 2015; Pulver et al., 2015). This is reminiscent of the reversal of peristalsis in the middle of forward locomotion observed in the freely behaving larvae upon activation of VT25803 cells (see Figure 3.3A).

Second, I used two-photon optogenetics to activate a single Wave neuron among the VT25803 cells. I expressed CsChrimson and GCaMP in VT25803 cells (Figure 3.5E) and first tested the efficiency and spatial resolution of the two-photon stimulation by imaging the activity of the Wave neuron itself. The two-photon stimulation efficiently activated the neuron with a spatial resolution of $\Delta x$, $\Delta y$ <10 μm and $\Delta z$ <18 μm, which is sufficient for single-cell stimulation among VT25803 cells (Figures 3.7A and 3.7B). I then examined whether Wave stimulation elicits fictive backward locomotion by monitoring the activity of other VT25803 cells, which show wave-like activities during fictive locomotion (Figures 3.5F and 3.7C–3.7C″). I observed backward motor waves following the stimulation of Wave neurons (Figure 3.5G) at a frequency significantly higher than in the control groups ($p = 0.024$, Fisher's exact test; Figures 3.5G and 3.5H). These results indicate that single-cell activation of Wave neurons in anterior abdominal segments is sufficient to trigger fictive backward locomotion.

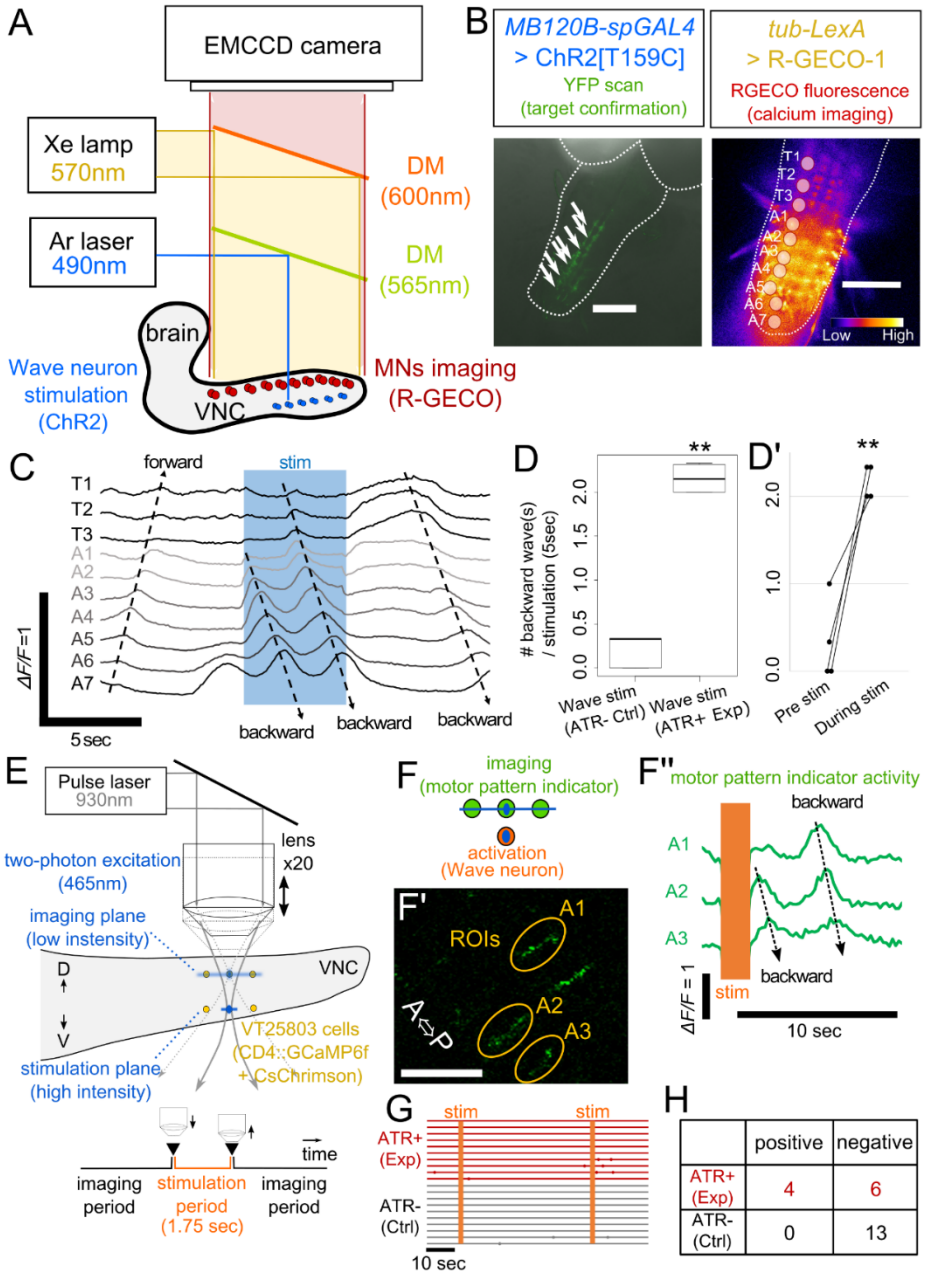


**Figure 3.5 Confined optogenetic activation of Wave neurons elicits fictive backward locomotion (see also Figures 3.6 and 3.7).**

(**A**) Scheme of one photon area-confined optogenetics assay. (**B**) Application of area-confined optogenetics assay on Wave neurons. Arrows: stimulation sites (Wave neurons). Circles: imaging ROIs (MNs dendrites visualized with *tub-LexA*. Scale bar =

100 $\mu$m. (**C**) Representative motor activity induced upon confined activation of Wave neurons. (**D, D'**) Quantification of the number of backward waves during the light stimulation with or without all-*trans* retinal (**D**, **: $p < 0.01$, Mann-Whitney's $U$ -test) and before or during the stimulation in ATR+ animals (**D'**, **: $p < 0.01$, paired $t$-test). (**E**) Scheme of two-photon optogenetics assay. Two-photon excitation was used for both calcium imaging and optogenetics. GCaMP and CsChrimson were expressed in *VT25803* cells. Light was applied at a low intensity during imaging to avoid activation of CsChrimson. During the stimulation period, the $Z$ plane is calibrated to the location of the target neuron and intense light is applied. (**F-H**) Backward motor waves were induced after the stimulation of Wave. (**F-F"**) Activities of the *VT25803*-positive segmental interneurons were used as a motor pattern indicator. (**G**) Raster plots of the backward waves. Transverse lines indicate individual animals. Dots indicate the occurrence of backward motor pattern. (**H**) Quantification of two-photon experiments. Animals that showed backward waves within three seconds after the end of light stimulation were counted as positive. Figures reproduced from Figure 3 in Takagi et al., 2017.

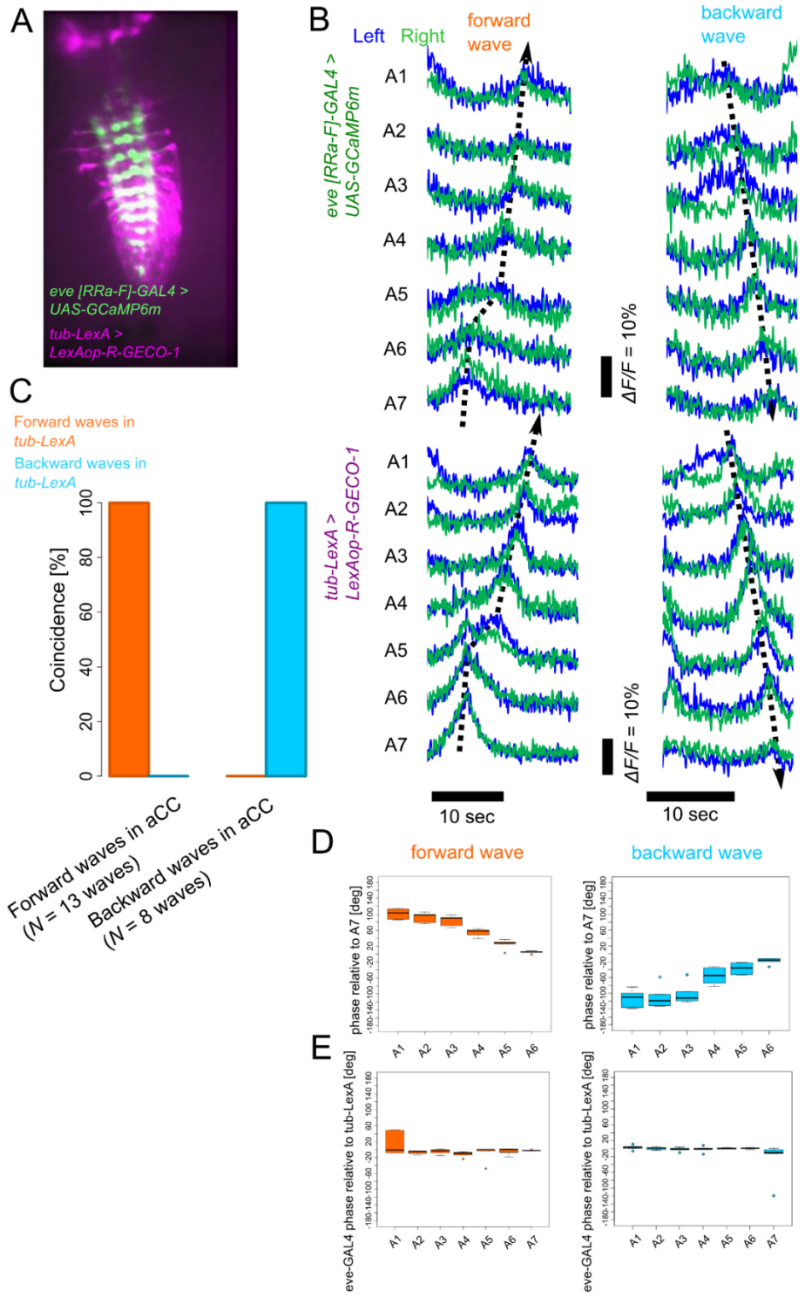


**Figure 3.6, related to Figure 3.5**

**(A)** Example image of dual-color calcium imaging of GCaMP6m driven by *eve[RRa-F]-GAL4* and RGECO-1 driven by *tub-LexA*. **(B)** Example trace of forward and backward waves detected with *eve[RRa-F] > GCaMP6m* and *tub > RGECO-1*, which

occur concurrently. (**C**) Quantification of the coincidence of waves detected with *eve[RRa-F] > GCaMP6m* and *tub > RGECO-1*. $p < 0.001$, Fisher's exact test. (**D**) Phase plot of the waves detected with *tub > RGECO-1*. Phase difference can be clearly observed between abdominal neuromeres A1 to A7. (**E**) Phase lag between *eve[RRa-F]-GAL4* and *tub-LexA*. Note that there is no phase difference. Figures reproduced from Figure S3 in Takagi et al., 2017.

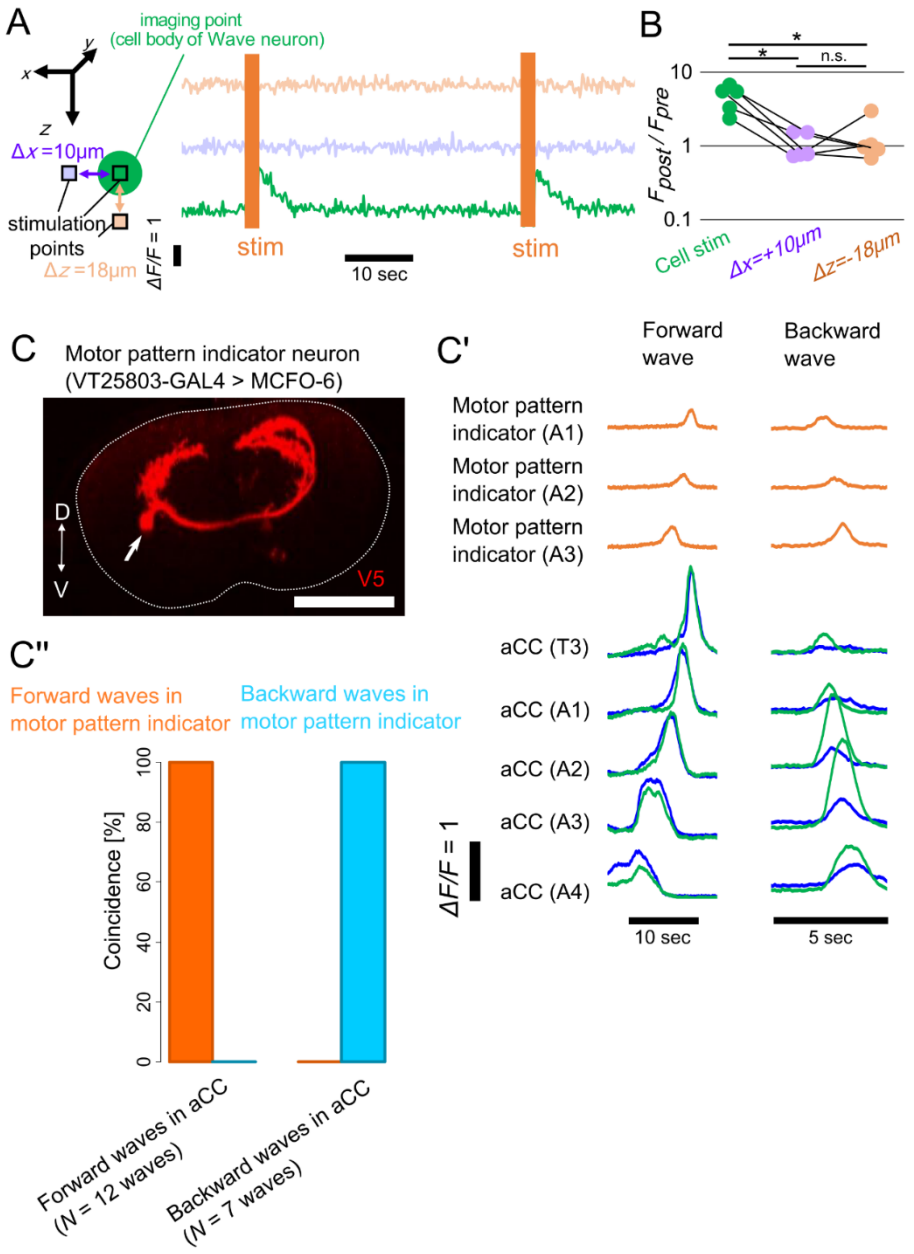


**Figure 3.7, related to Figure 3.5**

**(A**, **B)** Evaluation of the spatial resolution of the two-photon optogenetics. Stimulation of the cell body induces transient rise in activity (green), whereas stimulation in horizontally (purple) or vertically (orange) adjacent sites do not. *: $p < 0.05$, paired *t*-test followed by Bonferroni's correction. (**C-C"**) Characterization of motor pattern indicator

neuron in *VT25803-GAL4*. (**C**) Anterior view of motor pattern indicator neuron captured as MCFO clone. The arrow indicates the position of the cell body. (**C'**) Calcium imaging traces of motor pattern indicator neurons and aCC motoneurons (detected with GCaMP6 expressed in the two neurons). ROIs were placed around neurites of the two neurons that are clearly separated. Forward and backward waves detected in the two neurons occur concurrently. (**C")** Quantification of the coincidence of the waves detected in motor pattern indicator neurons and aCC motoneurons. The waves were separately detected in the two sets of traces, and their coincidence was examined. $p < 0.001$, Fisher's exact test. Figures reproduced from Figure S4 in Takagi et al., 2017.

Segment-Specific Role and Morphology of Wave Neurons

As described above, activation of cells targeted by the original *VT25803-GAL4* in the larvae induced backward locomotion. In contrast, activation of Wave neurons using the highly specific *MB120B-spGAL4*, surprisingly, induced bouts of wiggling and bending, which are an initial posture for rolling, and some rolling events, but much fewer incidences of backward locomotion (Data acquired by Mr. Benjamin T. Cocanougher and Dr. Marta Zlatic, Figure 4A in Takagi et al., 2017). A possible explanation for the difference in the activation phenotypes was segmental difference in GAL4-expression. While *MB120B-spGAL4* targeted Wave neurons in abdominal neuromeres from A2 to A6, *VT25803-GAL4* drove strong expression in these neurons in more anterior neuromeres (from A1 to A4). Since Wave neurons are second-order sensory interneurons, they might convey location-dependent sensory information and induce distinct behaviors depending on their location in the VNC.

To test this possibility, I again took advantage of the area-confined optogenetics assay and activated Wave neurons at different positions along the anterior-posterior axis. I observed that photostimulation in posterior neuromeres (A7 to A5) induced forward waves, whereas that in anterior neuromeres (A3-T1) induced backward waves (Figures 3.8A, 3.8B, and 3.9A; note that neurites but not cell bodies of Wave are present in T3–T1). Thus, Wave neurons elicit completely different motor outputs depending on the location of the activation, as was observed for localized activation of somatosensory inputs (Figure 3.1C). Surgical ablation of the brain did not abolish the induction of forward or backward waves (Figures 3.8C and 3.9B), suggesting that the downstream circuitry of Wave neurons inducing these behaviors is enclosed within the nerve cord. I also found that short-pulse stimulation (with a duration of 100 ms, where the timescale is far smaller than that of the fictive locomotion) was also sufficient to induce forward or backward waves depending on the stimulus site (Figures 3.9C and 3.9C'), suggesting that "gating" mechanisms that prolong the motor commands are present in the downstream circuitry. The segmental difference in Wave function could reflect segmental difference in the pattern of dendritic and axonal projections, which I found are spatially segregated in the neuron (Figure 3.9D). Indeed, I found that Wave neurons in neuromere A2 (Figure 3.8D) and A3 (Figure 3.9E) extended their dendrites and axons anteriorly and intersegmentally to thoracic segments, where the head touch is mainly sensed. (Due to head involution in larvae, thoracic segment 1 (T1) acts as the most anterior part of the animal.) In contrast, Wave neurons in neuromeres A4 (Figure 3.9E'), A5 (Figure 3.9E''), and A6 (Figure 3.8E) extended their dendrites and axons only in the neighboring abdominal segments. In particular, Wave neurons in A2 and A3 extend dendrites anteriorly, whereas those in A5 and A6 extend dendrites not only anteriorly but also posteriorly. Thus, the segmental differences in the projection pattern of Wave neurons (Figure 3.9F) are

closely correlated to the functional difference in evoking distinct behaviors (Figures 3.8B and 3.8C; summarized in Figure 3.8F).

It should be noted that a pair of Wave neurons in each segment were the only cells that express *MB120B-spGAL4* and thus could be unequivocally identified. Furthermore, Wave neurons in each neuromere share the same cell body position and the pattern of proximal axon projection to the neuropile as described above, although they differ in their distal axonal and dendritic arborizations. These observations strongly suggest that these neurons are segmental homologs with diverged neurite extension patterns.

To further confirm that activation of Wave neurons in vivo induces forward or backward locomotion in a segment-specific manner, I carried out FLP-Out optogenetics (see Chapter 2 for details) experiments to sparsely activate Wave neurons (using *MB120B-spGAL4* driver). I found that single-cell activation of Wave neurons in A4 increased forward locomotion, whereas that in A3 induces backward locomotion (Figures 3.10A–3.10C’’). In a case where Wave neurons in A3 and A4 are simultaneously activated, the larva showed wiggle/bend (Figure 3.10D) as observed in activation of Wave neurons in A2–A6 (Figure 4A in Takagi et al., 2017). Such wiggle/bend occurred only when Wave neurons in multiple segments were simultaneously activated (Figure 3.10D’). Taken together with the area-confined optogenetics experiments (Figure 3.8), I conclude that single-cell activation of Wave neurons in an anterior (A3) or posterior (A4) neuromere elicit backward or forward locomotion, respectively.

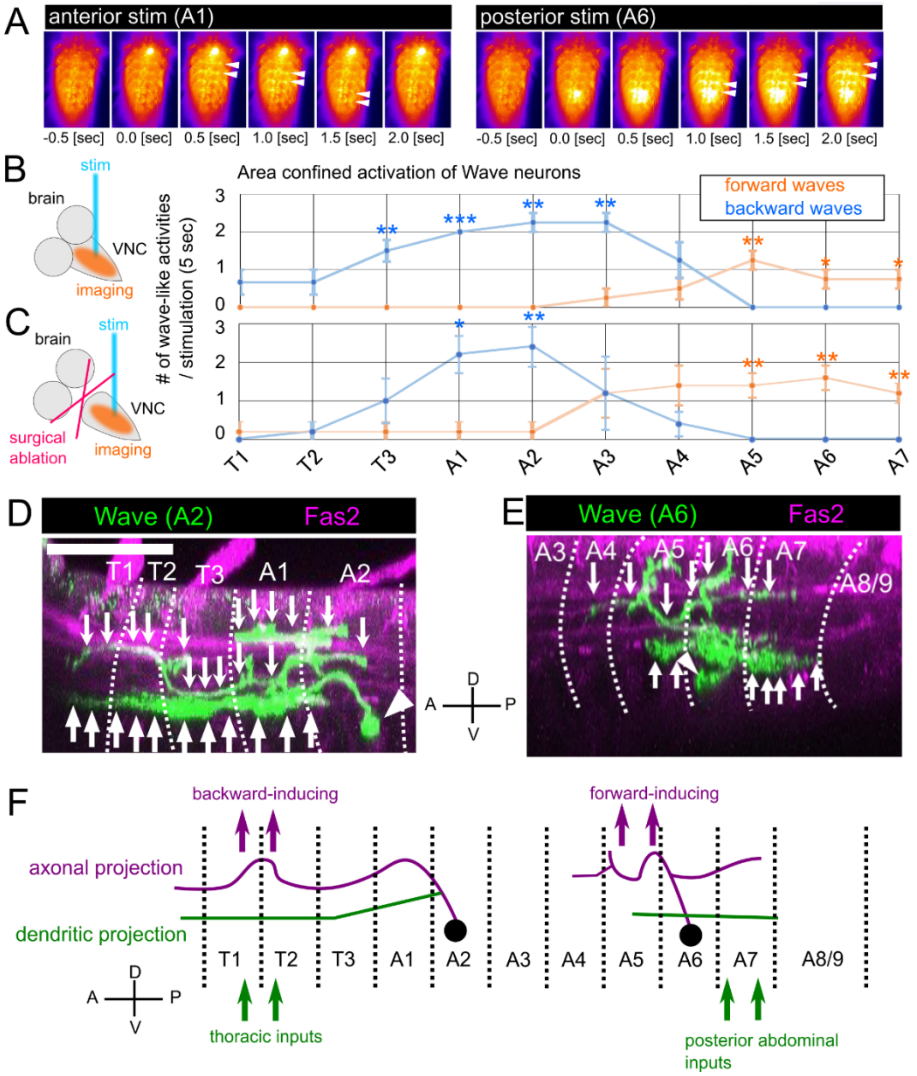


**Figure 3.8 Segmental difference in the function and morphology of Wave neurons (see also Figure 3.9).**

(**A, B**) Motor activity induced by confined activation of Wave neurons along the anterior-posterior axis by using the *MB120B-spGAL4* driver. Arrowheads in **A** indicate the site of wave-like motor activities. *: $p < 0.05$, **: $p < 0.01$, ***: $p < 0.001$, paired *t*-test ($n = 4$ animals for neuromeres A7-T3, $n = 3$ animals for neuromeres T2 and T1). (**C**) Confined activation of Wave neurons as in (**C**), but in the absence of the brain. $n = 5$ animals. (**D, E**) Segmental difference in the morphology (lateral view) of a Wave neuron

in A2 (**D**) and A6 (**E**) examined by the MCFO. Arrowheads indicate the location of cell bodies. Upward arrows indicate putative dendrites, whereas downward arrows indicate axons. Dashed lines indicate approximate segmental borders based on the location of the Fas2 tracts (TP1, TP4, and TP5; Landgraf et al., 2003). Scale bar = 50 $\mu$m. (**F**) Schematic lateral view of Wave neurons in neuromeres A2 (left) and A6 (right). Wave neurons in A2 extend their dendrites and axons anteriorly to thoracic neuromeres, whereas the neurons in A6 extend neurites in neighboring abdominal neuromeres, thus relaying synaptic inputs to outputs in distinct central regions. Figures modified and reproduced from Figure 4 in Takagi et al., 2017.

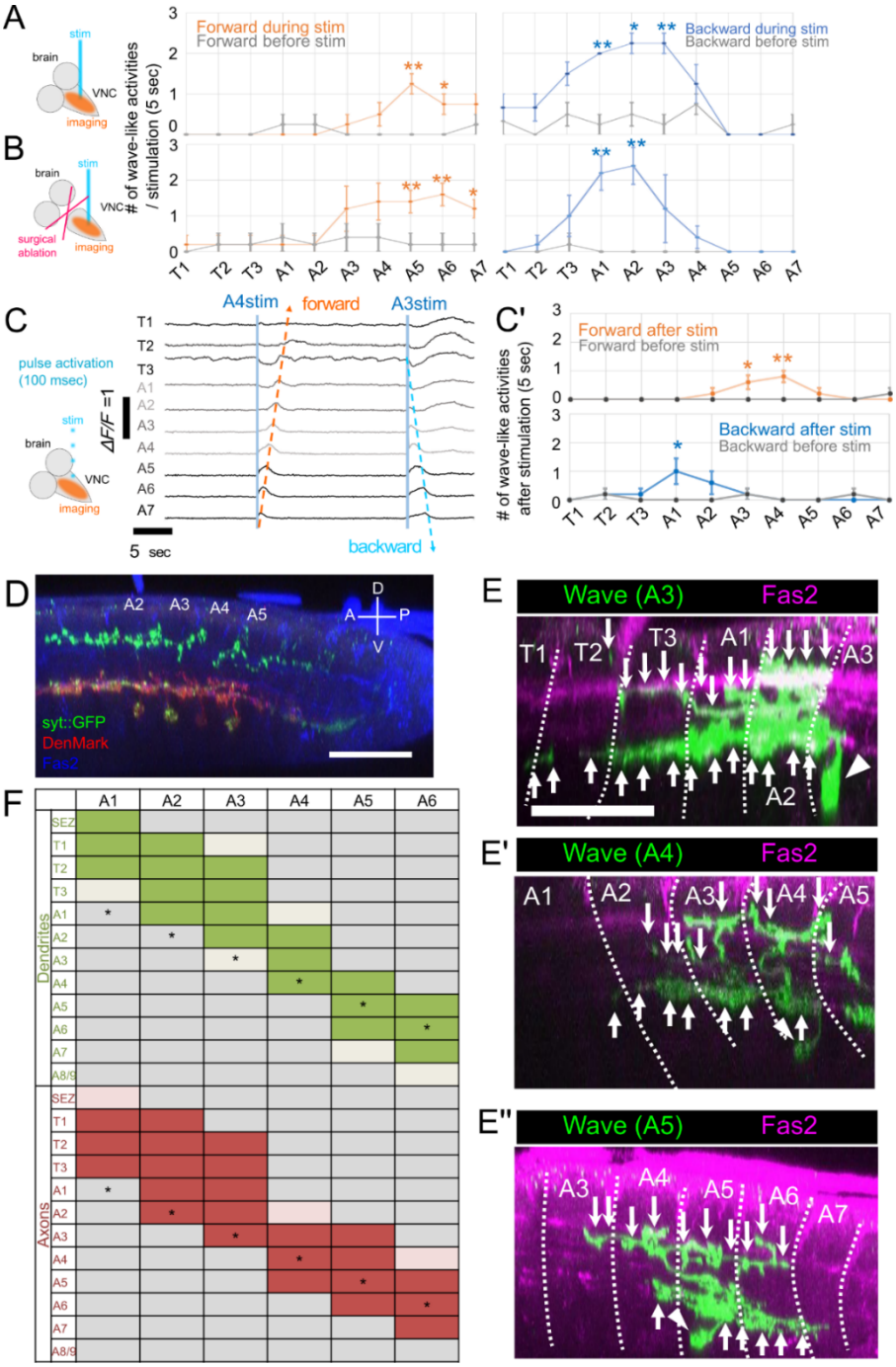


**Figure 3.9, related to Figure 3.8**

**(A, B)** The same experiment as in Figures 3.8B and C, but quantification was performed by comparing the number of waves before and during the stimulation. *: $p < 0.05$, **: $p < 0.01$, paired *t*-test ($n = 4$ animals for neuromeres A7-T3, $n = 3$ animals for neuromeres

T2 and T1). (**C, C'**) Transient activation of Wave neurons is sufficient to induce fictive forward and backward locomotion. Area-confined activation of Wave neurons along the anterior-posterior axis with short-pulse (100 msec) activation. (**C**) Example traces of induced forward and backward waves. (**C'**) Quantification conducted as in (**A, B)**. *: $p < 0.05$, **: $p < 0.01$, paired *t*-test ($n = 5$ animals for neuromeres A7-T2 and $n = 4$ for neuromere T1). (**D**) Pre- and post- synaptic sites of Wave neurons are spatially segregated to dorsal and ventral neurites, respectively. Scale bar = 50 $\mu$m. (**E-E"**) Segmental difference in the morphology (lateral view) of Wave neurons in A3 (**E**), A4 (**E'**), and A5 (**E"**) examined by the MCFO, as in Figures 4E and F. (**F**) Summarized neurite projection pattern of Wave neurons in each neuromere. Colored boxes indicate the presence of neurite projection (thin colors indicate weak projections). The projection pattern of Wave neurons in A1 is derived from the EM dataset (Figure 3.11A). *: neuromeres where the cell bodies reside. Figures reproduced from Figure S5 in Takagi et al., 2017.

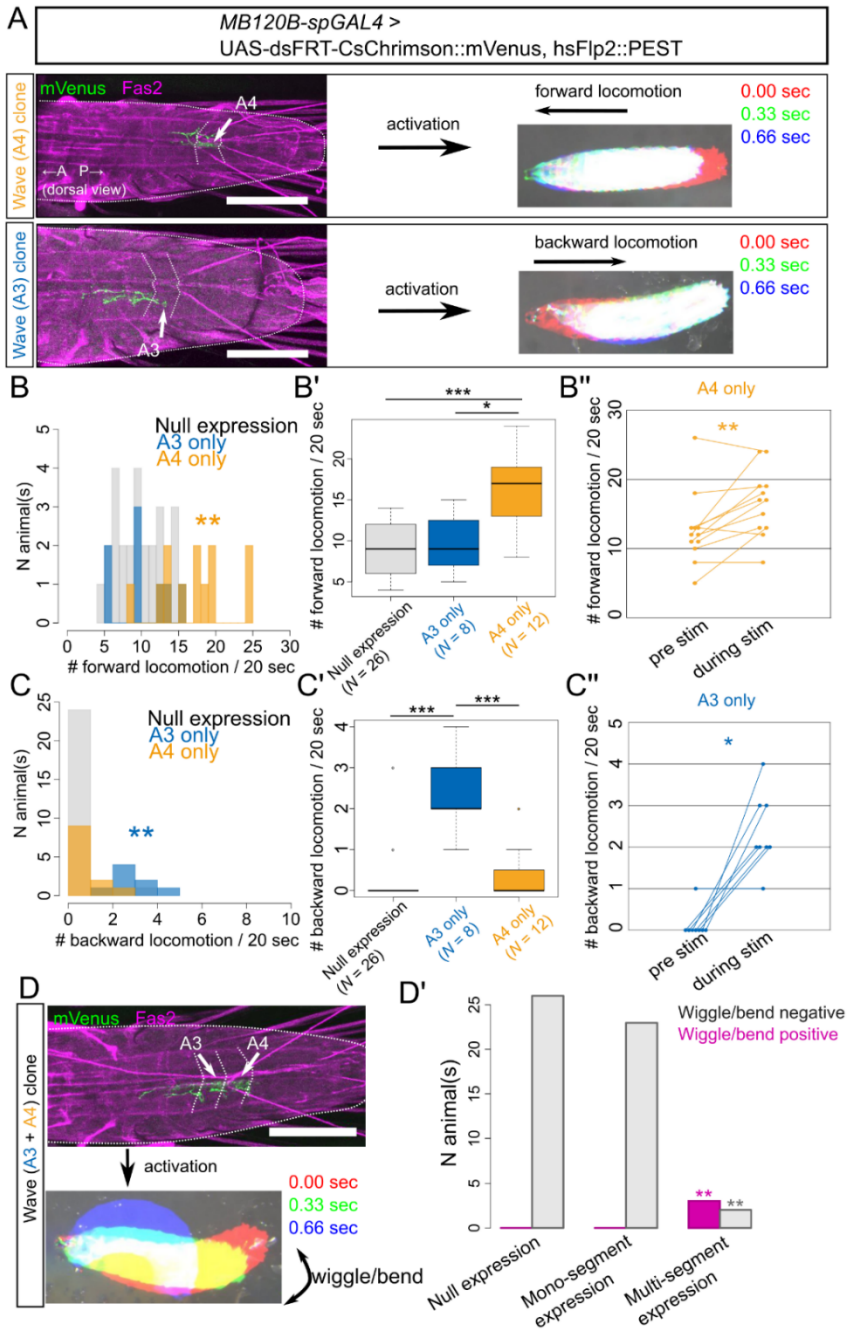


**Figure 3.10 Single-cell activation of Wave neurons *in vivo*.**

(**A**) Examples of single-cell activation of Wave neurons *in vivo* by using FLP-Out optogenetics. Activation of Wave neurons in A4 and A3 induced forward and backward locomotion, respectively. Left panels: expression pattern of CsChrimson::mVenus in

single Wave neurons. Arrows indicate the position of the cell bodies. Scale bar = 100 $\mu$m. Right panels: superimposed posture of a larva from three consecutive time frames upon light stimulation. While each larva was heading forward towards the left, the stimulation either promoted (forward) or reverted (backward) the locomotion directionality. (**B, C**) Histogram of locomotion events (**B**: forward, **C**: backward) during stimulation (with respect to Wave neuron expression patterns, two stimuli for each animal, 10 sec each). **: $p < 0.01$, Kolmogorov-Smirnov test followed by Holm-Bonferroni post-hoc analyses. (**B', C'**) Quantification of locomotion events (**B'**: forward, **C'**: backward) during stimulation. *: $p < 0.05$, ***: $p < 0.001$, Kruskal-Wallis test followed by Steel-Dwass post-hoc analyses. (**B", C"**) Comparison of locomotion events (**B'**: forward, **C'**: backward) before and during stimulation. Forward or backward locomotion significantly increased upon A4 or A3 activation, respectively. *: $p < 0.05$, **: $p < 0.01$, Wilcoxon's signed-rank test. (**D**) Combinatorial activation of Wave neurons in A4 and A3 induces wiggle/bend, which is an initial posture of rolling. (**D'**) Quantification of induced wiggle/bend. Wiggle/bend occurred only when Wave neurons in multiple segments were targeted. **: $p < 0.01$, Chi-square test followed by residual analyses. Figures reproduced from Figure 5 in Takagi et al., 2017.

Wave Neurons are Activated by Nociceptive Sensory Stimuli on the Head

I next asked when and how Wave neurons are activated. Calcium imaging of Wave activity in isolated CNSs undergoing fictive locomotion revealed that these neurons are not active during fictive backward or forward locomotion (Figures 3.11A and 3.11A').

I then tested whether activation of sensory neurons evokes responses in Wave neurons. Electrical stimulation of the nerve in an anterior segment (A1) induced an instant signal increase in Wave neurites in anterior neuromeres but not in posterior segments ($n$ = 5, Figure 3.11B). Conversely, nerve stimulation in a posterior segment (A7) activated Wave neurites in posterior neuromeres but not in anterior neuromeres ($n$ = 4; Figures 3.11C–3.11E). Thus, Wave neurons respond to sensory stimuli in a segment-specific manner. When I blocked neural transmission from MD IV ($n$ = 4, Figure 3.11E), the effect of nerve stimulation was largely abolished, indicating a major role played by MD IV in activating Wave neurons. These results suggest that Wave neurons are not part of the motor pattern generator but are rather transiently activated in response to noxious/mechanical stimuli to induce backward locomotion.

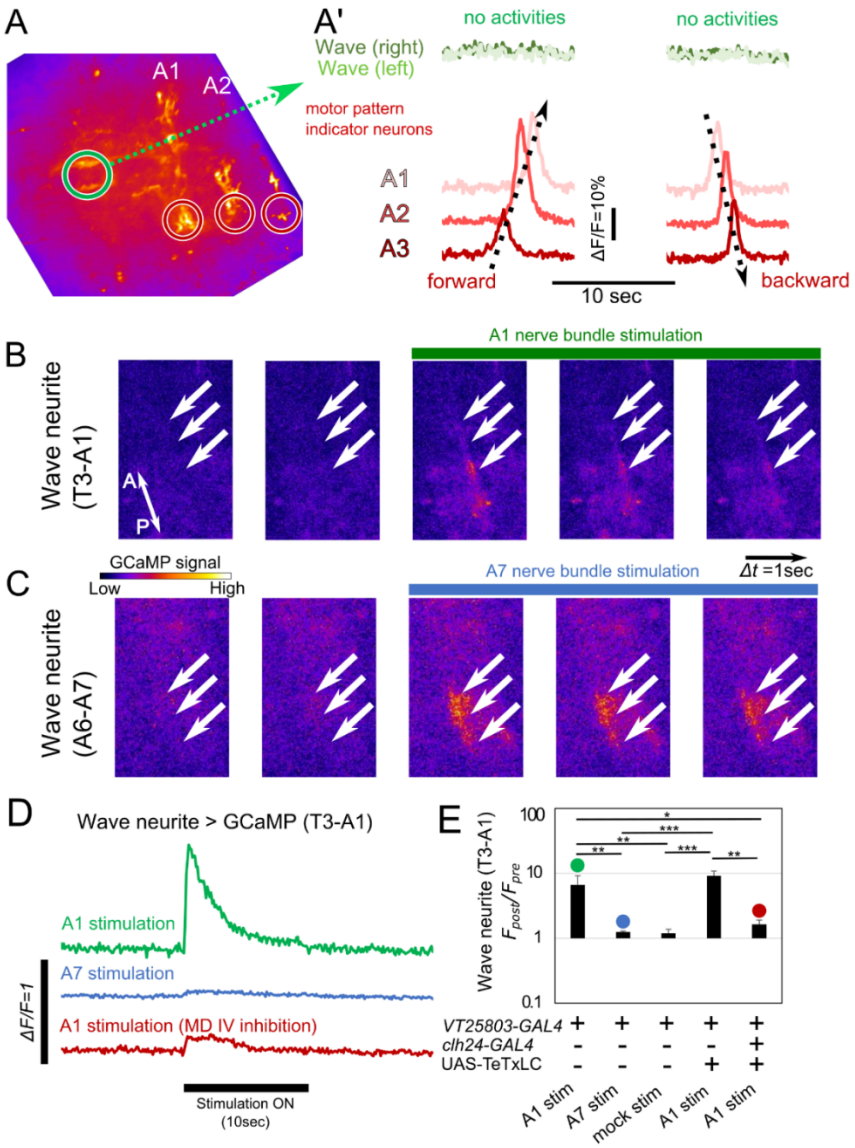


**Figure 3.11 Nociceptive sensory neurons activate Wave neurons in a segment-specific manner.**

(**A, A'**) Wave `neurons show no activities during fictive locomotion. (**A**) A sample view of calcium imaging using *VT25803-GAL4*, showing the ROIs in Wave neurites (green circle) and motor pattern indicator neurons (red circles, see Figures 3.7C-C"). (**A'**) Representative results of calcium imaging. (**B, C**) Wave neurons are activated by nociceptive sensory neurons. Examples of calcium imaging. Electrophysiological

stimulation to A1 nerve root elicits significant increase in GCaMP signals in Wave neurites between T3 and A1 neuromeres (arrows, **B**), whereas stimulation to A7 elicits signal increase in Wave neurites between A6 and A7 (arrows, **C**). (**D**) Example traces of calcium signals upon electrophysiological stimulation. (**E**) Quantification of signal increase evoked by nerve stimulation. 1st group: naive A1 stimulation, 2nd group: A7 stimulation, 3rd group: A1 mock stimulation (without suction), 4th group: control for the 5th group, 5th group: A1 stimulation with blocked transmission from MD IV. *: $p < 0.05$, **: $p < 0.01$, *: $p < 0.001$, no indications: $p > 0.05$, Tukey-Kramer's method after logarithmic transformation of jump rates. Figures reproduced from Figure 6 in Takagi et al., 2017.

Circuit Mapping Showed that Wave Neurons Relay Nociceptive Sensation to Motor Outputs

To understand how Wave neurons might receive the touch sensation on the head and induce backward locomotion, I mapped synapse-level circuits from a nanometer-scale EM volume of the whole CNS by using CATMAID software. I started by reconstructing a pair of Wave neurons in the A1 neuromere to identify all the arbors and synaptic sites. By mapping all the pre- and post-synaptic sites of Wave neurons, I found that dendritic and axonal neurites are clearly segregated (Figure 3.12A). Wave axons projected to the dorsal neuropile, while the dendrites extended in the ventro-medial region, where MD III/IV project (Grueber et al., 2007).

Next, I searched for the presynaptic and postsynaptic partners of Wave neurons. I adopted a previously described method (see Methods for details) that efficiently identifies neurons with a large number of synaptic connections, and bilaterally reconstructed strongly connected neurons thus identified (Figure 3.13). A majority of the presynaptic partners were found to be MD III and IV neurons (Figures 3.13B, 3.13C, and 3.14). Importantly, since Wave neurons in A1 extend dendrites anteriorly to the thoracic neuromeres, they receive synaptic inputs from MD III/IV in these segments (Figures 3.12B, 3.13B, and 3.13C). Thus, these neurons are well positioned to receive noxious stimuli on the most anterior part of the animal.

To understand how Wave neurons in neuromere A1 might initiate backward locomotion, I searched for the downstream pathway(s) that leads to motor circuits. I found that two of the strongly connected postsynaptic partners T07u and Swallowtail interneurons, whose cell bodies reside in neuromere T2, synapsed onto a class of premotor interneurons, A03a5 neurons, which in turn synapsed onto motoneurons in abdominal neuromeres (Figures 3.12D, 3.12D', and 3.13G). Since the four major postsynaptic partners of Wave converge directly or indirectly on A03a5, A03a5 neurons could be a key actuator of backward movement in this circuit.

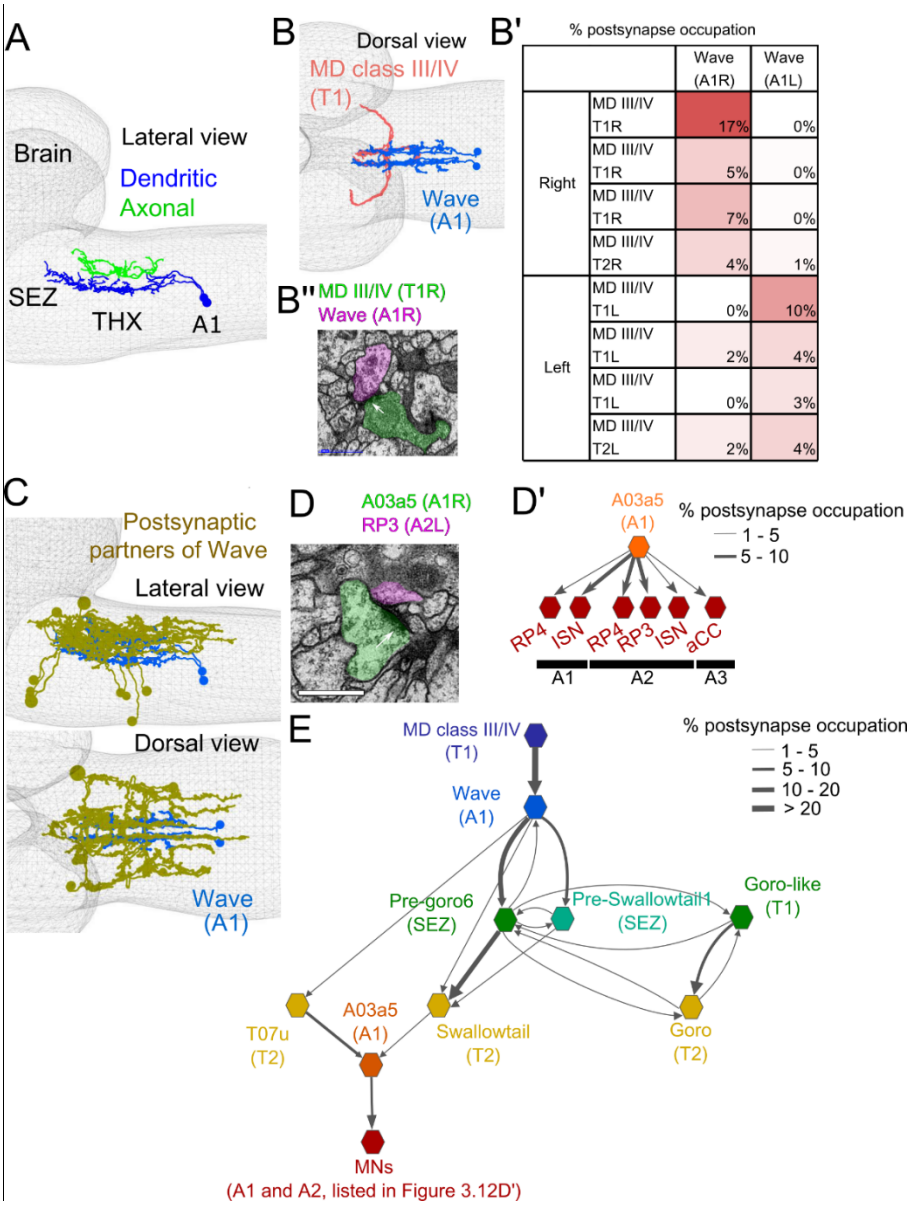


**Figure 3.12 Neuronal circuitry involving Wave neurons.**

**(A)** A reconstructed image of a pair of Wave neurons in A1. **(B)** MD III/IV neurons in thoracic segments are the major upstream partners of the Wave neurons. In the diagram **(B')**, circles and arrows represent neurons and synapses, respectively. In the EM image **(B")**, the arrow indicates the active zone of the presynaptic neuron. Scale bar = 500 nm. **(C)** Reconstruction of major downstream partners of the Wave neurons. **(D, D')** A03a5

neurons are indirect downstream partners of Wave neurons and synapses onto motoneurons. Scale bar = 500 nm. **(E)** Summarized circuit diagram of major synaptic partners of Wave neurons in A1. Each hexagon element represents a group of neurons, and the arrows indicate the synaptic connections. Figures modified and reproduced from Figure 7 in Takagi et al., 2017.

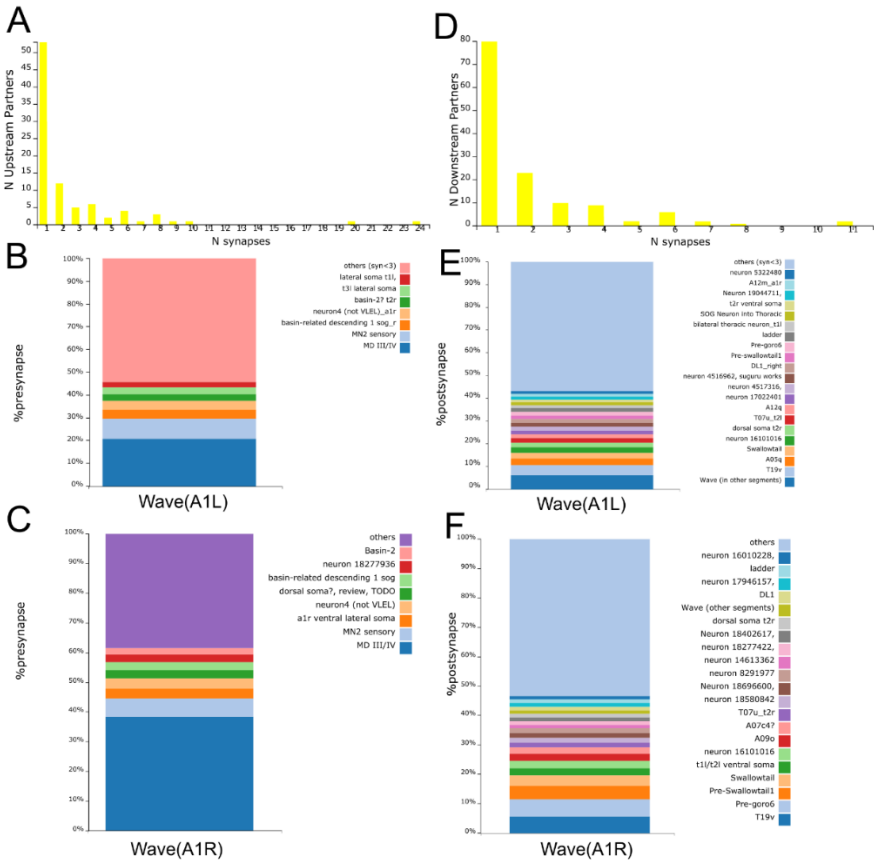


G

| pre \ post | | Wave (A1) | | Pre-goro6 (SEZ) | | Pre-Swallowtail1 (SEZ) | | T19v (T1) | | Swallowtail (T2) | | T07u (T2) | | A03a6 (A1) | |
|---|---|---|---|---|---|---|---|---|---|---|---|---|---|---|---|
| | | R | L | R | L | R | L | R | L | R | L | R | L | R | L |
| Wave (A1) | R | 1% | 0% | 7% | 7% | 4% | 5% | 2% | 4% | 2% | 3% | 4% | 0% | 0% | 0% |
| | L | 0% | 0% | 2% | 4% | 3% | 1% | 4% | 1% | 2% | 1% | 0% | 6% | 0% | 0% |
| Pre-goro6 (SEZ) | R | 0% | 2% | 0% | 0% | 3% | 0% | 0% | 0% | 7% | 9% | 0% | 0% | 0% | 0% |
| | L | 1% | 0% | 0% | 0% | 0% | 2% | 0% | 0% | 9% | 10% | 0% | 0% | 0% | 0% |
| Pre-Swallowtail1 (SEZ) | R | 0% | 0% | 7% | 0% | 0% | 0% | 0% | 0% | 3% | 2% | 0% | 0% | 0% | 0% |
| | L | 1% | 0% | 0% | 2% | 0% | 0% | 2% | 1% | 3% | 2% | 0% | 0% | 0% | 0% |
| T19v (T1) | R | 0% | 0% | 0% | 0% | 0% | 0% | 0% | 0% | 0% | 0% | 0% | 0% | 0% | 0% |
| | L | 0% | 0% | 0% | 0% | 0% | 0% | 0% | 0% | 0% | 0% | 0% | 0% | 0% | 3% |
| Swallowtail (T2) | R | 0% | 0% | 0% | 0% | 0% | 0% | 0% | 0% | 0% | 0% | 0% | 0% | 1% | 0% |
| | L | 0% | 0% | 0% | 1% | 0% | 0% | 0% | 0% | 1% | 0% | 0% | 0% | 0% | 3% |
| T07u (T2) | R | 0% | 0% | 0% | 0% | 0% | 0% | 0% | 0% | 0% | 0% | 0% | 0% | 0% | 5% |
| | L | 0% | 0% | 0% | 0% | 0% | 0% | 0% | 0% | 0% | 0% | 0% | 0% | 7% | 0% |
| A03a6 (A1) | R | 0% | 0% | 0% | 0% | 0% | 0% | 0% | 0% | 0% | 0% | 0% | 0% | 0% | 0% |
| | L | 0% | 0% | 0% | 0% | 0% | 0% | 0% | 0% | 0% | 0% | 0% | 0% | 0% | 0% |

**Figure 3.13, related to Figure 3.12**

**(A**, **D)** Distribution plot of presynaptic (**A**) and post synaptic (**D**) partners of Wave neurons in A1. Transverse axes show the number of neurons that are pre- or post-synaptic to a pair of Wave neurons. Horizontal axes show the number of synaptic

sites for each pre- or post-synaptic partner. (**B**, **C**, **E**, **F)** Identities of presynaptic (**B, C**) and post synaptic (**E, F**) partners of Wave neurons in the left (**B, E**) and right (**C, F**) side of A1. Transverse axes indicate the fraction of synaptic sites connected with each synaptic partner with respect to total synaptic sites in Wave neurons. Note that such quantification of synaptic fraction differs from that in Figure 3.12, which was calculated as the fraction of postsynapse occupation. **(G)** Adjacency matrix corresponding to the circuit diagram (Figure 3.12E), excluding SNs, Goro-like, and Goro neurons. The percentage in this figure denotes postsynapse occupations. Figures reproduced from Figure S6 in Takagi et al., 2017.


**Figure 3.14, related to Figure 3.12**

Dorsal views of major synaptic partners (pre: pink, post: yellow) of Wave neurons in A1.

Figures reproduced from Figure S7 in Takagi et al., 2017.

Wave and its Downstream Motor Circuits are Required for the Execution of Touch-Triggered Backward Response

I next studied the role of Wave neurons and the downstream A03a5 neurons in the execution of backward locomotion. I first investigated the requirement of Wave neurons in the touch-triggered backward response. I inhibited synaptic transmission of Wave neurons by expressing thermosensitive Shibire using the Wave neuron-specific GAL4 line (*MB120B-spGAL4*), and found a significant decrease in the number of backward locomotion performed in response to a head touch, either with a pinprick (Figure 3.15A) or gentle touch (Figures 3.16A and 3.16B). Thus, Wave neurons are not only sufficient for the induction of backward locomotion, but also necessary for the induction of backward locomotion in response to the head touch. After completing backward locomotion, the larvae normally continue the escape behavior by switching to forward locomotion. I found that this transition from backward to forward locomotion was also affected by Wave inhibition (Figure 3.15B). In contrast, I did not observe any defects in backward response to blue light (Figures 3.16C and 3.16D), another aversive stimulus for the larvae. This suggests that Wave neurons are specifically required for the induction of backward locomotion in response to mechanical stimuli but not to other noxious stimuli such as light.

I next characterized A03a5 neurons by using a specific GAL4 line (*SS02064-spGAL4*; generated by Dr. James W. Truman, Figure 3.15C). Immunostaining showed that pairs of A03a5 neurons are present in A2–A4 in this GAL4 line and are immunoreactive to anti-ChAT

and therefore consistent with being cholinergic (Figures 3.15D, 3.16E, and 3.16E'). Optogenetic activation of A03a5 neurons induced muscular contraction that led to tail flick (Figure 3.15E). Consistent with a role in this behavior, calcium imaging in isolated CNSs revealed that A03a5 neurons showed wave-like activities that propagate along the abdominal neuromeres both during forward and backward peristaltic locomotion (Figures 3.15F and 3.16F–3.16H). Although inhibition of A03a5 neurons with thermosensitive Shibire did not interfere with the peristaltic motion itself (data not shown), it resulted in significant decrease in the number of backward locomotion events performed in response to a pinprick on the head (Figure 3.15G). Taken together, these results suggest that the premotor A03a5 neurons are partially required for the execution of backward locomotion in response to noxious mechanical head stimuli

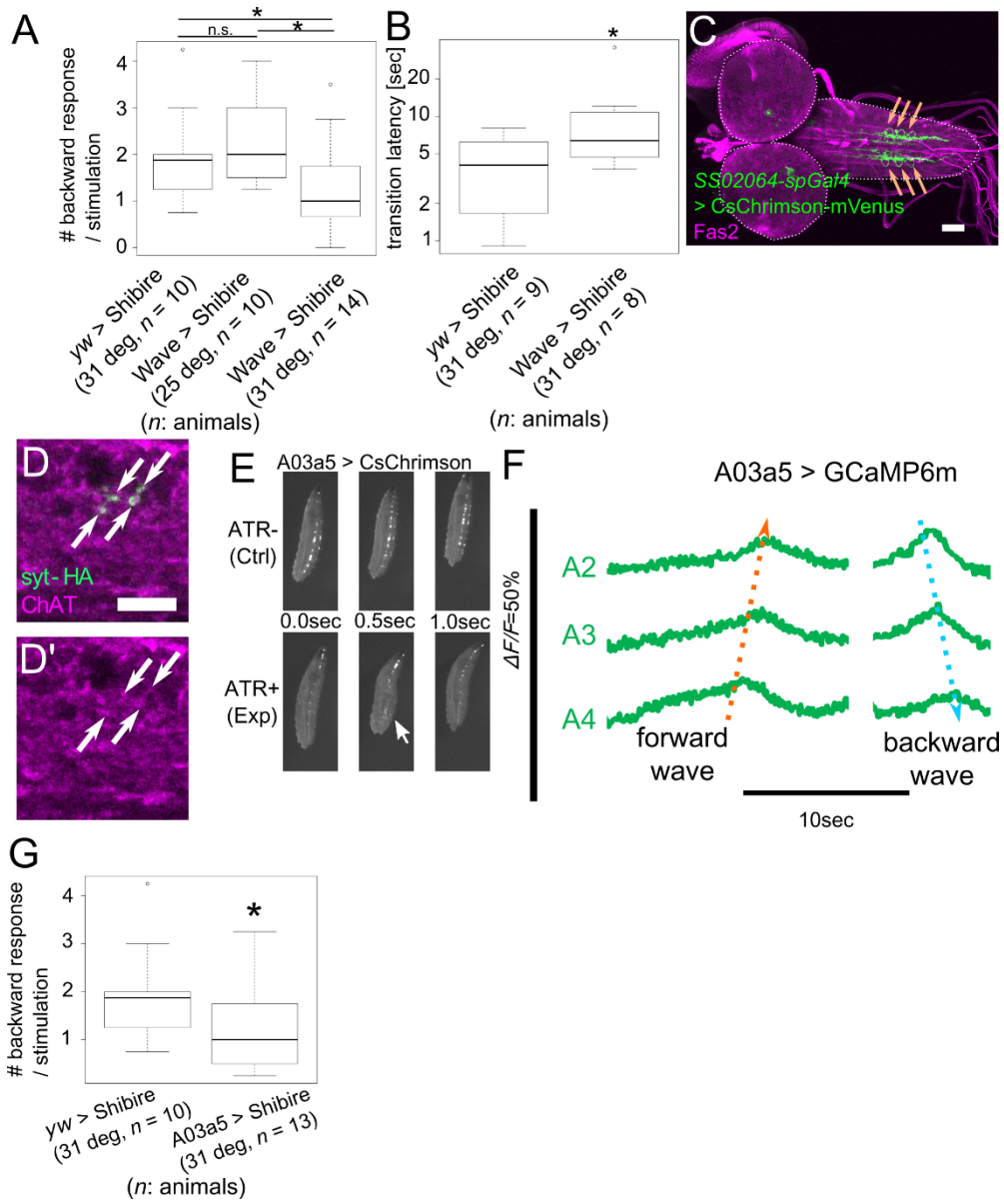


**Figure 3.15 Sensorimotor pathways recruited in anterior touch-triggered backward response.**

(**A, B**) Inhibiting Wave neurons decreases the number of head touch-triggered backward locomotion (**A**) and increases the latency in transit to forward locomotion (**B**). *: $p <$ 0.05, Mann-Whitney's *U* -test followed by Holm-Bonferroni post-hoc analysis. (**C**) Specific expression driven by *SS02064-spGAL4* in A03a5 neurons (orange arrows). Scale bar = 50 $\mu$m. (**D**) ChAT-positive puncta merged with presynaptic sites of A03a5.

Scale bar = 10 $\mu$m. (**E**) Optogenetic activation of A03a5 neurons induces tail-flip phenotype (arrow). $n$ = 8 for each group. **F**, Calcium imaging of A03a5 in an isolated CNS. (**G**) Inhibiting A03a5 neurons decreases the number of head touch-triggered backward locomotion. *: $p < 0.05$, Mann-Whitney's $U$ -test. Figures modified and reproduced from Figure 8 in Takagi et al., 2017.

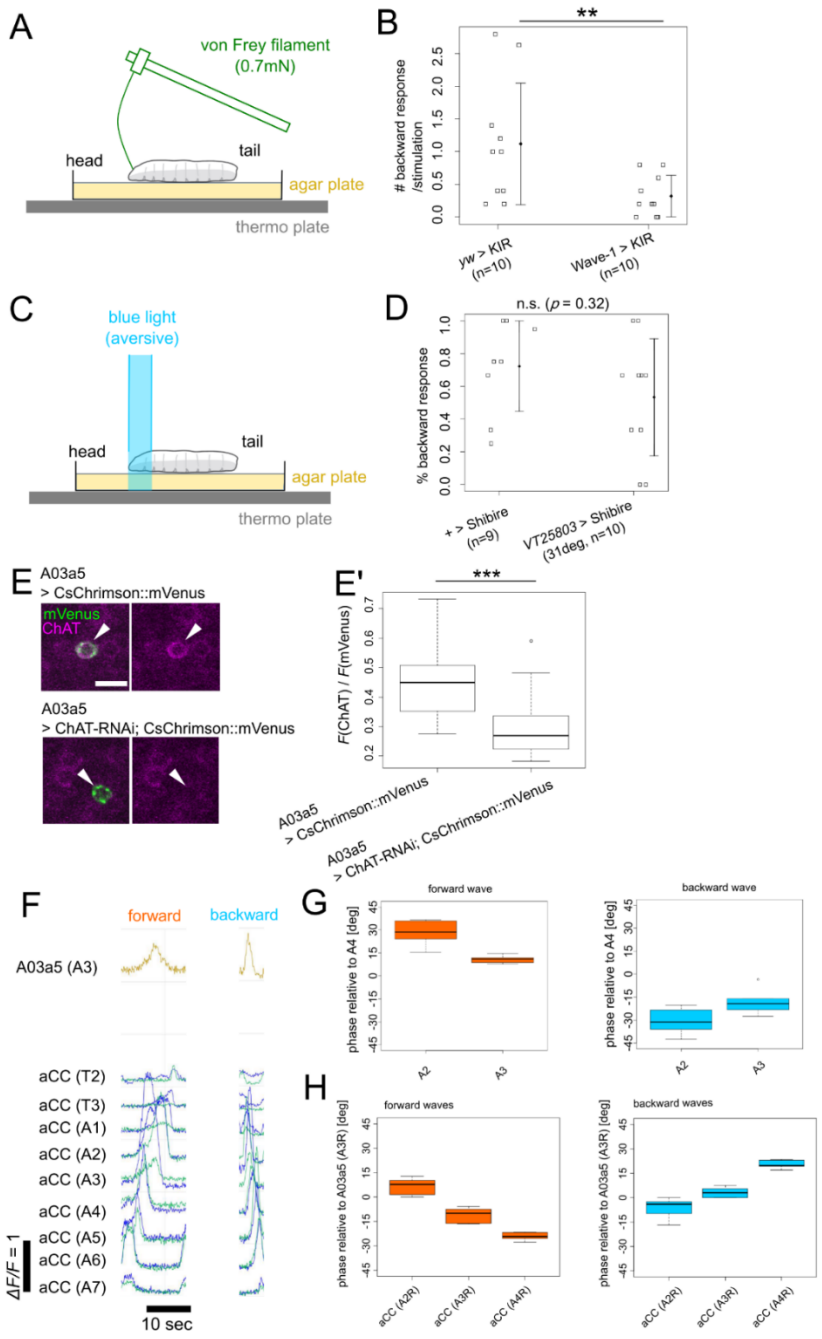


**Figure 3.16, related to Figure 3.15**

**(A)** Scheme of gentle touch assay using von Frey filament. **(B)** Inhibition of Wave neurons results in significant decrease of performed backward locomotion in response to gentle touch. **: $p < 0.01$, Mann-Whitney's *U*-test. **(C)** Scheme of blue light application

assay. **(D)** Inhibition of *VT25803-GAL4* does not reduce backward response to light application. Statistics: Mann-Whitney's *U*-test. **(E)** ChAT signals in A03a5 neurons detected with immunohistochemistry, which is diminished by ChAT-RNAi induction. Scale bar = 10 μm. (**E')** Quantification of the immunoreactivity to ChAT antibody. ***: $p < 0.001$, Mann-Whitney's *U*-test. (**F)** Calcium imaging traces of A03a5 neurons and aCC motoneurons. A03a5 neurons are active both during fictive forward and backward locomotion. (**G)** Phase plot of A03a5 neuron in multiple segments during forward and backward waves. (**H)** Phase plot of aCC motoneuron (A2, A3, and A4) with respect to A03a5 neurons in A3. Figures reproduced from Figure S8 in Takagi et al., 2017.

**Discussion**

My analyses revealed the neural circuits that span multiple layers of sensorimotor processing for action selection, from sensory perception to motor outputs, in which the Wave neurons function as a node linking localized somatosensory stimuli to distinct motor programs (Figure 3.17). My findings address crucial issues in sensorimotor control such as control by command neurons, circuit underpinnings of location specificity, and diversification of motor command.

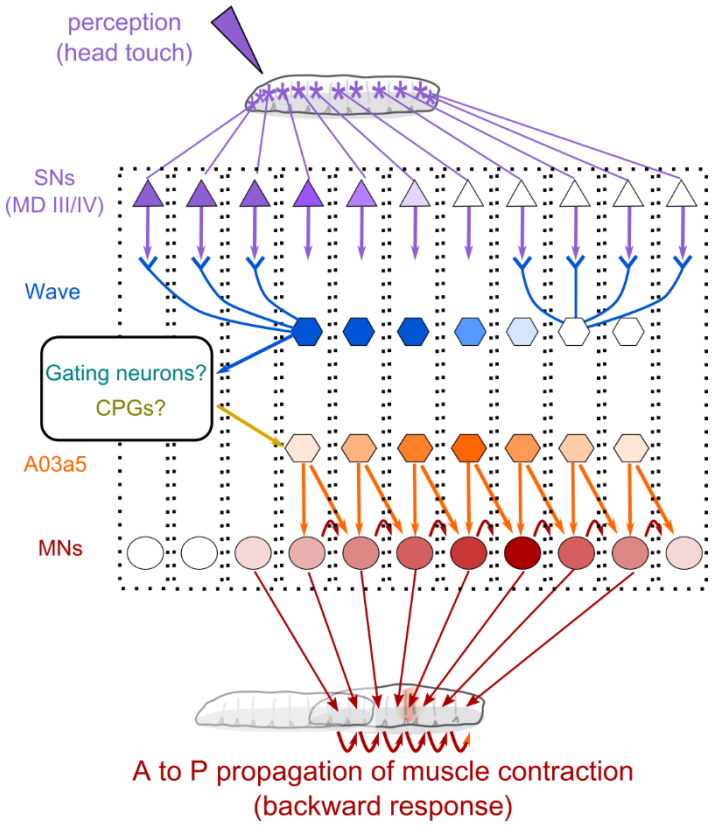


**Figure 3.17, Overall summary of the sensorimotor pathway that realizes backward motor outputs in response to head touch perception.**

Figure reproduced from Figure 8 in Takagi et al., 2017.

Command-like Neurons Elicit Larval Escape Behaviorss

The command neuron hypothesis has been widely appreciated as a general principle of action selection across the animal kingdom (Kupfermann and Weiss, 1978). In this study, I identified second-order somatosensory (Wave) neurons in anterior segments as candidate command neurons for larval backward locomotion. These neurons can be classified as command neurons according to the definition proposed by Kupfermann and Weiss (Kupfermann and Weiss, 1978), as follows. First, Wave neurons were activated by somatosensory stimuli that induce backward locomotion (Figure 3.11B). Second, gain-of-function analyses showed that their activation is

sufficient to induce backward locomotion (Figures 3.5C, 3.5D, 3.8B, 3.8C, 3.10A, and 3.10C). Finally, loss-of-function analysis showed that they are necessary for the execution of backward locomotion in response to a touch on the head (Figure 3.15A).

Regarding the nature of command neurons, two alternative hypotheses can be posed. The first hypothesis postulates a single, multisensory command-like neuron capable of inducing a specific behavior in response to multiple sensory modalities. The second hypothesis postulates multiple command-like neurons, such as one for each sensory modality, all evoking the same motor pattern. I have shown that a head-touch stimulus evokes backward locomotion via Wave neurons (Figures 3.15A, 3.16A, and 3.16B), whereas a light stimulus does so independently of Wave neurons (Figures 3.16C and 3.16D). These results are consistent with the second hypothesis, where distinct command-like neurons are independently capable of triggering the same pattern-generating circuits. I also found that activation of Wave neurons in posterior segments induces increased forward locomotion, both in the isolated CNS (Figures 3.8B and 3.8C) and intact animals (Figures 3.10A and 3.10B), and they are activated by somatosensory stimuli that induce forward locomotion (Figure 3.11C). These results suggest that posterior Wave neurons also function as command-like neurons for forward locomotion. Taken together, all Wave neurons could be command-like neurons for somatosensory-triggered locomotion, where the "sign" (forward or backward) depends on the axonal targeting of the excited Wave neuron.

Studies in the leech identified "trigger neurons" (that initiate a specific behavior) and "gating neurons" (that maintain the triggered behavior) as subclasses of command neurons (Brodfuehrer and Friesen, 1986). In this terminology, Wave neurons can be classified as trigger neurons. The observation that transient activation of Wave neurons suffices to trigger forward or

backward fictive locomotion (Figures 3.9C and 3.9C') suggests the presence of gating system(s) in the downstream circuitry, which sustain the triggered motor activity. The identity of the gating system(s) remains to be explored in future studies. One possibility is that some downstream neurons of Wave, such as Pre-goro6, Pre-Swallowtail1, T07u, and Swallowtail, act like gating neurons that fire throughout the motor episodes, as found in the leech (Brodfuehrer and Friesen, 1986). Alternatively, the downstream neurons may constitute pattern-generating circuit(s) that generates a sequence of motor activity. In this respect, it is interesting to note that the downstream circuits of the Wave include many recurrent or reciprocal connections that could maintain continuous motor activity and/or generate a pattern (Figure 3.12E).

I also identified A03a5, a novel premotor interneuron that reside downstream of an anterior Wave. Since motoneurons are activated by acetylcholine (Rohrbough and Broadie, 2002), A03a5 neurons are likely excitatory premotor interneurons (Fushiki et al., 2016; Hasegawa et al., 2016; Zwart et al., 2016), as neurons of the A03 lineage synapse onto motoneurons according to the EM dataset (Zwart et al., 2016). Optogenetic activation of A03a5 neurons induced muscular contraction that led to tail flick (Figure 3.15E), as was observed in activation of another class of cholinergic interneurons, CLI2 (Hasegawa et al., 2016). Thus, A03a5 may serve as a motor actuator for backward response to head touch.

Lateral Interaction between Distinct Command Systems

A behavioral response to a given sensory cue often consists of multiple motor programs. In the case of *Drosophila* larvae, a mechanical noxious touch (such as a pinprick) not only induces backward or forward locomotion, but also rolling (Hwang et al., 2007; Kim et al., 2012;

Ohyama et al., 2015; Robertson et al., 2013; Titlow et al., 2014; Tracey et al., 2003), depending on the strength and location of the stimuli. Hence, the basis of selection between locomotion or rolling escape behaviors should be implemented by the circuit architecture, possibly via lateral interaction between command neurons.

In the downstream circuits of Wave neurons, I found neural pathways to Goro neurons (Figure 3.12E), a pair of command-like neurons for rolling behavior (Ohyama et al., 2015). Wave neurons also receive synaptic inputs from the multisensory Basin neurons that trigger rolling (Ohyama et al., 2013). Thus, Wave pathways may facilitate rolling behavior in response to intense noxious inputs. Indeed, activating Wave neurons in segments A2-A6 did significantly increase rolling probability with respect to controls (Figure 4A in Takagi et al., 2017). Furthermore, I showed by clonal analyses that wiggling or bending (which are associated with the initial posture of rolling behavior) occurred only when Wave neurons in multiple segments were activated (Figures 3.10D and 3.10D'). Taken together, the lateral pathway from backward to rolling circuits may serve as a thresholding device, where rolling is induced instead of backward locomotion when the noxious inputs are detected in multiple body regions and exceed a certain threshold.

Segmental Interneurons are Diverged to Drive Adaptive Behaviors

A segmented architecture of the body and CNS is a common feature in vertebrates and invertebrates. The spinal cord in vertebrates, and nerve cord in invertebrates, are composed of homologous neuromeres, which receive afferent inputs from the corresponding body segment and send efferent outputs to the same or neighboring body parts. Thus, simple reflexes, such as

the knee-jerk reflex (Foster, 1877), can be induced in a location-dependent manner just by linking the afferents and efferents in the local circuits. In contrast, to induce more complex responses involving multiple body segments, neurons in distant neuromeres must be recruited. Just as I observed in the isolated nerve cord of the larvae, electrical stimulation of the spinal cord at different rostral-caudal levels induces distinct motor sequences (Barthélemy et al., 2006; Levine et al., 2014; Saltiel et al., 1998; Tresch and Bizzi, 1999). However, how homologous neuromeres drive distinct behaviors remains poorly understood.

Here, I have shown that functional and morphological divergence among segmentally repeated command (Wave) interneurons realizes segment-specific touch responses. Abdominal segments of *Drosophila* larvae contain largely the same sets of motoneurons, sensory neurons, and interneurons, each of which shares morphological characteristics across segments, including the cell-body position, axon projection, and dendritic arborization (Kohwi and Doe, 2013; Lacin and Truman, 2016; Landgraf et al., 1997; Schmid et al., 1999). While some sensory neurons (Merritt and Whitington, 1995) and somatosensory interneurons (e.g., A00c in Ohyama et al., 2015) have been shown to have segment-specific differences in their morphology, a functional significance of such segment-specific differences has not been investigated. Like other segmental neurons, Wave neurons are present in all abdominal segments and share common morphological features, such as the highly characteristic dorso-ventrally winding axon that extends along the anterior-posterior axis, a proximal neurite projection to the neuropile, and ther dendritic projection to the ventro-medial region of the neuropile, where the axons of MD IV and MD III terminate (Grueber et al., 2007). These neurons also share specific genetic features such as the expression of *VT25803-GAL4* and *MB120B-spGAL4*. However, segmentally homologous Wave neurons differ in their distal neurite extension pattern depending on the segment of origin

(Figures 3.8D–3.8F, and 3.9E–3.9E’’). Furthermore, activation of Wave neurons in anterior and posterior neuromeres trigger completely different motor patterns (i.e., backward versus forward locomotion). The segmental differences in neurite extension pattern and function are closely correlated. Thus, Wave neurons in different segments appear to acquire distinct functions by diverging their neurite extension pattern and thereby matching their receptive fields to appropriate motor outputs in a somatotopic arrangement. The notion that differences in postsynaptic targets among a single class of neurons may be responsible for inducing distinct behaviors is reminiscent of the sexual dimorphism of pheromone responses in adult flies (Datta et al., 2008).

Diversification of repeated segments is a universal strategy that animals use to evolve ethologically fit behaviors (Jarvis et al., 2012). During this process, the nervous system must evolve in concert with the body to ensure that sensory inputs from the body segments are locally and inter-segmentally linked to appropriate motor outputs. Previous studies in *Drosophila* have shown that diversification of neuromeres is controlled in part by Hox genes, which confer neuroblasts, the units for neuronal development, with segment-specific lineage properties (Jarvis et al., 2012). The offspring neurons thus generated self-assemble to form circuit architectures that mediate behaviors. The segmental boundary of anterior and posterior Wave neurons with distinct functional and morphological characteristics (Figure 3.8B) roughly corresponds to the expression boundary of the Hox gene *Abd-B* (Singh and Mishra, 2014). In the future, the study of command neurons such as the Wave neuron could inform us on how homologous neurons diverge in structure throughout development, possibly by differential recruitment of receptors for axon/dendrite guidance cues across segments under the regulation

of Hox and other spatially restricted transcription factors (Hilliard and Bargmann, 2006; Lu et al., 2009).

# Chapter 4. Formation of neuronal connectivity that regulates divergent action selection

This chapter is intentionally deleted from this PDF file as it contains unpublished data. The complete dissertation including this chapter will be made public on-line after publication in a peer-reviewed journal.

# Chapter 5. Conclusions

In this dissertation, I investigated the circuit mechanisms underlying somatotopic action selection from functional and developmental perspectives. Here, I would like to make concluding remarks on the present dissertation.

**Action selection circuitry**

How animals process sensory inputs, make a decision, and produce motor outputs has been a central question in ethology (Tinbergen, 1951). An answer to this question comprises distinct levels of analysis, such as development, mechanism, evolution, and adaptation (these categories are known as the Tinbergen's four questions; Tinbergen, 1963).

In this dissertation, I addressed the mechanistic and developmental aspects of this question by using a tactile-induced action selection in *Drosophila* larvae as a model. In Chapter 3, I identified a segment-specific wiring scheme present in *Drosophila* larvae. I showed that Wave neurons match their tactile receptive fields with appropriate motor programs, presumably by diverging their axon/dendrite extension patterns. In Chapter 4, I showed that shortening of Wave axons partially impaired motor commandability, suggesting a causal relationship between divergent axon/dendrite extension patterns and distinct motor commandability. Taking these together, I propose that segment-specific neurite extension of homologous command-like neurons mediates divergent action selection. As these neurons and the molecular mechanisms

are likely to be widely conserved across species, the present study may serve as a model to understand the "general principle" of action selection circuits.

The present study showed the circuit mechanisms of an action selection circuitry by taking advantage of cutting-edge optogenetics and connectomics. Furthermore, combination of optogenetics with a developmental approach helped clarify the significance of the morphology of the neurons on their function. Although the developmental mechanism shown in this dissertation may not be radically novel *per se*, it is reasonable that such a combination of developmental approaches with circuit analyses would reveal novel insights on how a circuit is gifted with its functions, such as by determining which of the synaptic partners among all are dominant in the function.

Besides development, blending distinct aspects of the Tinbergen's four questions may aid to understand new principles of action selection. For instance, searching for neuronal circuits that mediate tactile-based action selection in relevant insect species may help understand how the behavior has emerged through evolution and the generality of the behavioral strategy. By identifying and studying the function of "Wave circuitry orthologues" in distantly-related insect species, one may reveal the commonality and peculiarity underlying the segment-specific connectivity scheme (Takagi and Nose, 2018). Although such effort has been difficult to pursue due to the lack of accessibility to individual neurons in "non-model" species, recent development in genetic manipulation (such as the CRISPR/Cas9 system; Ran et al., 2013) is now opening a window towards such comparative approach. Although decades of studies on a select few "model" species have revealed the contribution of individual neurons and micro-circuitry to behaviors, comparative approach to elucidate how nervous system adapted to confer animals with unique behaviors would be an effective complementary way to extract

general principles of brain organization and function. It would be interesting for the community of neuroscience to revisit animal behaviors from developmental, evolutional, and adaptational perspectives to better understand “inside the black box”.

**Diversification of homologous ganglia**

The present study address segment-specificity of repeated ganglia (i.e. the function and morphology of homologous neurons between anterior and posterior neuromeres). A repetitive chain of modular units is a fundamental structure that can be found in the animal brain, such as the spinal cord, hindbrain, and neocortex (Burrows, 1996; Maruoka et al., 2017; Trevarrow et al., 1990). A common feature among such chains of ganglia is that each of the unit process external inputs and produce divergent functional outputs. In this dissertation, I have posed the possibility that segment-specific neurite guidance mechanisms underlie functional divergence of homologous neurons. Segmental differences of homologous units (in terms of morphology and function) are evident in distinct classes of neurons, such as the Rohon-Beard cells in the vertebrate spinal cord (Umeda et al., 2016) and the Mauthner cell homologs (MiD2cm and MiD3cm) in the fish hindbrain (Korn and Faber, 2005). Thus, it would be interesting to investigate the molecular divergence of these repeated units and to examine its significance on functional diversification. Such an approach would contribute to describing a brain function from molecular perspectives, which would be useful in understanding the mechanisms not only of action selection but also of broader brain functions.

# Notes on the dissertation

The detailed contribution of the collaborators is as follows:

Chapter 1

Prof. Akinao Nose helped with writing the manuscript.

Chapter 3

Mr. Benjamin Cocanougher ran the large-scale behavioral experiments, analyzed the data, and generated Figure 4A in Takagi et al., 2017.

Ms. Sawako Niki helped design the project.

Mr. Dohjin Miyamoto developed the area-confined optogenetics assay.

Dr. Hiroshi Kohsaka generated the *UAS-CD4-GCaMP6f* reporter line.

Dr. Hokto Kazama conceived and designed the two-photon optogenetics experiments.

Dr. Richard Fetter generated the ssTEM dataset.

Dr. James Truman provided reagents and generated Figure S2F in Takagi et al., 2017.

Dr. Marta Zlatic provided reagents and supervised the project.

Dr. Albert Cardona helped in EM reconstruction and writing of the manuscript.

Prof. Akinao Nose supervised the project and helped with writing the manuscript.

Chapter 4

Prof. Akinao Nose supervised the project and helped with writing the manuscript.

All the figures included in this dissertation was generated by the author himself.

The text was written originally by the author himself, with modifications based on suggestions from the collaborators listed above.

A part of this dissertation is published as follows:

- Takagi, S., Cocanougher, B.T., Niki, S., Miyamoto, D., Kohsaka, H., Kazama, H., Fetter, R.D., Truman, J.W., Zlatic, M., Cardona, A., & Nose, A (2017). Divergent Connectivity of Homologous Command-like Neurons Mediates Segment-Specific Touch Responses in *Drosophila*. *Neuron* 96, 1373–1387.e6

  (Reproduced in Chapter 3)
- Takagi, S. & Nose, A. (2018) Circuit architecture for somatotopic action selection in invertebrates. *Neurosci. Res.*, 10.1016/j.neures.2018.08.008

  (Reproduced in Chapter 1)

The inclusion of text and figures from these two publications for the current dissertation is permitted under the Cell Press (https://www.cell.com/trends/editorial-policies) and Elsevier (https://www.elsevier.com/about/policies/copyright/permissions) policy.

# Acknowledgements

I would like to express my gratitude to those who helped me with my work.

I would first like to express my deep gratitude to my mentor, Prof. Akinao Nose. This work has been built up through his limitless support, invaluable advice, and in sharing generous time for discussion. I would also like to thank Dr. Hiroshi Kohsaka for his support, advice, and encouragement. I also gratefully acknowledge Ms. Sawako Niki, Messrs. Ben Cocanougher, Dohjin Miyamoto, Drs. Hokto Kazama, Richard Fetter, Jim Truman, Marta Zlatic, and Albert Cardona for the collaboration.

I would like to thank Akira Fushiki, Casey Schneider-Mizell, Ingrid Andrade, Javier Valdes Aleman, Laura Herren, and Maarten Zwart for their contributions to EM reconstructions, Takako Morimoto for advice on electrophysiological stimulation experiments, Yoshiko Tsuchimoto for assistance in the two-photon experiments, Atora Yamada for assistance in the behavioral experiments, Karen Hibbard and Gerald Rubin's lab for the use of CsChrimson FLP-Out flies prior to publication, Chris Doe and Aref Arzan Zarin for their critical reading of the manuscript, and Matthias Landgraf for sharing unpublished observations. I would also like to thank Cynthia Hughes, Miki Fujioka, Richard Baines, Stefan Pulver, Toshihiro Kitamoto, Tzumin Lee, Yuh Nung Jan, Bloomington *Drosophila* Stock Center, Kyoto *Drosophila* Stock Center, Vienna *Drosophila* Research Center, and Developmental Studies Hybridoma Bank for

providing reagents. This work was supported by the HHMI Janelia Visitor Program, the Advanced Leading Graduate Course for Photon Science (ALPS), and a JSPS Research Fellowship for Young Scientists (DC2, 18J10483). I would like to acknowledge Linda Edwards for her proofreading of the current dissertation.

I would like to acknowledge the defense committee members for invaluable comments and suggestions on the dissertation: Profs. Kuniyoshi L. Sakai, Masaki Sano, Chikara Furusawa, Yasushi Okada, and Tetsuya Tabata.

I would like to express my gratitude to all the past and present lab members:
Drs. Eri Hasegawa, Yuki Itakura, Akira Fushiki, Teruyuki Matsunaga, Tappei Kawasaki, Youngtaek Yoon, Mss. Yumi Sakamaki, Maki Kusano, Messrs. Shunsuke Takagi, Yoshiki Maruta, Dohjin Miyamoto, Yingtao Liu, Hitoshi Maruo, Yasuhide Lee, Tatsuya Takatori, Jeonghyuk Park, Atsuki Hiramoto, Xiyang Sun, Xiangsunze Zeng, Shoya Ohura, Yuji Matsuo, Kazuki Tomatsu, Hiroto Nakabayashi, Kazushi Fukumasu, Shinsuke Inaba, and Xu Zhang. Mss. Kasumi Shibahara, Toshie Naoi, and Sawako Niki are greatly acknowledged for their excellent assistance.

Finally, my family, who have always stretched out their helping hands (and paws), are greatly acknowledged. This dissertation is dedicated to them.

# References

Abraira, V.E., and Ginty, D.D. (2013). The sensory neurons of touch. Neuron *79*, 618–639.

Aso, Y., Siwanowicz, I., Bräcker, L., Ito, K., Kitamoto, T., and Tanimoto, H. (2010). Specific dopaminergic neurons for the formation of labile aversive memory. Curr. Biol. *20*, 1445–1451.

Baines, R.A., Uhler, J.P., Thompson, A., Sweeney, S.T., and Bate, M. (2001). Altered electrical properties in Drosophila neurons developing without synaptic transmission. J. Neurosci. *21*, 1523–1531.

Barthélemy, D., Leblond, H., Provencher, J., and Rossignol, S. (2006). Nonlocomotor and Locomotor Hindlimb Responses Evoked by Electrical Microstimulation of the Lumbar Cord in Spinalized Cats. J. Neurophysiol. *96*, 3273–3292.

Berndt, A., Schoenenberger, P., Mattis, J., Tye, K.M., Deisseroth, K., Hegemann, P., and Oertner, T.G. (2011). High-efficiency channelrhodopsins for fast neuronal stimulation at low light levels. Proc. Natl. Acad. Sci. U. S. A. *108*, 7595–7600.

Berni, J. (2015). Genetic dissection of a regionally differentiated network for exploratory behavior in drosophila larvae. Curr. Biol. *25*, 1319–1326.

Berni, J., Pulver, S.R., Griffith, L.C., and Bate, M. (2012). Autonomous circuitry for substrate exploration in freely moving Drosophila larvae. Curr. Biol. *22*, 1861–1870.

Bezares-Calderón, L.A., Berger, J., Jasek, S., Verasztó, C., Mendes, S., Gühmann, M., Almeda, R., Shahidi, R., and Jékely, G. (2018). Neural circuitry of a polycystin-mediated hydrodynamic startle response for predator avoidance. Elife *7*.

Bidaye, S.S., Machacek, C., Wu, Y., and Dickson, B.J. (2014). Neuronal Control of Drosophila. Science. *344*, 97–101.

Brand, A.H., and Perrimon, N. (1993). Targeted gene expression as a means of altering cell fates and generating dominant phenotypes. Development *118*, 401–415.

Brodfuehrer, P.D., and Friesen, W.O. (1986). From stimulation to undulation: a neuronal pathway for the control of swimming in the leech. Science *234*, 1002–1004.

Burrows, M. (1996). The Neurobiology of an Insect Brain (Oxford University Press).

Chalfie, M., Sulston, J.E., White, J.G., Southgate, E., Thomson, J.N., and Brenner, S. (1985). The neural circuit for touch sensitivity in Caenorhabditis elegans. J. Neurosci. *5*, 956–964.

Clyne, J.D., and Miesenböck, G. (2008). Sex-Specific Control and Tuning of the Pattern Generator for Courtship Song in Drosophila. Cell *133*, 354–363.

Datta, S.R., Vasconcelos, M.L., Ruta, V., Luo, S., Wong, A., Demir, E., Flores, J., Balonze, K., Dickson, B.J., and Axel, R. (2008). The Drosophila pheromone cVA activates a sexually dimorphic neural circuit. Nature *452*, 473–477.

Duan, B., Cheng, L., Bourane, S., Britz, O., Padilla, C., Garcia-Campmany, L., Krashes, M., Knowlton, W., Velasquez, T., Ren, X., et al. (2014). Identification of spinal circuits transmitting and gating mechanical pain. Cell *159*, 1417–1432.

Edwards, D.H., Heitler, W.J., and Krasne, F.B. (1999). Fifty years of a command neuron: The neurobiology of escape behavior in the crayfish. Trends Neurosci. *22*, 153–161.

Feinberg, E.H., VanHoven, M.K., Bendesky, A., Wang, G., Fetter, R.D., Shen, K., and Bargmann, C.I. (2008). GFP Reconstitution Across Synaptic Partners (GRASP) Defines Cell Contacts and Synapses in Living Nervous Systems. Neuron *57*, 353–363.

Fire, A., Xu, S., Montgomery, M.K., Kostas, S.A., Driver, S.E., and Mello, C.C. (1998). Potent and specific genetic interference by double-stranded RNA in Caenorhabditis elegans. Nature *391*, 806–811.

Foster, M. (1877). A Text Book of Physiology (Macmillan).

Fujioka, M., Lear, B.C., Landgraf, M., Yusibova, G.L., Zhou, J., Riley, K.M., Patel, N.H., and Jaynes, J.B. (2003). Even-skipped, acting as a repressor, regulates axonal projections in Drosophila. Development *130*, 5385–5400.

Fushiki, A., Zwart, M.F., Kohsaka, H., Fetter, R.D., Cardona, A., and Nose, A. (2016). A circuit mechanism for the propagation of waves of muscle contraction in Drosophila. Elife *5*, 1–23.

Gao, S., Guan, S.A., Fouad, A.D., Meng, J., Kawano, T., Huang, Y.-C., Li, Y., Alcaire, S., Hung, W., Lu, Y., et al. (2018). Excitatory motor neurons are local oscillators for backward locomotion. Elife *7*, e29915.

Di Giminiani, P., Petersen, L.J., and Herskin, M.S. (2013). Nociceptive responses to thermal and mechanical stimulations in awake pigs. Eur. J. Pain (United Kingdom) *17*, 638–648.

Golic, K.G., and Lindquist, S. (1989). The FLP recombinase of yeast catalyzes site-specific recombination in the Drosophila genome. Cell *59*, 499–509.

Green, C.H., Burnet, B., and Connolly, K.J. (1983). Organization and patterns of inter- and intraspecific variation in the behaviour of Drosophila larvae. Anim. Behav. *31*, 282–291.

Grueber, W.B., Ye, B., Yang, C.-H., Younger, S., Borden, K., Jan, L.Y., and Jan, Y.-N. (2007). Projections of Drosophila multidendritic neurons in the central nervous system: links with peripheral dendrite morphology. Development *134*, 55–64.

Hasegawa, E., Truman, J.W., and Nose, A. (2016). Identification of excitatory premotor interneurons which regulate local muscle contraction during Drosophila larval locomotion. Sci. Rep. *6*, 1–13.

Hilliard, M.A., and Bargmann, C.I. (2006). Wnt signals and Frizzled activity orient anterior-posterior axon outgrowth in C. elegans. Dev. Cell *10*, 379–390.

Hotta, Y., and Benzer, S. (1970). Genetic dissection of the Drosophila nervous system by means of mosaics. Proc. Natl. Acad. Sci. U. S. A. *67*, 1156–1163.

Hotta, Y., and Benzer, S. (1972). Mapping of Behaviour in Drosophila Mosaics. Nature *240*, 527–535.

Hughes, C.L., and Thomas, J.B. (2007). A sensory feedback circuit coordinates muscle activity in Drosophila. Mol. Cell. Neurosci. *35*, 383–396.

Hwang, R.Y., Zhong, L., Xu, Y., Johnson, T., Zhang, F., Deisseroth, K., and Tracey, W.D. (2007). Nociceptive Neurons Protect Drosophila Larvae from Parasitoid Wasps. Curr. Biol. *17*, 2105–2116.

Inoue, M., Takeuchi, A., Horigane, S., Ohkura, M., Gengyo-Ando, K., Fujii, H., Kamijo, S., Takemoto-Kimura, S., Kano, M., Nakai, J., et al. (2015). Rational design of a high-affinity, fast, red calcium indicator R-CaMP2. Nat. Methods *12*, 64–70.

Islam, S.S., and Zelenin, P. V. (2008a). Modifications of Locomotor Pattern Underlying Escape Behavior in the Lamprey. J. Neurophysiol. *99*, 297–307.

Itakura, Y., Kohsaka, H., Ohyama, T., Zlatic, M., Pulver, S.R., and Nose, A. (2015). Identification of inhibitory premotor interneurons activated at a late phase in a motor cycle during drosophila larval locomotion. PLoS One *10*, 1–24.

Jarvis, E., Bruce, H.S., and Patel, N.H. (2012). Evolving specialization of the arthropod nervous system. Proc. Natl. Acad. Sci. *109*, 10634–10639.

Kernan, M., Cowan, D., and Zuker, C. (1994). Genetic dissection of mechanosensory transduction: Mechanoreception-defective mutations of drosophila. Neuron *12*, 1195–1206.

Kim, S.E., Coste, B., Chadha, A., Cook, B., and Patapoutian, A. (2012). The role of Drosophila Piezo in mechanical nociception. Nature *483*, 209–212.

Kitamoto, T. (2001). Conditional modification of behavior inDrosophila by targeted expression of a temperature-sensitiveshibire allele in defined neurons. J. Neurobiol. *47*, 81–92.

Kitamoto, T. (2002). Conditional disruption of synaptic transmission induces male-male courtship behavior in Drosophila. Proc. Natl. Acad. Sci. *99*, 13232–13237.

Klapoetke, N.C., Murata, Y., Kim, S.S., Pulver, S.R., Birdsey-Benson, A., Cho, Y.K., Morimoto, T.K., Chuong, A.S., Carpenter, E.J., Tian, Z., et al. (2014). Independent optical excitation of distinct neural populations. Nat. Methods *11*, 338–346.

Kohsaka, H., Takasu, E., Morimoto, T., and Nose, A. (2014). A group of segmental premotor interneurons regulates the speed of axial locomotion in drosophila larvae. Curr. Biol. *24*, 2632–2642.

Kohwi, M., and Doe, C.Q. (2013). Temporal fate specification and neural progenitor competence during development. Nat. Rev. Neurosci. *14*, 823–838.

Korn, H., and Faber, D.S. (2005). The Mauthner Cell Half a Century Later: A Neurobiological Model for Decision-Making? Neuron *47*, 13–28.

Kristan, W.B.J. (1982). Sensory and Motor Neurones Responsible for the Local Bending Response in Leeches. J. Exp. Biol. *96*, 161–180.

Kristan, W.B., Calabrese, R.L., and Friesen, W.O. (2005). Neuronal control of leech behavior. Prog. Neurobiol. *76*, 279–327.

Kupfermann, I., and Weiss, K.R. (1978). The command neuron concept. Behav. Brain Sci. *1*, 3.

Lacin, H., and Truman, J.W. (2016). Lineage mapping identifies molecular and architectural similarities between the larval and adult Drosophila central nervous system. Elife *5*, 1–28.

Lai, S.-L., and Lee, T. (2006). Genetic mosaic with dual binary transcriptional systems in Drosophila. Nat. Neurosci. *9*, 703–709.

Landgraf, M., Bossing, T., Technau, G.M., and Bate, M. (1997). The origin, location, and projections of the embryonic abdominal motorneurons of Drosophila. J. Neurosci. *17*, 9642–9655.

Levine, A.J., Hinckley, C.A., Hilde, K.L., Driscoll, S.P., Poon, T.H., Montgomery, J.M., and Pfaff, S.L. (2014). Identification of a cellular node for motor control pathways. Nat. Neurosci. *17*, 586–593.

Lewis, J.E., and Kristan, W.B.J. (1998). A neuronal network for computing population vectors in the leech. Nature *391*, 76–79.

Lima, S.Q., and Miesenböck, G. (2005). Remote control of behavior through genetically targeted photostimulation of neurons. Cell *121*, 141–152.

Lockery, S.R., and Kristan, W.B. (1990a). Distributed processing of sensory information in the leech. I. Input-output relations of the local bending reflex. J. Neurosci. *10*, 1816–1829.

Lockery, S.R., and Kristan, W.B. (1990b). Distributed processing of sensory information in the leech. II. Identification of interneurons contributing to the local bending reflex. J. Neurosci. *10*, 1816–1829.

Lockery, S.R., and Sejnowski, T.J. (1992). Distributed processing of sensory information in the leech. III. A dynamical neural network model of the local bending reflex. J. Neurosci. *12*, 3877–3895.

Lu, B., Wang, K.H., and Nose, A. (2009). Molecular mechanisms underlying neural circuit formation. Curr. Opin. Neurobiol. *19*, 162–167.

Luan, H., Peabody, N.C., Vinson, C.R., and White, B.H. (2006). Refined Spatial Manipulation of Neuronal Function by Combinatorial Restriction of Transgene Expression. Neuron *52*, 425–436.

Lue, N.F., Chasman, D.I., Buchman, A.R., and Kornberg, R.D. (1987). Interaction of GAL4 and GAL80 gene regulatory proteins in vitro. Mol. Cell. Biol. *7*, 3446–3451.

Ma, Z., Stork, T., Bergles, D.E., and Freeman, M.R. (2016). Neuromodulators signal through astrocytes to alter neural circuit activity and behaviour. Nature *539*, 428–432.

Marder, E., and Bucher, D. (2001). Central pattern generators and the control of rhythmic movements. Curr. Biol. *11*, R986-96.

Marr, D. (2010). Vision : a computational investigation into the human representation and processing of visual information (MIT Press).

Maruoka, H., Nakagawa, N., Tsuruno, S., Sakai, S., Yoneda, T., and Hosoya, T. (2017). Lattice system of functionally distinct cell types in the neocortex. Science *358*, 610–615.

McClellan, A.D. (1989). Control of Locomotion in a Lower Vertebrate, the Lamprey: Brainstem Command Systems and Spinal Cord Regeneration. Am. Zool. *29*, 37–51.

Mittenthal, J.E., and Wine, J.J. (1973). Connectivity patterns of crayfish giant interneurons: visualization of synaptic regions with cobalt dye. Science *179*, 182–184.

Nagel, G., Szellas, T., Huhn, W., Kateriya, S., Adeishvili, N., Berthold, P., Ollig, D., Hegemann, P., and Bamberg, E. (2003). Channelrhodopsin-2, a directly light-gated cation-selective membrane channel. Proc. Natl. Acad. Sci. U. S. A. *100*, 13940–13945.

Nakai, J., Ohkura, M., and Imoto, K. (2001). A high signal-to-noise Ca 2 + probe composed of a single green fluorescent protein. Nat. Biotechnol. *19*, 137–141.

Nern, A., Pfeiffer, B.D., and Rubin, G.M. (2015). Optimized tools for multicolor stochastic labeling reveal diverse stereotyped cell arrangements in the fly visual system. Proc. Natl. Acad. Sci. *112*, E2967–E2976.

Nicolaï, L.J.J., Ramaekers, A., Raemaekers, T., Drozdzecki, A., Mauss, A.S., Yan, J., Landgraf, M., Annaert, W., and Hassan, B.A. (2010). Genetically encoded dendritic marker sheds light on neuronal connectivity in Drosophila. Proc. Natl. Acad. Sci. U. S. A. *107*, 20553–20558.

Ohyama, T., Jovanic, T., Denisov, G., Dang, T.C., Hoffmann, D., Kerr, R.A., and Zlatic, M. (2013). High-Throughput Analysis of Stimulus-Evoked Behaviors in Drosophila Larva Reveals Multiple Modality-Specific Escape Strategies. PLoS One *8*, e71706.

Ohyama, T., Schneider-Mizell, C.M., Fetter, R.D., Aleman, J.V., Franconville, R., Rivera-Alba, M., Mensh, B.D., Branson, K.M., Simpson, J.H., Truman, J.W., et al. (2015). A multilevel multimodal circuit enhances action selection in Drosophila. Nature *520*, 633–639.

Orlovsky, G., Deliagina, T.G., and Grillner, S. (1999). Neuronal Control of LocomotionFrom Mollusc to Man (Oxford University Press).

Palmer, C.R., Barnett, M.N., Copado, S., Gardezy, F., and Kristan, W.B. (2014). Multiplexed modulation of behavioral choice. J. Exp. Biol. *217*, 2963–2973.

Penfield, W., and Boldery, E. (1937). Somatic Motor And Sensory Representation In The Cerebral Cortex Of Man As Studied By Electrical Stimulation. Brain *60*, 389–443.

Perkins, L.A., Holderbaum, L., Tao, R., Hu, Y., Sopko, R., McCall, K., Yang-Zhou, D., Flockhart, I., Binari, R., Shim, H.-S., et al. (2015). The Transgenic RNAi Project at Harvard Medical School: Resources and Validation. Genetics *201*, 843–852.

Piggott, B.J., Liu, J., Feng, Z., Wescott, S.A., and Xu, X.Z.S. (2011). The Neural Circuits and Synaptic Mechanisms Underlying Motor Initiation in C. elegans. Cell *147*, 922–933.

Pirri, J.K., McPherson, A.D., Donnelly, J.L., Francis, M.M., and Alkema, M.J. (2009). A Tyramine-Gated Chloride Channel Coordinates Distinct Motor Programs of a Caenorhabditis elegans Escape Response. Neuron *62*, 526–538.

Pulver, S.R., Bayley, T.G., Taylor, A.L., Berni, J., Bate, M., and Hedwig, B. (2015). Imaging fictive locomotor patterns in larval *Drosophila*. J. Neurophysiol. *114*, 2564–2577.

Ran, F.A., Hsu, P.D., Lin, C.-Y., Gootenberg, J.S., Konermann, S., Trevino, A.E., Scott, D.A., Inoue, A., Matoba, S., Zhang, Y., et al. (2013). Double Nicking by RNA-Guided CRISPR Cas9 for Enhanced Genome Editing Specificity. Cell *154*, 1380–1389.

Robertson, J.L., Tsubouchi, A., and Tracey, W.D. (2013). Larval Defense against Attack from Parasitoid Wasps Requires Nociceptive Neurons. PLoS One *8*, 1–9.

Rohrbough, J., and Broadie, K. (2002). Electrophysiological Analysis of Synaptic Transmission in Central Neurons of *Drosophila* Larvae. J. Neurophysiol. *88*, 847–860.

Saalfeld, S., Cardona, A., Hartenstein, V., and Tomančák, P. (2009). CATMAID: Collaborative annotation toolkit for massive amounts of image data. Bioinformatics *25*, 1984–1986.

Saltiel, P., Tresch, M.C., and Bizzi, E. (1998). Spinal Cord Modular Organization and Rhythm Generation: An NMDA Iontophoretic Study in the Frog. J. Neurophysiol. *80*, 2323–2339.

Schmid, A., Chiba, A., and Doe, C.Q. (1999). Clonal analysis of Drosophila embryonic neuroblasts: neural cell types, axon projections and muscle targets. Development *126*, 4653–4689.

Schneider-Mizell, C.M., Gerhard, S., Longair, M., Kazimiers, T., Li, F., Zwart, M.F., Champion, A., Midgley, F.M., Fetter, R.D., Saalfeld, S., et al. (2016). Quantitative neuroanatomy for connectomics in Drosophila. Elife *5*.

Sen, R., Wu, M., Branson, K., Robie, A., Rubin, G.M., and Dickson, B.J. (2017). Moonwalker Descending Neurons Mediate Visually Evoked Retreat in Drosophila. Curr. Biol. *27*, 766–771.

Singh, N.P., and Mishra, R.K. (2014). Role of abd-A and Abd-B in Development of Abdominal Epithelia Breaks Posterior Prevalence Rule. PLoS Genet. *10*, e1004717.

Sweeney, S.T., Broadie, K., Keane, J., Niemann, H., and O'Kane, C.J. (1995). Targeted expression of tetanus toxin light chain in Drosophila specifically eliminates synaptic transmission and causes behavioral defects. Neuron *14*, 341–351.

Takagi, S., and Nose, A. (2018). Circuit architecture for somatotopic action selection in invertebrates. Neurosci. Res. *10.1016/j.neures.2018.08.008.*

Takagi, S., Cocanougher, B.T., Niki, S., Miyamoto, D., Kohsaka, H., Kazama, H., Fetter, R.D., Truman, J.W., Zlatic, M., Cardona, A., et al. (2017). Divergent Connectivity of Homologous Command-like Neurons Mediates Segment-Specific Touch Responses in Drosophila. Neuron *96*, 1373–1387.e6.

Terada, S.-I., Matsubara, D., Onodera, K., Matsuzaki, M., Uemura, T., and Usui, T. (2016). Neuronal processing of noxious thermal stimuli mediated by dendritic Ca2+ influx in Drosophila somatosensory neurons. Elife *5*.

Tinbergen, N. (1951). The study of instinct (Oxford University Press).

Tinbergen, N. (1963). On aims and methods of Ethology. Z. Tierpsychol. *20*, 410–433.

Titlow, J.S., Rice, J., Majeed, Z.R., Holsopple, E., Biecker, S., and Cooper, R.L. (2014). Anatomical and genotype-specific mechanosensory responses in Drosophila melanogaster larvae. Neurosci. Res. *83*, 54–63.

Tracey, W.D., Wilson, R.I., Laurent, G., and Benzer, S. (2003). painless, a Drosophila gene essential for nociception. Cell *113*, 261–273.

Tresch, M.C., and Bizzi, E. (1999). Responses to spinal microstimulation in the chronically spinalized rat and their relationship to spinal systems activated by low threshold cutaneous stimulation. Exp. Brain Res. *129*, 401–416.

Trevarrow, B., Marks, D.L., and Kimmel, C.B. (1990). Organization of hindbrain segments in the zebrafish embryo. Neuron *4*, 669–679.

Tsubouchi, A., Caldwell, J.C., and Tracey, W.D. (2012). Dendritic filopodia, ripped pocket, NOMPC, and NMDARs contribute to the sense of touch in Drosophila larvae. Curr. Biol. *22*, 2124–2134.

Umeda, K., Ishizuka, T., Yawo, H., and Shoji, W. (2016). Position- and quantity-dependent responses in zebrafish turning behavior. Sci. Rep. *6*, 27888.

White, J.G., Southgate, E., Thomson, J.N., and Brenner, S. (1986). The structure of the nervous system of the nematode Caenorhabditis elegans. Philos. Trans. R. Soc. Lond. B. Biol. Sci. *314*, 1–340.

Wiersma, C.A.G., and Ikeda, K. (1964). Interneurons commanding swimmeret movements in the crayfish, Procambarus clarki (girard). Comp. Biochem. Physiol. *12*, 509–525.

Wilson, D.M. (1961). The Central Nervous Control of Flight in a Locust. Exp. Biol. 471–490.

Xiang, Y., Yuan, Q., Vogt, N., Looger, L.L., Jan, L.Y., and Jan, Y.N. (2010). Light-avoidance-mediating photoreceptors tile the Drosophila larval body wall. Nature *468*, 921–926.

Yan, Z., Zhang, W., He, Y., Gorczyca, D., Xiang, Y., Cheng, L.E., Meltzer, S., Jan, L.Y., and Jan, Y.N. (2013). Drosophila NOMPC is a mechanotransduction channel subunit for gentle-touch sensation. Nature *493*, 221–225.

Zemelman, B. V., Lee, G.A., Ng, M., and Miesenböck, G. (2002). Selective photostimulation of genetically chARGed neurons. Neuron *33*, 15–22.

Zhang, W., Yan, Z., Jan, L.Y., and Jan, Y.N. (2013). Sound response mediated by the TRP channels NOMPC, NANCHUNG, and INACTIVE in chordotonal organs of Drosophila larvae. Proc. Natl. Acad. Sci. *110*, 13612–13617.

Zhao, Y., Araki, S., Wu, J., Teramoto, T., Chang, Y.-F., Nakano, M., Abdelfattah, A.S., Fujiwara, M., Ishihara, T., Nagai, T., et al. (2011). An Expanded Palette of Genetically Encoded Ca2+ Indicators. Science. *333*, 1888–1891.

Zhong, L., Hwang, R.Y., and Tracey, W.D. (2010). Pickpocket Is a DEG/ENaC Protein Required for Mechanical Nociception in Drosophila Larvae. Curr. Biol. *20*, 429–434.

Zwart, M.F., Pulver, S.R., Truman, J.W., Fushiki, A., Fetter, R.D., Cardona, A., and Landgraf, M. (2016). Selective Inhibition Mediates the Sequential Recruitment of Motor Pools. Neuron. *91*, 615-628.